



Interactions between synaptic plasticity and switches in brain states for memory consolidation: a modeling study.

*Master thesis realised with the aim of obtaining the degree of Master in
Biomedical Engineering*

Caroline Minne

Promotor:

Guillaume Drion

Jury members:

Guillaume Drion

Christophe Phillips

Vincent Seutin

Pierre Sacré

Davide Ruffoni

UNIVERSITY OF LIÈGE
FACULTY OF APPLIED SCIENCES
ACADEMIC YEAR 2020 - 2021

Interactions between synaptic plasticity and switches in brain states for memory consolidation: a modeling study.

Caroline Minne

Supervisor: G. Drion

Master in Biomedical Engineering, University of Liège

Academic year 2020-2021

Abstract

Once a day, every individual lay down and becomes unconscious. Isn't sleep a strange thing to do? Despite the risks associated to it, our ancestors used to sleep too, suggesting that it should provide an evolutionary advantage. Thus, it rises a fundamental question: *why do we sleep?* Among all essential functions of sleep, research has proved its preponderant role in memory formation and consolidation. At the cellular level, memory is achieved through processes referred to as *synaptic plasticity* and translating the remarkable ability of the brain to constantly evolve due to various stimuli. Furthermore, differences in the neuronal firing patterns have been highlighted between wake and sleep: during sleep, neurons are bursting while during wake, neurons show a tonic firing pattern.

Memory is an abstract concept, it is not a simple task to understand the processes behind it. As experimental evidence provides insights about how plasticity is induced, modeling techniques reproducing experimental data can give insights about memory mechanisms. Literature is broad concerning plasticity modeling. In this work, a concise review of phenomenological models is conducted.

Then, some of them are implemented in a conductance-based model able to switch from *waking* to *sleep* i.e. from *tonic* to *bursting* activity. Compared to simplified spiking neuron model, this conductance-based model is a powerful tool to be able to faithfully replicate neuronal behavior in a waking and sleeping period. Reproduction of experimental protocols are carried in *tonic* mode as well as the impact of variability in the firing pattern to mimic more *in vivo* situations. As the ultimate goal of this thesis is to see the impact of existing models on memory consolidation during sleep, their robustness and behaviour during a bursting period are investigated. It led to unsatisfactory results regarding memory consolidation, highlighting the limitations of those phenomenological models. The behaviour of the models implemented highly depends on the method used to bound the synaptic weight in-between extreme values. Finally, insights about neuromodulation are suggested as improvements.

Acknowledgements

I would like to express my sincere appreciation to my supervisor Guillaume Drion, who dedicated a lot of time and expertise for the well accomplishment of this work, as well as the opportunity to work in a subject that I truly enjoyed. I am extremely grateful for his PhD student, Kathleen Jacquerie, who gave her time, energy and heart in the supervision of this work. I admire her patience, rigorousness as well as her aesthetic skills.

I also take this opportunity to express my sincere gratitude for having spent this semester in the good company of Chloé Marchal and Chloé Preud'homme who provided the moral support and friendship necessary in these times of crisis. It was truly a pleasure to work along their sides.

I must express my very profound gratitude to Juliette, Pol who, directly or indirectly, have lent their helping hands in this work, and among others, to Louise-Marie, Antoine, Alice, and my family for providing me with unfailing support throughout my years of study, especially this one.

Liège, June 9th, 2021

Caroline Minne

Contents

1	Introduction	1
1.1	Motivation: the link between sleep and memory	1
1.2	Structure	2
I	Background	5
2	Elements of neurophysiology and neuronal modeling	7
2.1	Neurons	7
2.1.1	Morphology	7
2.1.2	Excitability and electrical signalling	7
2.1.3	Communication between two neurons	9
2.2	Wake/sleep cycle	9
2.2.1	States Characteristics	9
2.2.2	Thalamus	10
2.2.3	Bursting types	11
2.3	Neuronal modeling	11
2.3.1	Conductance-based models	11
2.3.2	Integrate-and-fire models	13
2.4	Summary	17
3	Synaptic Plasticity: from a biological perspective	19
3.1	Short-term synaptic plasticity	19
3.2	Long-term plasticity	20
3.2.1	Properties	20
3.2.2	Long-term plasticity mechanisms	22
3.3	Experimental (long-term) induction protocols	25
3.3.1	How experimental induction protocols are carried?	25
3.3.2	The main synaptic plasticity drivers	25
3.4	Summary	30
II	Synaptic plasticity from a modeling point of view	31
4	State-of-the-art	33
4.1	Rate-based	35
4.2	Spike timing-based	36
4.2.1	Classical STDP: Pair-based model	36

4.2.2	Triplet models	39
4.2.3	Voltage-based models	40
4.2.4	Three-factor rule	41
4.2.5	Combination of models	43
4.2.6	Sleep adaptation	44
4.2.7	Burst	45
4.3	Modeling specifications	45
4.4	Summary	48
III	Computational study	49
5	Integration of synaptic rule in a switching network: validation in <i>tonic</i> mode	51
5.1	Model integration in conductance-based circuit (ECI)	52
5.1.1	Pair-based model from [Abbott and Nelson, 2000, Graupner et al., 2016]	52
5.1.2	Triplet model from [Pfister and Gerstner, 2006, Graupner et al., 2016]	53
5.1.3	Voltage-dependent model [Clopath et al., 2010]	53
5.2	Experiments	53
5.2.1	Reproduction of STDP protocol	54
5.2.2	Adding variability	57
5.2.3	Reproduction of frequency effect on STDP protocol	61
5.3	Summary	65
6	Compatibility of plasticity rules with memory consolidation during sleep in <i>bursting</i> mode	67
6.1	In a perfect world	68
6.1.1	Synapse with low connectivity	69
6.1.2	Synapse with high connectivity	71
6.2	In a realistic world	72
6.2.1	Synapse with low connectivity	74
6.2.2	Synapse with high connectivity	75
6.3	Summary and conclusion	76
IV	Conclusions and Perspectives	79
7	Conclusion and perspectives	81
7.1	Thesis summary	81
7.2	Perspectives	82
7.2.1	A variety of models	82
7.2.2	The importance of neuromodulation	82
	Appendices	A1
A	Neurophysiology basis	A1
A.1	Action potential mechanism	A1
A.2	Nernst Potential of main ions	A2

B	Thalamus mechanisms during sleep	A3
B.1	T-Type current	A3
B.2	Spindles	A3
C	Conductance-based model	A5
C.1	Connection between cells	A6
D	Plasticity rules and computational details	A7
D.1	Pair-based model	A7
D.2	Triplet model	A8
D.3	Voltage-dependent model [Clopath et al., 2010]	A9
D.4	UP-mediated learning rule from [González-Rueda et al., 2018]:	A9
D.5	Dynamical evolution of the synaptic weight	A9
D.6	Variability in ionic conductances	A9
E	Supplementary results	A10
E.1	Bursts parameters for the different simulations	A10
	Bibliography	A16

Acronyms

AMPAr α -amino-3-hydroxy-5-methyl-4-isoxazolepropionic acidreceptor. 9, 22–24

EEG Electroencephalogram. 9–11, A4

EPSC Excitatory Post-Synaptic Current. 25, 26, 38

EPSP Excitatory Post-Synaptic Potentiation. 8, 9, 19, 25, 26, 38, 71, A4

GABA Aminobutyric Acid. 9, 36, 42

LTD Long-term depression. 20–23, 25–28, 40, 41, 43, 45, 53, A9

LTP Long-term potentiation. 20–23, 25–28, 40, 41, 43, 45, 53, A9

NMDAr N-methyl-D-aspartate receptor. 9, 22, 38

SHY Synaptic Homeostasis Hypothesis of Sleep. 44, 45, 47, 67, 68, 83, 84

STDP Spike timing-dependent plasticity. v, 25, 28, 29, 36–39, 41–45, 47, 54, 56, 61, 63, 81–84

SWS Slow-Wave Sleep. 9–11, 44, 45, 47

Chapter 1

Introduction

1.1 Motivation: the link between sleep and memory

It has been shown that memories are consolidated in the brain by synaptic changes and that sleep is essential for memory consolidation. One of the first study linking sleep and memory was realised by [Jenkins and Dallenbach, 1924], who performed a study in which two men had to learn a list of syllables with no meaning. The conclusion was clear: the performance of the subjects were significantly better after sleeping than staying awake during the same amount of time. Since then, a high amount of studies have been carried out, proving the memory function of sleep and more importantly its role in the consolidation of memories as an evolutionary process [Diekelmann and Born, 2010, Vorster and Born, 2015, Rennó-Costa et al., 2019]. As an example, sleep deprivation leads to less memory performance among other cognition mechanisms [Killgore, 2010].

In parallel, at the cellular level, synaptic plasticity in-between neurons (*i.e.* change of neuronal connection strengths) is a widely accepted candidate in the recall and storage of information [Stuchlik, 2014, Martin et al., 2000, Wang et al., 2005]. Modification of synapses by plasticity mechanisms should allow the brain to store, maintain and retrieve memories [Rennó-Costa et al., 2019, Takeuchi et al., 2014]. FIGURE 1.1 sketches the concept of memory consolidation in a simplified way.

As experimental evidence keeps growing, computational studies can help deepen the role of sleep in learning by simulating different theories. Indeed, there is no consensus on a single plasticity rule that would explain how learning affects the brain [González-Rueda et al., 2018].

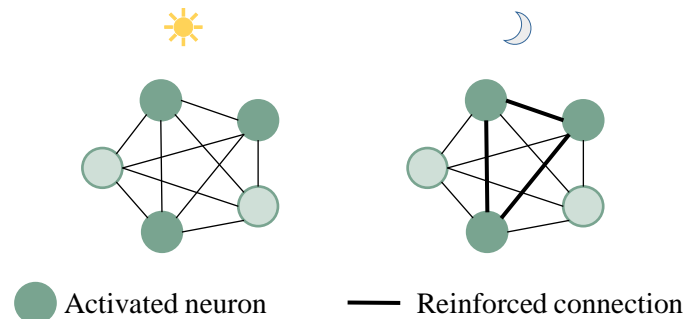


Figure 1.1 – *Concept of memory consolidation (simplified)*. During the day, learning occurs and some neurons are activated (left). During the night, the connections between the activated neurons strengthen so that memory is consolidated (right).

In the context of this thesis which focuses on studying the sleep impact on memory consolidation in

a computational way, the following questions will be answered:

- *What are the neuronal features that can be modeled and how can they be modeled?* (CHAPTER 2)
- *What is synaptic plasticity and how can it be modeled?* (CHAPTERS 3 AND 4)
- *Are the models existing from the literature compatible not only with learning during the day (CHAPTER 5) but also with the theory of memory consolidation during sleep (CHAPTER 6)?*

1.2 Structure

To answer those questions, this thesis is divided into four main parts:

Part I first introduces neurophysiology fundamentals. The communication between neurons is investigated as well as the different firing patterns associated to the different brain states at the cellular level: during *sleep*, neurons are *bursting* while during *waking* neurons are firing in *tonic* mode. Then, modeling techniques are presented to describe neuronal activity (CHAPTER 2).

In CHAPTER 3, synaptic plasticity basis from a biological perspective is given. Mainly, it investigates how the connection in-between two neurons is modulated by their respective activities and that the strength of a synaptic connection can either be *depressed* or *potentiated*.

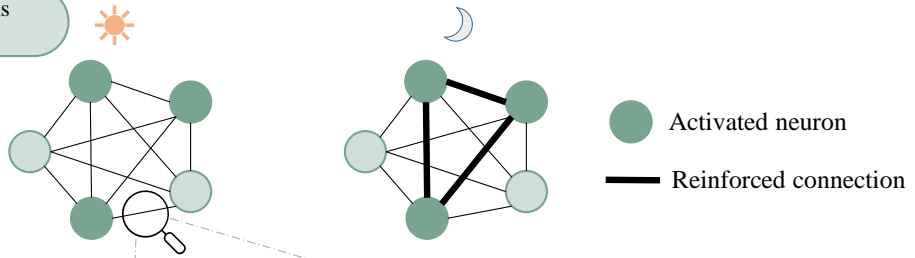
Part II focuses on synaptic plasticity modeling. The literature is broad, models can be either mathematical or very biologically-detailed. They reproduce experimental plasticity induction protocols. However, no consensus exists. Models can either be phenomenological or biophysical and this thesis focuses on phenomenological ones. Thus, in CHAPTER 4, a systematic and rigorous state-of-the-art has been realised in order to offer a global vision of the different existing models.

Part III is dedicated to the implementation of phenomenological models taken from the literature review. The first contribution consists in implementing them into a conductance-based circuit able to switch from tonic to firing mode. Then, in CHAPTER 5, different experimental protocols in *tonic* mode are carried to check out if the models have been well implemented and fitted to experimental data. However, no computational protocols have been realised for *bursting* mode (*i.e.* during sleep). Therefore, CHAPTER 6 focuses on testing the behaviour of those models during sleep to see if they allow memory consolidation.

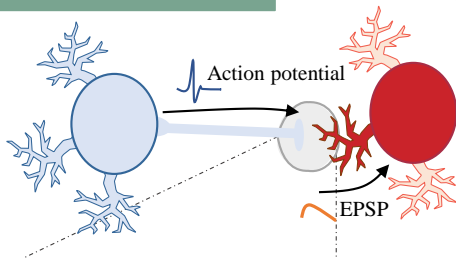
Part IV draws the conclusion regarding the implementation of the chosen phenomenological models in tonic and bursting mode as well as their implication for memory consolidation. As limitations in terms of robustness and unsatisfactory results are highlighted, investigations of potential perspectives to improve the models are enumerated.

STRUCTURE & MOTIVATION

Memory consolidation happens during sleep



Part I: BACKGROUND



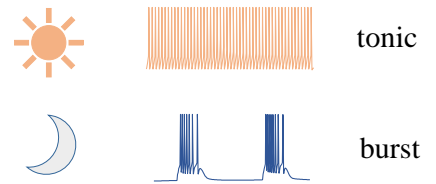
Synaptic strength depends on

- Neurotransmitter release
- Number of receptors
- Efficacy of receptors

And is witnessed by EPSP change:



Firing patterns

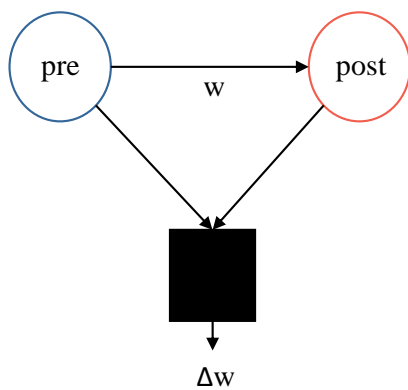


Modeling synaptic plasticity
Phenomenological models

Implementing models in
sleep with bursting pattern

Part II: PHENOMENOLOGICAL MODELS

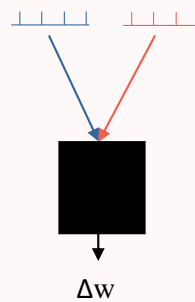
Computational models:
State-of-the-art



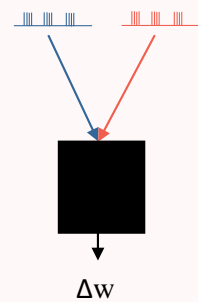
Part III: COMPUTATIONAL STUDY

Implementation of learning rules

- Reproduction of models
- Fitting experimental protocols



- Are they still valid during sleep?



Part I

Background

Chapter 2

Elements of neurophysiology and neuronal modeling

2.1 Neurons

Neurons are a specific type of cells at the basis of the neural system. They are composed of the same main components as any cell type: a *nucleus* containing the genetic information, a *plasma membrane* isolating the cell from the extracellular matrix and different *organelles* such as Golgi apparatus, mitochondria, etc. having distinct functions

2.1.1 Morphology

Distinction of neurons compared to other cells show its specific function: *communication* via *electrical signalling*. Indeed, neurons show various morphologies, specific organisation of membrane elements and specific components to allow contacts between each other.

Neurons, to allow their main function which is communication, show a typical morphology with structural branching, see FIGURE 2.1 A [Purves, 2004]:

- *Dendritic processes*: arborisation from the cell body receiving synaptic inputs from other neurons usually thanks to small protrusions from the membrane called *dendritic spines*.
- *Axon*: unique extension from the neuronal cell body conducting information via electrical signalling (*action potential*, see A.1).

2.1.2 Excitability and electrical signalling

The main characteristic of neurons is their *excitability*, *i.e.* they can be excited by an electrical stimulation. The axon initial segment (called *axon Hillock*) is the point of initiation of the electrical wave at the basis of electrical signal transmission: the *action potential (AP)* (see detailed mechanism A.1). If the dendritic inputs are large enough, an *AP* propagates from the axon hillock to the end of the axon, reaching the postsynaptic neuron and information is transmitted [Purves, 2004] .

Plasma membrane is a key component in neuron signalling machinery. It consists of a phospholipid bilayer which is permeable to small molecules and water, diffusing mainly following their concentration gradients or by osmosis. However, it is impermeable to other large molecules and more importantly to ions. The communication mechanism of neurons mainly relies on ionic flows through the membrane, thus requiring transmembrane proteins ion channels changing the permeability of the membrane to specific ions.

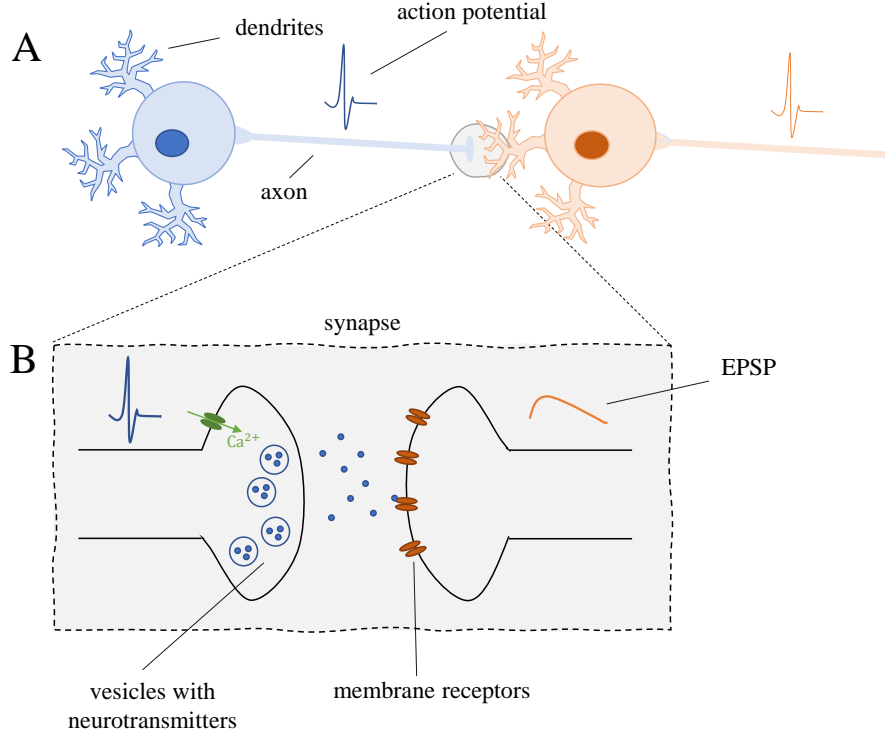


Figure 2.1 – *Schematic representation of neurons and communication at an excitatory synapse* **A.** A presynaptic neuron (blue) sends information through its axon via an action potential until its synaptic terminal and communicates with the postsynaptic neuron (red) through its dendrites. Signals of all dendrites are collected and processed in the soma of the postsynaptic neuron and possibly an action potential is triggered. **B.** At the synapse, neurotransmitters are released following presynaptic action potential. Neurotransmitters bind to postsynaptic membrane receptors (red). This results in membrane potential change (EPSP) in the postsynaptic dendrites. (*inspired from [Graupner, 2017]*)

Since the plasma membrane isolates intra- and extracellular components, each ion has a electrochemical potential and ion flow is driven by electric and chemical forces. On one hand, positive charges are attracted by negative charges and vice versa. On the other hand, difference in concentration of a specific ion between the two compartments drives ions to equilibrate the two concentrations. It gives rise to a difference of intracellular and extracellular potential, called *membrane potential* ($V_m = V_{in} - V_{out}$).

Electrochemical equilibrium for one specific ion corresponds to a specific membrane potential defined as the *Nernst potential*:

$$V_{\text{Nernst}} = \frac{RT}{zF} \ln \frac{[\text{ion}]_{\text{out}}}{[\text{ion}]_{\text{in}}} \quad (2.1)$$

where R is a gas constant, T is the temperature (deg K), F the Faraday's constant and z is the valence.

However, different ions are present in different concentrations across the membrane, mainly Na^+ , K^+ , Ca^{2+} , Cl^- . In addition to the electrical potentials, the concentration gradients result in different Nernst potentials (see TABLE A.2 in APPENDIX A) and the membrane potential results of the mixture of all of them, depending on the permeability of the different ion channels.

It follows the Goldman-Hodgkin-Katz equation:

$$V_m = \frac{RT}{F} \ln \left(\frac{P_{Na^+} [Na^+]_{out} + P_{K^+} [K^+]_{out} + P_{Cl^-} [Cl^-]_{in}}{P_{Na^+} [Na^+]_{in} + P_{K^+} [K^+]_{in} + P_{Cl^-} [Cl^-]_{out}} \right) \quad (2.2)$$

where P_{ion} is the permeability of the specific ion channel in the membrane.

2.1.3 Communication between two neurons

A typical transmission of information between two neurons requires connection between the axon from a neuron and dendrites from another neuron. This area is called a *synapse* and the transmitting and target cells are called respectively pre- and postsynaptic neurons. The communication between the pre- and postsynaptic terminals can be achieved by chemical synapses or electrical synapses. A schematic representation can be found on Figure 2.1 B. The ones of interest for this thesis are also the more common and are chemical. Communication happens through the secretion by the presynaptic cell of small molecules, the *neurotransmitters*, binding to receptors in the postsynaptic cell and released from the presynaptic terminal thanks to calcium entry following an action potential. On one hand, the main neurotransmitter released by excitatory neurons is glutamate and binds to postsynaptic receptors called AMPAR (α -amino-3-hydroxy-5-methyl-4-isoxazolepropionic acid receptor) and NMDAR (*N*-methyl-D-aspartate receptor). On the other hand, inhibitory presynaptic neuron releases GABA (*aminobutyric acid*) as neurotransmitters which binds $GABA_A$ and $GABA_B$ postsynaptic receptors. In excitatory (*resp.* inhibitory) synapses, this results in a excitatory post-synaptic potential (*EPSP*) (*resp.* inhibitory post-synaptic potential (*IPSP*)) in the postsynaptic neuron [Graupner, 2017, Purves, 2004] (see TABLE 2.1). This way, information is collected to the dendrites and then processed in the cell body.

Synapse type	Neurotransmitter	Receptors	Postsynaptic response
Excitatory	glutamate	AMPA	EPSP
		NMDA	
Inhibitory	GABA	$GABA_A$	IPSP
		$GABA_B$	

Table 2.1 – Summary of main released neurotransmitters, postsynaptic receptors and response at excitatory and inhibitory synapses

2.2 Wake/sleep cycle

The brain has been shown to constantly evolve and switch between different cortical states. In 1887, Caton was the first investigator to observe that the pattern of cortical activity was dependent on the state of the animal [Caton, 1887]. A state is considered to be a stable recurring set of neural conditions for a significant period of time. A diversity of cortical states has been established going from Slow-Wave-Sleep (*SWS*), REM (*Rapid-Eye-Movement*) sleep, quiet waking, active waking and attentive state [Zagha and McCormick, 2014]. In this work, the focus will be made on SWS, active waking and mainly the transition between those two.

2.2.1 States Characteristics

The characteristics of those states at both network and cellular levels have been well studied. As it can be seen in FIGURE 2.2 (A), the electroencephalogram (*EEG*, displaying the activity of the neocortex) shows at the network level that SWS is characterised by slow oscillatory UP and DOWN states of large amplitude (10-20mV) while the waking state shows oscillations of reduced amplitude and high frequency. The UP-DOWN states observed during SWS are due to synchronisation of pyramidal cells in the neocortex, switching from silent to active states altogether. Conversely, during waking, those cells show reduced synchronisation and thus lower amplitude oscillations at the population level [Zagha and McCormick, 2014].

Obviously, this switch does not occur spontaneously. It is controlled by different neuromodulators. Mostly, the releasing of acetylcholine (*ACh*), noradrenaline (*NE*), serotonin (*5-HT*), dopamine (*DA*) and histamine (*HA*) are possible mechanisms of state-dependent transitions of activities [Zagha and McCormick, 2014].

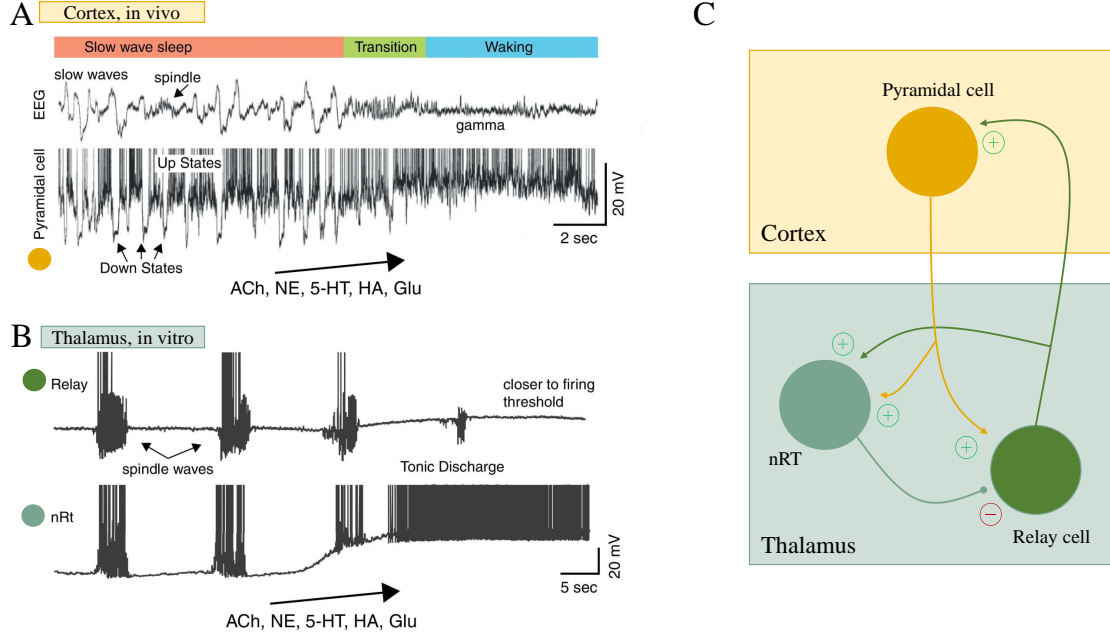


Figure 2.2 – *State-dependent changes at the network and cellular level in the neocortex and thalamus.* **A.** In the neocortex, SWS is characterised at the network level by slow waves (10-12[Hz]) of high amplitude and by synchronized UP and DOWN states at the cellular level. Waking state, after a transition phase resulting by augmentation of ACh, NE, 5-HT, Ha, Glu levels, shows lower amplitude and high frequencies at the network level. This is due to desynchronisation at the cellular level. **B.** In the thalamus, nRT cells and relay cells exhibits bursting firing patterns during SWS and tonic discharge during waking. **C.** Schematic representation of thalamocortical interactions. Inhibition is represented in blue and excitation in red. While TRN inhibits relay cells in the thalamus, relay cells excite cortex and TRN cells. Cortex also shows excitatory connections to the relay cells of the thalamus [Zagha and McCormick, 2014]. (*adapted from [Zagha and McCormick, 2014, Purves, 2004]*)

However, the wake/sleep switch induction cannot be mentioned without zooming at a deeper level and introducing the role of the thalamus and its dynamics.

2.2.2 Thalamus

The thalamus is the first relay station for the incoming information from external stimuli. It is composed of different nuclei - *relay* nuclei relaying the information to the cortex that have *excitatory* functions and nuclei from the *thalamic reticular nucleus* (*TRN* or *nRT*) that are *inhibitory* neurons.

The *relay* neurons send excitatory inputs to the TRN and to the neocortex while the *TRN* sends inhibitory connections to the relay neurons (FIGURE 2.2 (C)). In this way, the TRN are able to influence the flow of information between the thalamus and the cortex. Those interconnections between the different neurons from different brain areas are at the basis of the mechanism of the generation of different oscillation rythms in thalamocortical networks. Indeed, depending on the state, they exhibit different firing patterns (FIGURE 2.2 (B)) :

- *Waking*: the EEG shows low amplitude and high frequency rhythm. The cellular level of thalamic

cells corresponds to a tonic firing pattern, *i.e.* simple action potential firing.

- *Sleep*: the EEG shows large amplitude and low frequency. This corresponds to the synchronisation of burst firing, *i.e.* high frequency action potentials generation, at the cellular level.

2.2.3 Bursting types

As briefly introduced in the previous section, the concept of *bursting* can be defined as a distinct firing mode of the neurons in which action potentials are discharging at a very high frequency, followed by periods of silence. However, different kind of '*bursting*' types can be distinguished.

Endogenous bursting

The bursting ability of the thalamic neurons that induces the sleep state (see FIGURE 2.2 (B)) is due to an additional ionic current in the membrane. It has been shown that, when the cell is hyperpolarised under a certain threshold, a calcium current can be measured. This current is called T-Type Calcium current or low-threshold Ca^{2+} current [Jacquerie, 2018, McCormick and Bal, 1997, Steriade et al., 1993]. For more details on the bursting mechanism see APPENDIX B.

Exogenous bursting

While thalamic cells have intrinsic bursting properties, evidence is lacking concerning the presence of T-Type ionic currents in pyramidal cells in the cortex. It has been shown that a small portion of cortical cells have intrinsic bursting ability due to other ionic currents [Franceschetti et al., 1995]. However, as stated, the slow oscillations in *SWS* recorded by the EEG at the cortex level are due to UP and DOWN states, *i.e.* respectively high activity and silent activity at the cellular level. This dynamics in cortical cells firing pattern is driven by the thalamic endogenous bursts, whose pattern is passed on to the cortex thanks to the thalamocortical loop shown in FIGURE 2.2 (C) [Purves, 2004].

2.3 Neuronal modeling

Biological neurons can be modeled by mathematical structures and equations in order to reproduce the biophysical characteristics of their membranes and their qualitative properties.

Different modeling techniques can be used for this purpose, focusing either on complete and faithful representation of neuron behaviour (such as *conductance-based* models) or either on qualitative aspects of neurons properties like excitability (such as *integrate-and-fire* models). The interesting point is that the first one describes a more biological model while the second one describes a more mathematical model that separates itself from biological parameters.

2.3.1 Conductance-based models

Neuron, particularly its membrane, can easily be equivalently represented as an electrical circuit using mathematical modeling (FIGURE 2.3).

Conductance-based models represent faithful interpretation of excitable cells in which current flows through the membrane. It was first put forth by [Hodgkin and Huxley, 1952] studying the squid giant axon.

The ions channels can be represented as resistors with dynamic regulation of their conductance (g_{ion}) to reach open - closed states. Consequently, the flow of ions gives rise to an ionic current following Ohm's law as:

$$I_{ion} = g_{ion}(V_m - V_{ion}) \quad (2.3)$$

where the term $(V_m - V_{ion})$ accounts for the electrochemical force drove by the electrochemical gradient. The phospholipid bilayer of the membrane is impermeable to ions and acts as a capacitance (C), since it accumulates ions to its intracellular and extracellular sides. Change in the distribution of charges across that capacitance drives a capacitive current defined as :

$$I_C = C \frac{dV_m}{dt} \quad (2.4)$$

where $\frac{dV_m}{dt}$ is the variation of the membrane potential per unit of time.

Using Kirchoff law and generalising to a set of n ionic currents, we obtain :

$$C \frac{dV_m}{dt} = - \sum_n g_{ion} (V_m - V_{ion}) + I_{app} \quad (2.5)$$

where I_{app} is an applied current and represents an external stimulus. Hodgking and Huxley, creators of the original conductance-based model, identified three types of current:

$$I_{ion} = I_K + I_{Na} + I_{leak} \quad (2.6)$$

, where I_{leak} represents the passive movement of ions through the membrane.

Moreover, the ion channels are voltage-gated. Consequently, the membrane permeability to specific ions is a dynamic process. To model this dynamic, Hodgkin and Huxley introduced activation and inactivation gate variables that will be dependent on the membrane potential. By voltage-clamp experiments, they modeled the conductances of ion channels by assuming them to be proportional to these activation/inactivation gate variables [Hodgkin and Huxley, 1952].

The (in)activation variables are modeled by a system of first-order differential equations (*ODE*), considering $m_{ion,\infty}$, $h_{ion,\infty}$ as the steady-state values and $\tau_{m,ion}$, $\tau_{h,ion}$ as the time constants of respectively the activation (m) and inactivation variable (h). These two variables are voltage-dependent.

$$\begin{aligned} C \dot{V}_m &= -\bar{g}_{Na} m_{Na}^3 h_{Na} (V_m - V_{Na}) - \bar{g}_K m_K^4 (V_m - V_K) - g_L (V_m - V_L) + I_{app} \\ \dot{m}_{Na} &= \frac{m_{Na,\infty}(V_m) - m_{Na}}{\tau_m N_M(V_m)} \\ \dot{h}_{Na} &= \frac{h_{Na,\infty}(V_m) - h_{Na}}{\tau_h M(V_m)} \\ \dot{m}_K &= \frac{m_{K,\infty}(V_m) - m_K}{\tau_{m_K}(V_m)} \end{aligned} \quad (2.7)$$

The solution of this system of ODEs is plotted in FIGURE 2.4 (A) for a constant applied current from 20 to 75[ms].

Note that the bursting firing pattern introduced in SECTION 2.2.3 is obtained simply by adding T-Type ionic current in the conductance-based model. As it can be seen in FIGURE 2.4 (B) in which a

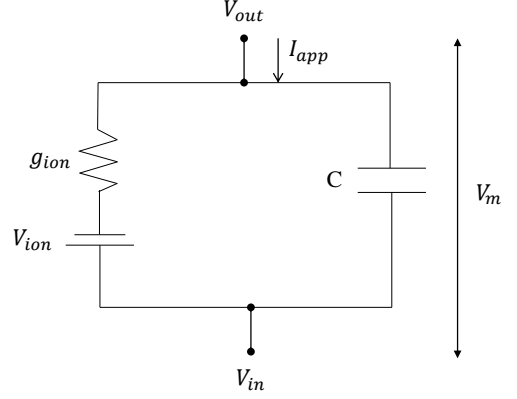
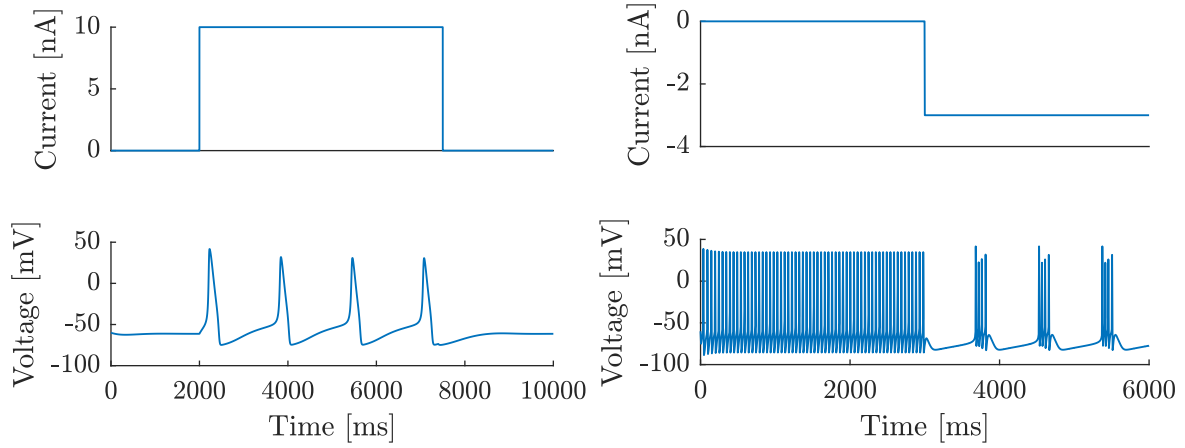


Figure 2.3 – *Modeling of the membrane as an electrical circuit.* The membrane is modelled by a capacitance (C), any ion channel is represented by a dynamic conductance g_{ion} and is driven by its Nernst potential V_{ion} , the applied current is I_{app} and the total circuit has a potential $V_m = V_{in} - V_{out}$ which is the membrane potential [Jacquerie, 2018].



(a) *Resolution of Hodgkin-Huxley system of equations.* (b) *Burst and tonic firing patterns.* **(top)** Time course evolution of applied current. At 3000ms, applied current $I_{app} = 10$ [nA] from 20 [ms] to an hyperpolarising current is applied (-3 [nA]). 75[ms]. **(bottom)** Time evolution of membrane potential. **(bottom)** Membrane voltage evolution, from tonic mode to bursting mode.

Figure 2.4 – Resolution of systems of equations of conductance based models based on (a) classical Hodgkin-Huxley (HH) model and (b) HH model with additional ionic currents sensitive to hyperpolarisation (mostly T-Type Calcium channels).

conductance-based model has been implemented with ionic currents sensitive to hyperpolarisation, an hyperpolarisation of the cell leads to a bursting firing pattern.

One of the advantages of those conductance-based models is that one can add as many ion channels as wanted. It is therefore helpful to better understand mechanisms contributing to action potential generation, repetitive firing and bursting, and so on. However, as complexity increases with the number of differential equations, those models require more computation time and the dynamics of the model becomes more difficult to understand. Reduction of conductance-based models help to reduce this complexity and show the same qualitative dynamics.

2.3.2 Integrate-and-fire models

While it has been mentioned that conductance-based models can be highly accurate, they are difficult to analyse due to their high complexity. An alternative to lower the complexity is achieved by focusing on the spiking activity (*i.e.* the ability to generate action potentials) and getting rid of the ion channel modeling. This gives rise to simple spiking neurons models. In those models, the action potential is seen as a discrete event, fully characterised by its firing time. The detailed shape obtained from the ion interactions is replaced by a mathematical description ("integrate"). As soon as the membrane voltage reaches a certain threshold, the value is reset to a resting value and spikes ("fire"). However, the capacitive effect of the membrane is kept.

Integrate-and-fire (*IF*) models are a type of simple spiking neurons. They have first been developed in the work of Lapicque (1907) [Lapicque, 1907] that studied the electrical excitation of nerves and have then been adapted to neurons.

Leaky integrate-and-fire

Leaky integrate-and-fire models are probably the best known example of spiking neuron models. According to this model, a neuron can be represented by an RC circuit with a threshold potential driven by an input current, see FIGURE 2.5 [Gerstner et al., 2014].

Using the law of current conservation, the driving current is thus split in two components:

$$I(t) = I_R + I_C \quad (2.8)$$

Considering membrane impermeability, it can be modeled by a capacitance C leading to a capacitive current:

$$I_C = C \frac{du(t)}{dt} \quad (2.9)$$

The resistance corresponds to a leak term reflecting the diffusion of ions through the membrane and results to a current:

$$I_R = \frac{u(t) - u_{rest}}{R} \quad (2.10)$$

where u_{rest} is the resting potential of the membrane.

The driving current is thus

$$I(t) = C \frac{du(t)}{dt} + \frac{u(t)}{R} \quad (2.11)$$

Multiplying the equation by R and introducing the time constant $\tau_m = RC$, we obtain the following equation corresponding to the leaky integrator in electrical engineering, called the equation of a passive membrane for the neuroscience field:

$$\tau_m \frac{du}{dt} = -[u(t) - u_{rest}] + RI(t) \quad (2.12)$$

To see the behaviour of this circuit, let's find the solution of this equation with no input. We assume as an initial condition that for $t = t_0$ the membrane potential is at $u_{rest} + \Delta u$ and for $t > t_0$ $I(t) = 0$. The solution is therefore: [Gerstner et al., 2014]:

$$u(t) - u_{rest} = \Delta u \exp\left(-\frac{t - t_0}{\tau_m}\right) \quad \text{for } t > t_0 \quad (2.13)$$

As it can be intuitively expected, with no input current, the membrane potential $u(t)$ decays exponentially to its resting state with the characteristic time of the decay given by τ_m .

Considering now the case where $I \neq 0$. The current injected is due to spikes coming from other neurons or artificial stimulus and is accumulating through time, while the voltage is decaying exponentially due to the leak term. If the threshold voltage θ is reached, the action potential firing time is kept and the voltage is reset to its resting potential u_{rest} :

$$u(t) \rightarrow u_{rest} \quad \text{if } u(t) = \theta \quad (2.14)$$

The spikes train S_i of the neuron is fully represented by its spike times $t_i^{(f)}$:

$$S_i(t) = \sum_f \delta(t - t_i^{(f)}) \quad (2.15)$$

As an example, applying a constant current I_0 leads to a regular firing pattern and leads to the time course displayed in FIGURE 2.6 (A). Indeed, resolving the differential equation (2.12) for

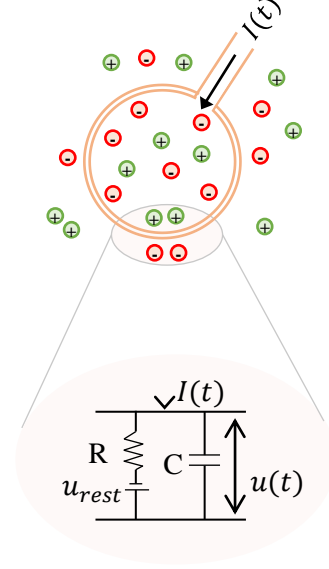


Figure 2.5 – *Neuron modeling by a leaky integrate-and-fire*. Accumulation of charges across the membrane is represented by a capacitance C and the passive leakage of ions through the membrane is represented by a resistance R . The membrane has a resting potential u_{rest} and an external current $I(t)$ is injected. (*adapted from [Gerstner et al., 2014]*)

$I = I_0$, with initial condition $u(t_0) = u_{rest}$ for $t = t_0$ and for a simulation $t_0 < t$ leads to the solution [Gerstner and Kistler, 2002]:

$$u(t) = u_{rest} + RI_0 \left[1 - \exp \left(-\frac{t - t_0}{\tau_m} \right) \right] \quad (2.16)$$

The membrane potential thus increases from its initial value u_{rest} to the threshold value (θ) when it "fires" and is reset to u_{rest} . Note that $\lim_{t \rightarrow +\infty} u(t) = RI_0$ such that if $RI_0 < \theta$, the neuron cannot fire since the threshold value is never reached [Gerstner and Kistler, 2002].

Increase in the applied current leads to an increase in the firing rate since the voltage accumulation until the threshold occurs faster. Frequency as a function of constant applied current with or without refractory period is displayed in FIGURE 2.6 (B) [Gerstner and Kistler, 2002].

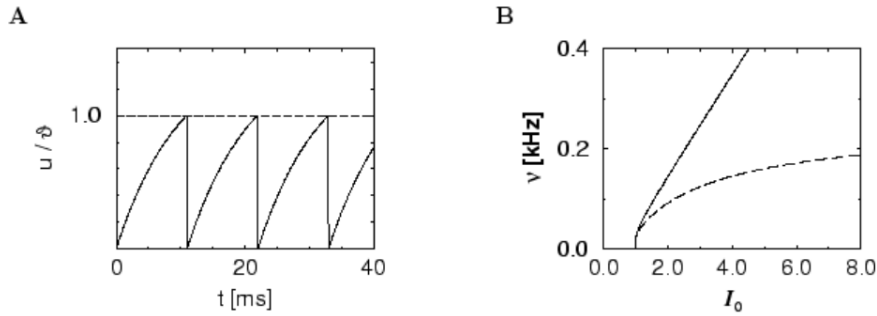


Figure 2.6 – *Leaky Integrate-and-Fire dynamics under a constant current*. **A.** Temporal evolution of the membrane voltage. Potential is accumulated until reaching the spiking threshold θ , then is reset to its resting potential. **B.** Firing rate as a function of applied current I_0 [Gerstner and Kistler, 2002].

Quadratic integrate-and-fire

While leaky integrate-and-fire's differential equations are linear, there is also complexification of spiking neurons by introduction of non-linearity, generally written as [Gerstner and Kistler, 2002]:

$$\tau \frac{du}{dt} = F(u) + G(u)I \quad (2.17)$$

A specific instance, and one of the most used, is the quadratic model written as:

$$\tau \frac{du}{dt} = a_0(u - u_{rest})(u - u_c) + RI \quad (2.18)$$

where u_{rest} is the value at which the membrane potential comes back after reaching the threshold voltage and parameters $a_0 > 0$, $u_c > u_{rest}$. This parameter u_c can be interpreted as the voltage needed for action potential triggering by a short current pulse.

One-dimensional phase plane of equation 2.18 is plotted in FIGURE 2.7 for different I . This phase plane is an easy tool to understand the behaviour of the model. The sign of $\frac{du}{dt}$ helps to understand the convergence towards the fixed point and so gives its attraction. Increasing the applied current I moves upward the nullcline. Therefore, we can study the excitability of the model for different applied currents. The intersection of the function with the x-axis gives the fixed points, and the surrounding values of $\frac{du}{dt}$ states their stability. As can be seen in FIGURE 2.7 (A) u_{rest} is stable and u_c unstable for $I = 0$. On one hand, an initial $u < u_{rest}$, the voltage decays to the resting potential ($\frac{du}{dt} > 0$) and for

an initial $u_{rest} < u < u_c$, $\frac{du}{dt} < 0$ such that u is attracted to the fixed point u_{rest} . On the other hand, for an initial $u > u_c$, the voltage keeps increasing because $\frac{du}{dt} > 0$ and thus a spike is initiated.

However, for $I > 0$, the parabolic curve ($\frac{du}{dt}$ as a function of u) is displaced in the phase plane in the positive values such as (for a certain I) $\frac{du}{dt} < 0$ for all u . This gives rise to repetitive firing (see FIGURE 2.7 [Gerstner and Kistler, 2002]).

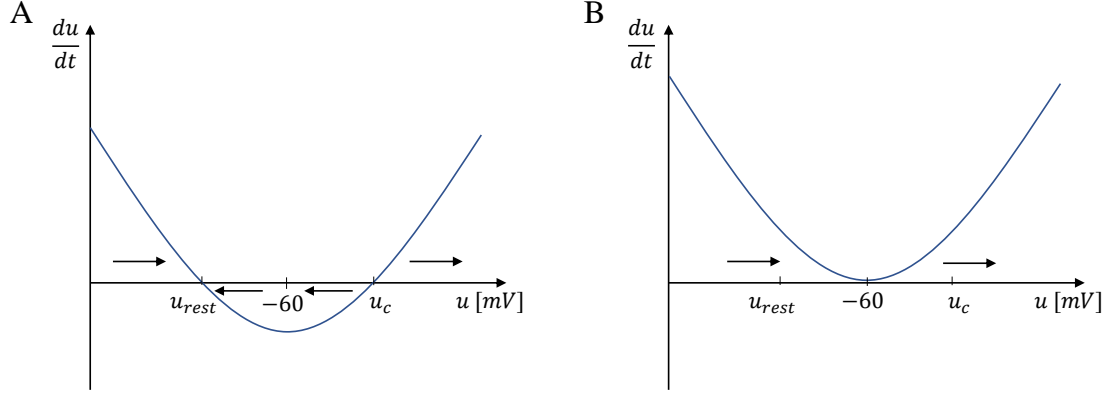
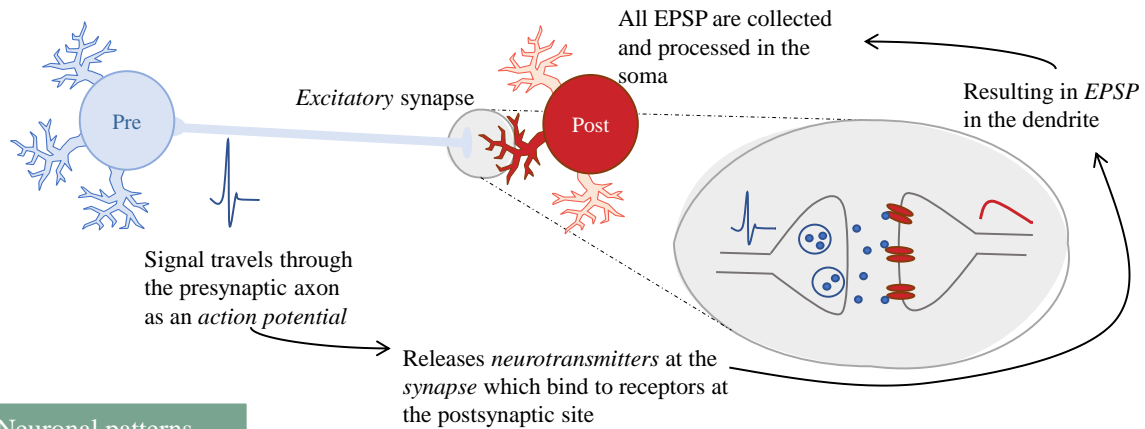


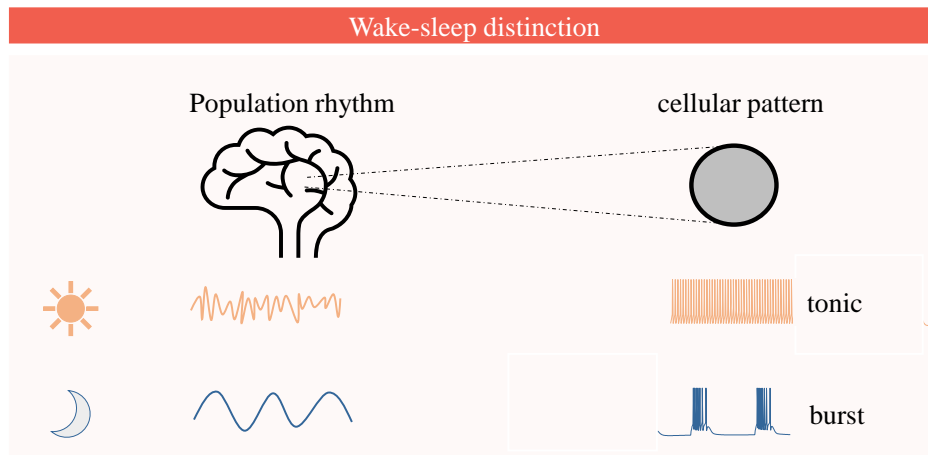
Figure 2.7 – *Quadratic integrate-and-fire model*. One-dimensional phase plane for **A.** $I = 0$ **B.** $I \neq 0$ (adapted from [Gerstner and Kistler, 2002])

2.4 Summary

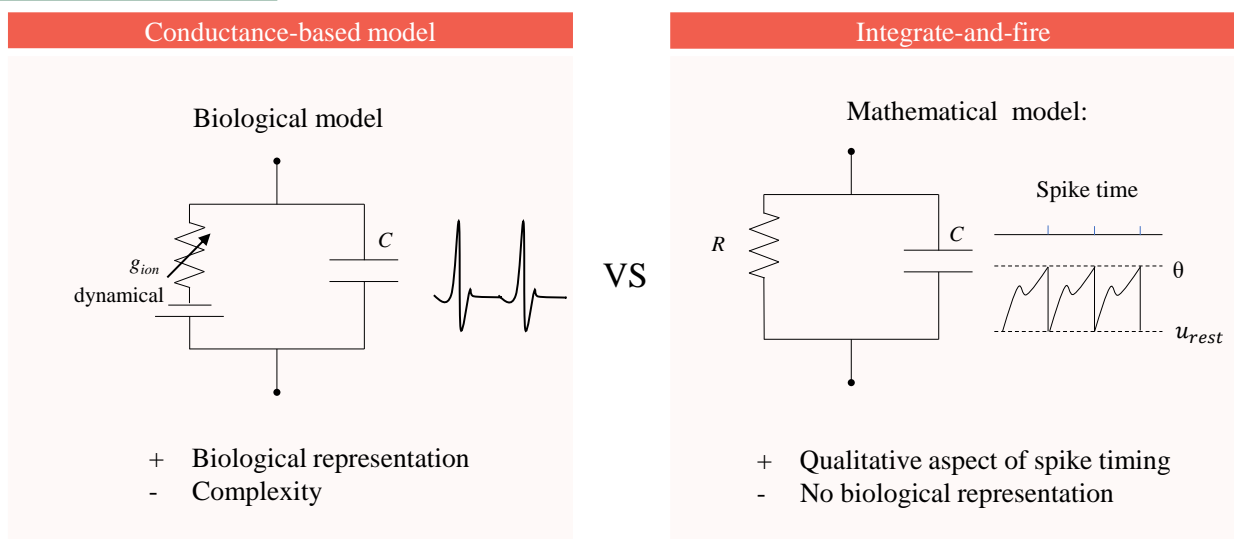
NEURONS AT CELLULAR AND POPULATION SCALE



Neuronal patterns



Neuronal modeling



Chapter 3

Synaptic Plasticity: from a biological perspective

Synaptic plasticity is a fascinating property of the brain and has been thought for centuries to play a role in its early development but also in learning and memory [Citri and Malenka, 2008]. This term refers to the ability of synapses to modify their strengths. It is a critical aspect of memory. For the last decades, different hypotheses about the link between plasticity and learning have risen but they all share a common ground stating that :

"Activity-dependent synaptic plasticity is induced at appropriate synapses during memory formation and is both necessary and sufficient for the information storage underlying the type of memory mediated by the brain area in which that plasticity is observed." [Martin et al., 2000]

At an excitatory synapse, the strength of the connection between a presynaptic neuron and a postsynaptic neuron is related to the amplitude of the postsynaptic neuron potentiation (EPSP). It can be modulated by different parameters acting at different locations in the synapse:

- *At the presynaptic level:* the number of neurotransmitters released, the pool of neurotransmitters available, the action potential frequency, ...
- *At the postsynaptic level:* the number and the efficiency of postsynaptic receptors, gene expression, ...

Plasticity can happen at different time-scales, the term of short-term plasticity refers to changes that last for seconds to minutes while long-term plasticity refers to synaptic changes that persist for hours, days or lifetime.

3.1 Short-term synaptic plasticity

Plasticity in a time scale from seconds to minutes is referred to as short-term plasticity. It can express by synaptic changes increasing efficiency in synaptic transmission, called *facilitation*, or in a decrease in the synaptic connection called *depression*. Short-term plasticity manifests by a change in the post-synaptic potential. At an excitatory synapse, an action potential in the presynaptic neuron gives rise to an excitatory post-synaptic potential (EPSP).

A simple protocol to quantify the change in synaptic strength is to stimulate a presynaptic neuron in such a way that two action potentials are induced at the presynaptic terminal. The consequences of two close action potentials are explained by the fact that the effects of the first are not completely

finished when the second one occurs. Precisely, the *calcium binding in the presynaptic terminal* and the *release of synaptic vesicles* require some time before going back to their resting states. However, those two events have contradictory effects [Meriney and Fanselow, 2019, Citri and Malenka, 2008]:

- On one hand, calcium ion binding increases the number of neurotransmitters released following a second action potential because new calcium ions entering the nerve terminal add up to the ones already present in the cell due to the first action potential. Since the release of neurotransmitters is triggered by those ions, the probability of release increases with the amount of calcium ions.
- On the other hand, the fusion of synaptic vesicles with the membrane has the opposite effect: it reduces the probability of neurotransmitter release. The recycling or replacing of the synaptic vesicles carrying neurotransmitters takes some time. Thus, shortly after a first action potential the vesicles have not been replaced yet and the second action potential triggers less neurotransmitters release. This phenomenon is known as *vesicle depletion*.

The relative effect of each of those two factors depends on the initial synaptic efficiency. If in a short time-scale, two action potentials are firing, two scenarios are possible (FIGURE 3.1):

1. *Facilitation*: At initially weaker synapses, the effect of vesicle depletion is relatively lower than the effect of residual calcium. Thus, a second action potential will increase the probability of neurotransmitter release.
2. *Depression*: At initially stronger synapses, the phenomenon of vesicle depletion occurs and predominates the effect of the calcium. The probability of neurotransmitter release decreases because of the lack of vesicles available due to the first action potential.

3.2 Long-term plasticity

In the case of long-term memory, long-term plasticity is key. While experiments are made in a reduced preparation such as a brain slice, how to prove that a link between learning and the observed long-term plasticity exists? [Martin and Morris, 2002] proposed 4 criteria to assess if learning is based on synaptic plasticity:

1. *Detectability*: the synaptic changes occurring after learning should be experimentally detected.
2. *Mimicry*: learning can be directly induced by changing appropriate synapses in the brain.
3. *Anterograde alteration*: preventing plasticity should also prevent memory formation.
4. *Retrograde alteration*: altering synaptic strength after learning should also alter the memory itself.

3.2.1 Properties

Long-term plasticity is **bidirectional**. Increase in synaptic connection is called long-term potentiation (*LTP*) while a decrease is called long-term depression (*LTD*). Following the idea in the late 19th century by Ramón y Cajal [Ramón y Cajal, 1894] that learning was associated with the reinforcement of existing pathways between neurons and the formation of new ones, Jerzy Konorski [Konorski, 1948] was the first to use the term "synaptic plasticity" and approximately at the same time, Donald Hebb (1949) gave his famous definition of his interpretation of plasticity, giving rise to what is called now Hebbian plasticity [Hebb, 1949]:

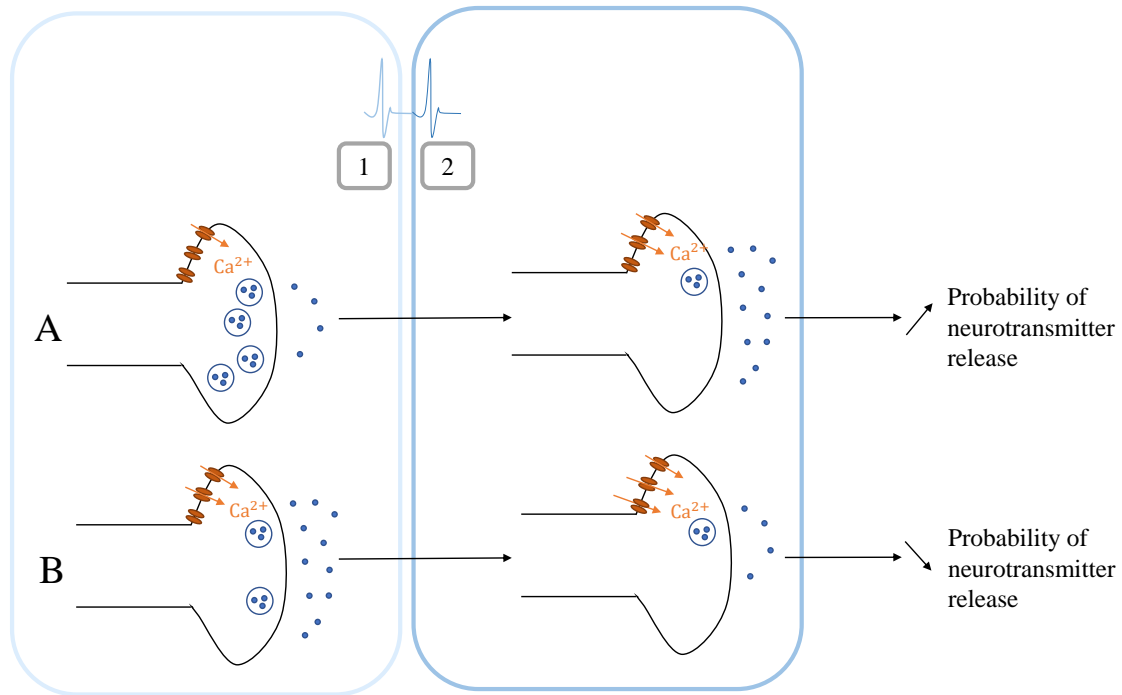


Figure 3.1 – *Short-term plasticity following two presynaptic action potentials. A. Synapse with an initially low probability of release.* The first AP triggers only a low amount of vesicles fusion and thus the second action potential can release more neurotransmitters because there were enough vesicles available. The vesicle depletion effect was weaker than the residual calcium effect. This results in facilitation. *B. Synapse with an initially high probability of release.* The opposite scenario happens: the first AP triggers the release of a lot of neurotransmitters, resulting in vesicle depletion. At the time of the second AP, not enough vesicles are available. Vesicle depletion effect is higher than residual calcium effect, resulting in depression (adapted from [Meriney and Fanselow, 2019]).

"When an axon in cell A is near enough to excite cell B and repeatedly and persistently takes part in firing it, some growth process or metabolic change takes place in one or both cells such that A's efficiency in firing B is increased."

This explains that LTP requires the activity of both presynaptic and postsynaptic cells at a local synapse. However, several pitfalls indicate that this rule alone cannot explain plasticity on its whole. Indeed, potentiation alone will cause all synaptic efficacies to saturate at their maximal level and would be non-selective. Also, several experimental results cannot be explained by LTP on its own. Thus, the bidirectionality principle [Cooper et al., 1979, Bienenstock et al., 1982]. Hebb postulate alone thus fails to explain every aspect of plasticity. Introduction of bidirectionality idea in plasticity by the concept of LTD helps to resolve those limitations and has been demonstrated experimentally (see SECTION 3.3).

Classical LTP in the hippocampus also exhibits the following properties, illustrated in FIGURE 3.2:

- **cooperativity** : the probability to induce LTP increases with the number of afferent neurons stimulated at the same time.
- **associativity** : a weak stimulus can be efficient if a strong afferent is applied to the same target at the same time.
- **specifity** : LTP is induced only in the afferent neurons submitted to an efficient direct or indirect stimulation.

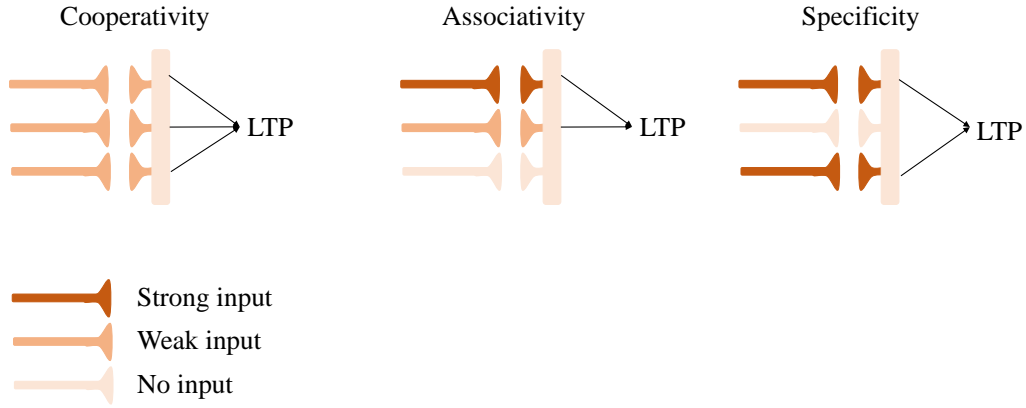


Figure 3.2 – *Properties of LTP. (adapted from [Kandel et al., 2000])*

It demonstrates that synaptic plasticity can either be *homosynaptic* (specificity) and *heterosynaptic* since weak stimulation in a synapse can lead to plasticity events if a neighbouring synapse is highly stimulated (cooperativity) or if weak inputs add up (associativity).

3.2.2 Long-term plasticity mechanisms

NMDAr-based plasticity at the postsynaptic site

To understand the molecular mechanism underlying LTP and LTD, it is important to develop the role of the two main receptors present at the postsynaptic side of excitatory synapses: the glutamate receptors AMPA and NMDA. AMPA receptors are permeable to Na^+ and K^+ while NMDA receptors are permeable to Ca^{2+} , K^+ and Na^+ ions. Both types bind glutamate but NMDAr is blocked by Mg^{2+} ions that are released in a voltage-dependent way. Thus, NMDAr are able to detect two coincident events: glutamate binding and depolarisation of the postsynaptic neuron. If the postsynaptic cell has depolarised enough thanks to AMPA receptors letting ionic flow following glutamate binding, Mg^{2+} is removed from NMDAr. This allows Ca^{2+} to enter the cell and acting as a second messenger, Ca^{2+} triggers LTP by a cascade of events (the details are not relevant in the context of this thesis) [Purves, 2004]. This process relying on the activation of NMDAr is referred to as *LTP induction*.

The *expression* phase of LTP relies of synaptic changes in long-term arising from changes in the sensitivity to the neurotransmitter (glutamate). In excitatory synapses, several observations state that postsynaptic glutamate receptors (AMPA) are dynamically regulated. Thanks to Ca^{2+} signalling, additional AMPA receptors can be inserted into the membrane (see FIGURE 3.3 B). Similarly, LTD is associated with the removal of AMPA receptors by internalisation in the postsynaptic cell.

Another form of plasticity expression is the change of biophysical properties of AMPA receptors still due to calcium concentration. Mainly, an increase or decrease in the conductance of AMPAR increases or decreases the synaptic strength [Citri and Malenka, 2008]. NMDAr might also be dynamically regulated but [Ferreira et al., 2017] but strong evidence is lacking regarding this subject.

In order for the synaptic plasticity to last several hours after stimulation (*maintenance*), modification in gene expression and synthesis of new proteins are needed and are also triggered by Ca^{2+} signalisation [Purves, 2004, Korb and Finkbeiner, 2011].

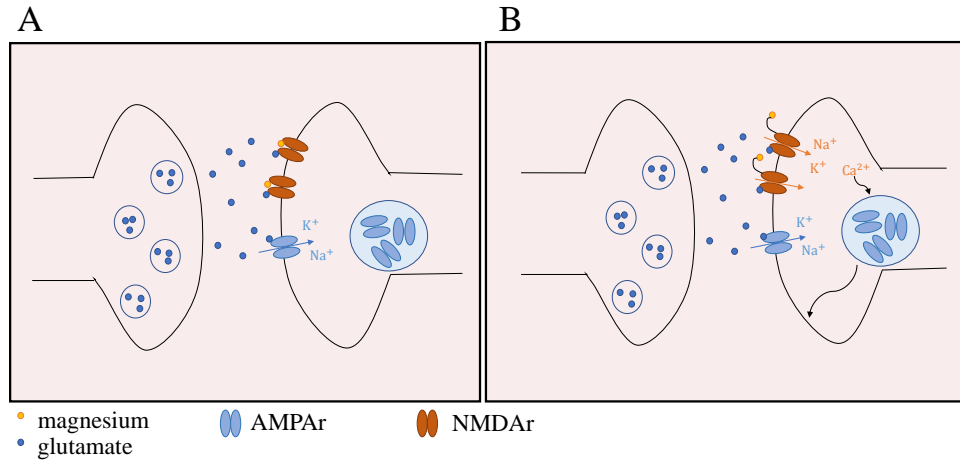


Figure 3.3 – *Induction mechanism of LTP at excitatory synapses.* AMPA receptors are permeable to sodium ions and NMDA receptors to Ca^{2+} , K^{+} and Na^{+} ions. Both are sensitive to glutamate released by the presynaptic cell but the latter are blocked by Mg^{2+} ions. **A.** At resting potential, if glutamate coming from the presynaptic terminal binds to the receptors, Na^{+} enters the cell through AMPAR. **B.** After a certain depolarisation threshold, Mg^{2+} is removed from NMDA receptors and Ca^{2+} ions enter the cells, triggering LTP expression. Illustrated here is one aspect of LTP expression: Ca^{2+} triggers, by a cascade of events, the insertion of new AMPAR to the membrane. (*adapted from [Purves, 2004]*)

Presynaptic plasticity

Another type of plasticity coexists with the well-documented NMDA-dependent plasticity explained above. The latter involves plasticity mechanisms at the postsynaptic site but presynaptic mechanisms of plasticity involving decrease or increase of neurotransmitter release also exist and are induced by calcium signalling as well. It has been demonstrated initially at hippocampal mossy fibers and cerebellar parallel fibers synapses but the list of other brain regions expressing this kind of presynaptic plasticity has grown [Yang and Calakos, 2013].

Structural Plasticity: at both pre- and postsynaptic level

Additionally, dendritic spines at the postsynaptic sites are likely to vary in volume and number [Segal, 2005, De Vivo et al., 2017]. This phenomenon is called *structural plasticity*. Thanks to kinase signalisation, a late phase of plasticity can induce the production either of new synaptic contacts and/or growing of the spine (associated to LTP) or either pruning of old ones and/or shrinkage (associated to LTD). The strength of synaptic connection and volume of the dendritic spine seems to be linked [Bosch and Hayashi, 2012].

An illustration of the different long-term plasticity expression mechanisms can be found in FIGURE 3.4. All the different plasticity types at different time scales are summarised in TABLE 3.1.

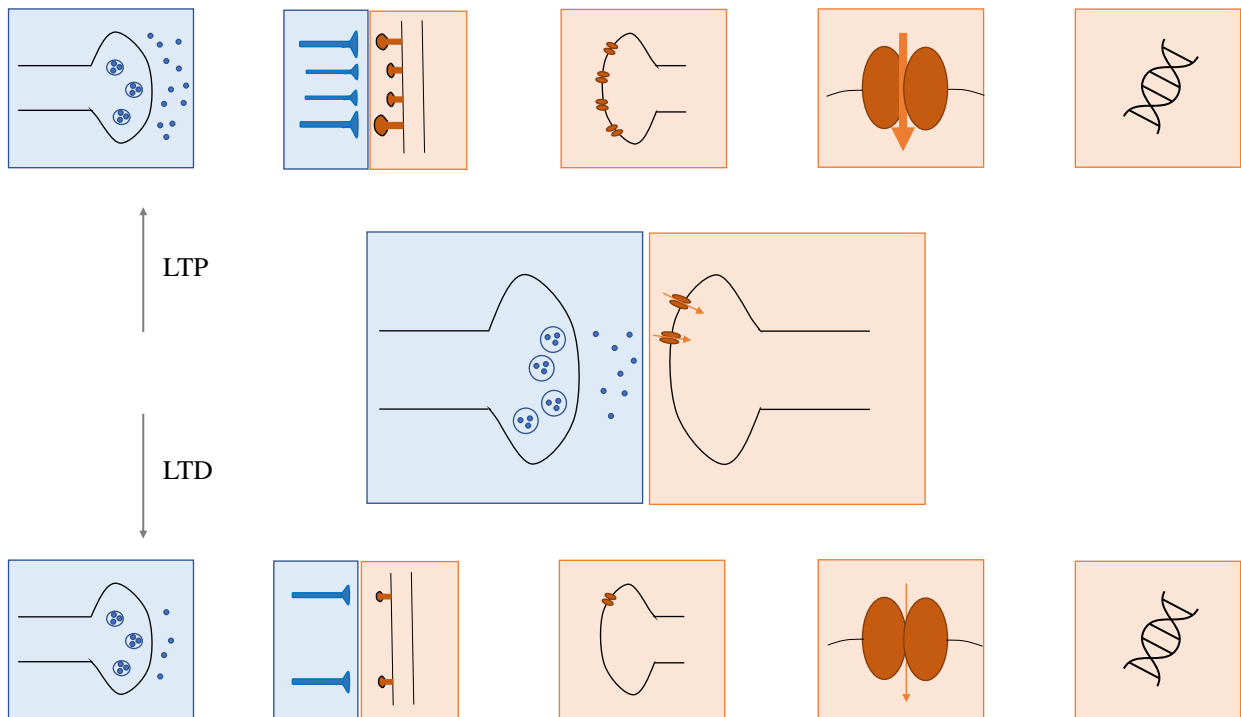


Figure 3.4 – *Long-term synaptic plasticity expression*. In blue, changes concerning the presynaptic site. In red, changes concerning the postsynaptic site. From left to right: change in probability of neurotransmitter release, change in volume and number of dendritic spines, change in AMPA receptors number, change in receptor conductance and gene expression.

		Locus of plasticity	Dominant mechanism	Consequences
Short-Term	Depression	Presynaptic	Vesicle depletion	\searrow p release
	Potentiation		Calcium binding	\nearrow p release
Long-Term	Potentiation (Depression)	Presynaptic	Calcium	\nearrow # NT released (\searrow # NT released)
		Postsynaptic	Calcium cascade	\nearrow # AMPAr (\searrow # AMPAr)
				\nearrow AMPAr efficiency (\searrow AMPAr efficiency)
			Kinase cascade	gene expression \nearrow synaptic contact, \nearrow dendritic spines size (\searrow synaptic contact, \searrow dendritic spines size)

Table 3.1 – *Summary of synaptic plasticity types* and their expression types. *p* release means the probability of neurotransmitter release, # the number of *NT* (neurotransmitters) or *AMPAr* (AMPA receptors).

3.3 Experimental (long-term) induction protocols

Experimental protocols have been realised in order to induce LTP/LTD. This allows obtaining experimental data by varying one parameter at a time and to see their impact on synaptic strength change.

3.3.1 How experimental induction protocols are carried?

Typical protocols using extracellular electrodes follow the following steps:

- (a) measure of initial EPSP or EPSC (*excitatory postsynaptic current*) in postsynaptic neuron induced by an action potential in the presynaptic neuron.
- (b) induction protocol specific to the experiment
- (c) measure of EPSP or EPSC difference before and after the protocol

FIGURE 3.5 shows an example of an induction protocol.

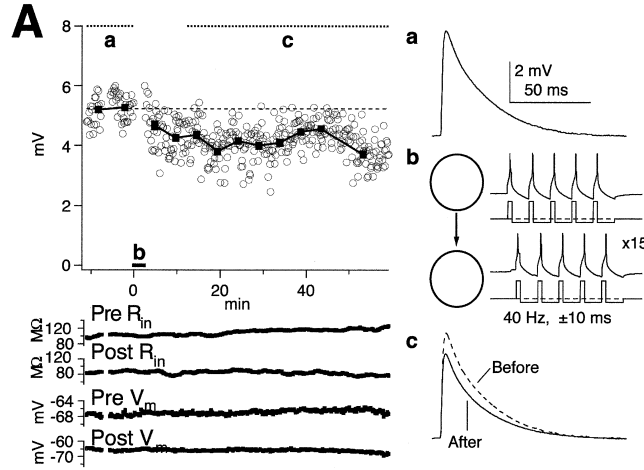


Figure 3.5 – *Experimental STDP protocol* **a.** experimental measure of the initial EPSP amplitude. **b.** Induction protocol: stimulation of the two cells with 15 times 5 spikes at a frequency of 40[Hz] and a delay of $t_{post} - t_{pre} = 10$ [ms] **c.** measure of the difference of EPSP amplitude before and after the protocol [Sjöström et al., 2001]

3.3.2 The main synaptic plasticity drivers

Three main components seem to have importance in initiation of long-term plasticity: the *spiking rate*, the *voltage* of the postsynaptic cell and the *spike timing* difference between pre- and postsynaptic cell.

A visual summary of the different experimental findings can be found in FIGURE 3.6.


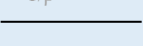
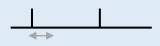
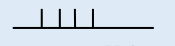
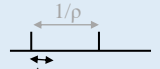
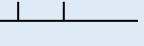
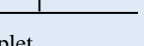
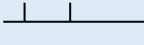
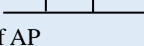
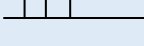
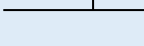
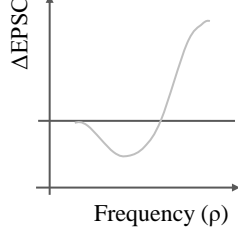
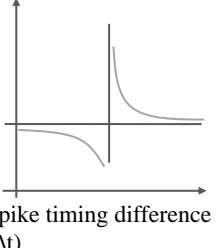
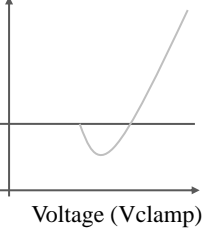
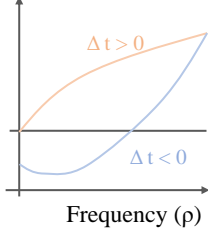
Rate-based protocol	Pairing protocol	Effect of postsynaptic voltage-clamp	Frequency effect in pairing protocols	Various spike patterns
Pre-  Post-  $1/\rho$	 Δt	 V_{clamp}	 $1/\rho$ Δt	<u>Triplet</u>   <u>Quadruplet</u>   <u>Burst of AP</u>  
 $\Delta EPSC$ Frequency (ρ)	 Spike timing difference (Δt)	 Voltage (V_{clamp})	 $\Delta t > 0$ $\Delta t < 0$ Frequency (ρ)	

Figure 3.6 – *Summary of experimental findings using different induction protocol.* From left to right: rate-based [Bliss and Lømo, 1973, Dudek and Bear, 1995] (*hippocampus*), pairing protocol [Bi and Poo, 1998] (*hippocampus*) [Markram et al., 1997] (*cortex*), postsynaptic voltage-clamp [Artola et al., 1990] (*cortex*) [Ngezahayo et al., 2000] (*hippocampus*), frequency change in pairing protocol [Sjöström et al., 2001, Markram et al., 1997] (*cortex*) and other various spike patterns [Wang et al., 2005] (*hippocampus*), [Froemke and Dan, 2002, Nevian and Sakmann, 2006] (*cortex*). **(blue background)** Schematic representation of the experimental protocol, in grey the varying parameter. **(graphs)** Experimental curves changes in EPSC amplitude.

Rate-based induction

In 1973, Bliss and Lomo [Bliss and Lømo, 1973] were the first to demonstrate plasticity at a single synapse experimentally by stimulating hippocampal path. They recorded in the dentate gyrus increase in synaptic transmission efficiency.

A conditioning stimulus (high-frequency stimulus for a few seconds) is sent to the conditioning pathway (FIGURE 3.7 (B)) while the control pathway is unstimulated. If there is no change in the control pathway but an increase in the magnitude of the EPSP or EPSC in the conditioning pathway, homosynaptic LTP in this synapse has been induced (FIGURE 3.7 (C)). Since presynaptic and postsynaptic activity in close temporal proximity is required for LTP, this is consistent with Hebb's idea.

As it has been previously demonstrated, LTP alone is not sufficient. LTD was also observed in the hippocampus induced by low-frequency stimulus (0.5-10Hz) [Dudek and Bear, 1995, Mulkey and Malenka, 1992]. Induction protocols of bidirectional plasticity induced by different rates of presynaptic stimulation are often referred to as rate-based protocols.

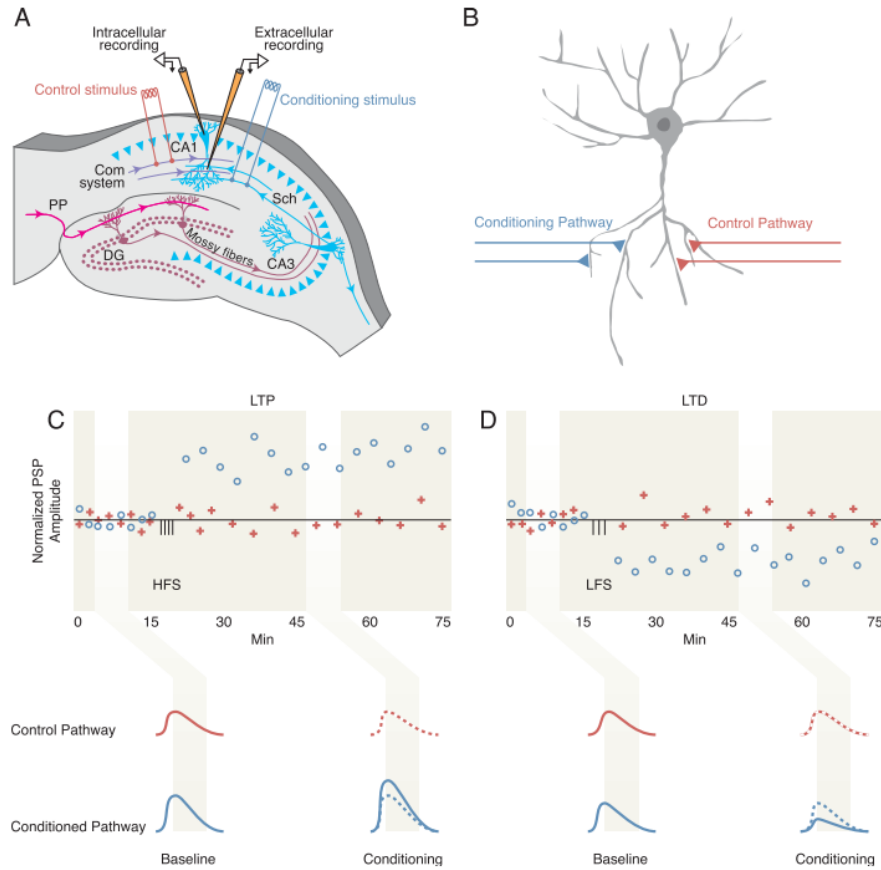


Figure 3.7 – *Induction of rate-dependent plasticity.* **A.** Intracellular and extracellular recordings are carried out in CA1 synapses in the hippocampus. **B.** Schematic representation of a CA1 neuron conditioning and control pathways. **C.** High-frequency stimulation. Only the conditioning pathway receives HF stimulation. In both pathways, postsynaptic potentials are recorded before and after the stimulation. LTP is observed only in the conditioning pathway. **D.** Low-frequency stimulation. LTD is induced only in the conditioning pathway [Heidelberg et al., 2014]

Voltage-clamp induction

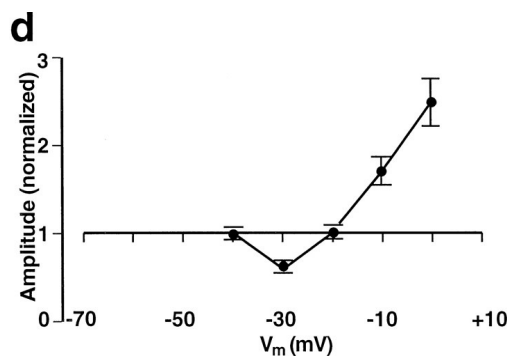


Figure 3.8 – *Experimental findings of [Ngezahayo et al., 2000]* LTP occurs above a certain postsynaptic voltage, while LTD occurs at lower voltages.

Rate-based protocols do not consider the post-synaptic cell behaviour and other protocols allow the control of the post-synaptic cell. One of them is a patch-clamp protocol, in which the post-synaptic

cell is depolarised at a certain voltage by voltage-clamp and is paired to low-frequency presynaptic stimulation. LTP induction occurs if the postsynaptic cell is depolarised sufficiently while LTD occurs at lower depolarisation values [Heidelberg et al., 2014]. Such voltage dependence in plasticity has been shown in rat visual cortex [Artola et al., 1990] and hippocampus and can be seen in FIGURE 3.8 [Ngezahayo et al., 2000].

Spike Timing-Dependence Plasticity

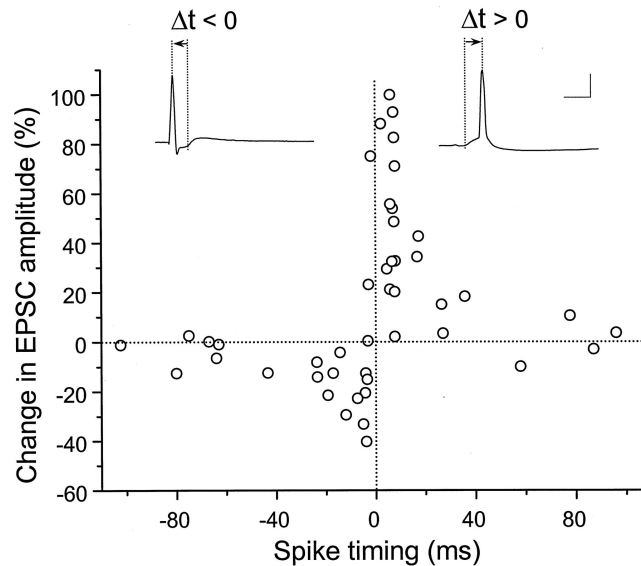


Figure 3.9 – *Experimental findings of [Bi and Poo, 1998] in the hippocampus.* Classical STDP windows depending on the spike timing difference of the pre- and postsynaptic neuron. Pairings were repeated at 1Hz.

Another very common protocol considering also the control of the postsynaptic cell gave rise to the well-known concept of *Spike Timing-Dependent Plasticity (STDP)*. In this protocol, the pre- and postsynaptic cells are stimulated with a certain delay between the two.

In cultured hippocampal neurons, experiments have shown that repetitive firing induces a change in synaptic efficiency as a function of the time delay and that the direction of the change depends on the relative timing of the spikes at a millisecond time-scale in the cortex [Markram et al., 1997] and in the hippocampus [Bi and Poo, 1998]. On one hand, if the pre-synaptic neuron spikes *before* the post-synaptic spikes, LTP occurs (see FIGURE 3.9). On the other hand, if a presynaptic spike occurs *after* a post-synaptic spike, LTD is observed. Those observations are in line with Hebb’s postulate.

However, the long-term modification induced by this protocol varies in different brain areas as experiments in different slices preparations have shown [Abbott and Nelson, 2000]. Differences can be observed in FIGURE 3.10.

Also, other spiked-timing protocols have shown that STDP depends on the frequency of the firing rate in such a way that potentiation increases with firing rate [Sjöström et al., 2001] in the cortex.

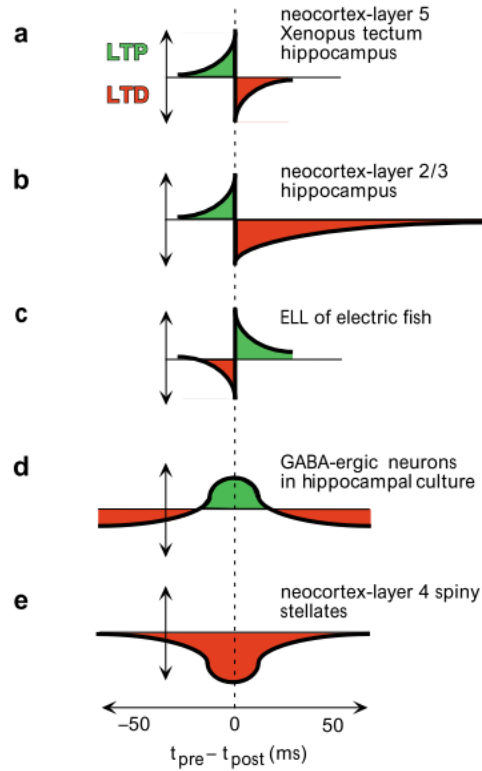


Figure 3.10 – *Spike Timing-Dependent Plasticity (STDP) evoked by repeated pre- and postsynaptic firing in different preparations* [Abbott and Nelson, 2000].

Various spiking patterns

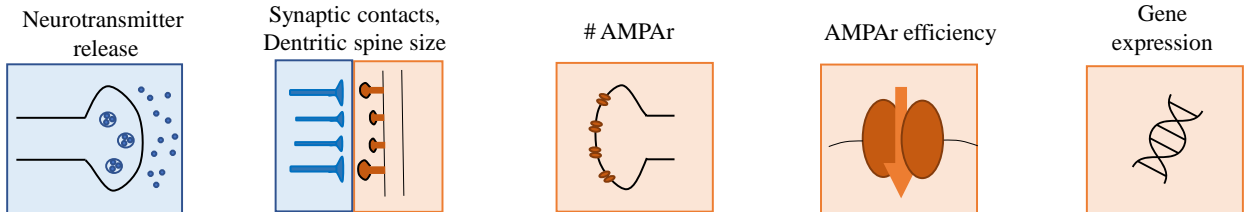
Other patterns have been experimentally induced and resulting synaptic change evaluated. Here is an enumeration of the most common:

- *Triplet* or *quadruplet* pairing protocols (three or four spikes instead of two) have also been experimented in the hippocampus [Wang et al., 2005] and in the cortex [Froemke and Dan, 2002] (triplets).
- *Postsynaptic 'bursts'* (*i.e.* repetitive AP in a short period of time) of 1, 2 or 3 spikes paired with one single presynaptic spike induced experimentally in the cortex [Nevian and Sakmann, 2006]. Note that those bursts are not the same as endogenous T-type bursting patterns evoked in CHAPTER 2.

3.4 Summary

SYNAPTIC PLASTICITY

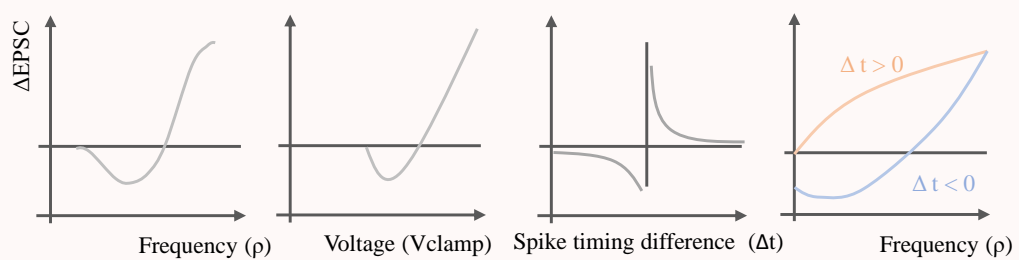
Plasticity mechanisms



	Locus	Dominant mechanism	Consequences
Short-term	Presynaptic	Vesicle depletion	Proba NT release
		Calcium binding	
Long-term	Presynaptic	Calcium	# NT release
	Postsynaptic	Calcium cascade	# AMPAR
			AMPA efficiency
		Kinase cascade	Gene expression
			Synaptic contacts and dendritic spines size

Experimental evidence

Main experimental findings in different brain areas



• Hippocampus

• Hippocampus
• Cortex

• Hippocampus
• Cortex

• Cortex

Part II

Synaptic plasticity from a modeling point of view

Chapter 4

State-of-the-art

In the field of computational neurosciences, computational models of synaptic plasticity replicating experimental data are being actively investigated. Two modeling approaches can be distinguished [Graupner, 2017]:

1. *Phenomenological models of plasticity* using the times or frequency of action potentials fired by neurons to estimate the synaptic strength changes. This approach focuses on abstract equations able to fit experimental data rather than trying to explain the molecular processes underneath.
2. *Biophysical models of plasticity* using biological variables to track the change in synaptic strength (such as Ca^{2+} concentration, a cascade of kinase activation, ...) to explain plasticity.

This thesis only focuses on *phenomenological models* of synaptic plasticity. As summarised in FIGURE 4.1, the goal of this project is to use models, seen as black boxes, taking spike timings or rates from pre- and postsynaptic neurons as inputs and providing synaptic weight change as output. Moreover, CHAPTER 2 provides insights on firing pattern variation between waking and sleep states. While most common models focus on tonic firing (*i.e.* wake), the ultimate purpose is thus to see if those models are compatible with bursting firing mode (*i.e.* sleep).

Consequently, a review of the literature is built in order to find and classify already implemented models. The aim of this review is to investigate learning rules used in the literature.

Mainly, phenomenological models can be divided into two subgroups: *rate-based* and *spike timing-based*. The latter are becoming more prominent in the recent literature. Nevertheless, main principles of rate-based models have been addressed in this review.

Concerning the recent literature, the different rules of spike timing-based models have been introduced, focusing on how they can be mathematically modeled. Then, for each category, the conclusions of various authors are summarised and the possible limitations of such models are addressed.

The different key-modeling assumptions in the various models have been identified such as:

- **The network size:** two neurons, small circuit, large network, ...
- **The neuron model:** integrate-and-fire model, conductance-based model, ...
- **The definition of the synaptic weight** in the model
- **The protocol** on which their model is fitted
- The mechanism inducing the **wake/sleep switch** if it is investigated
- **The memory task** on which the model has been tested : associative memory, ...

- The phenomenological **learning rule**.

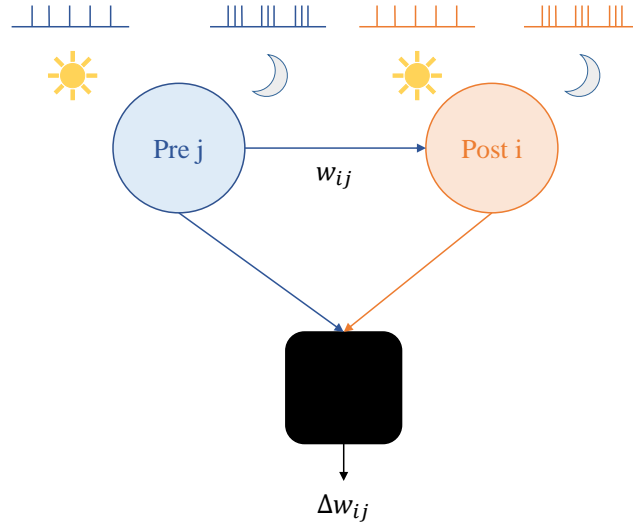


Figure 4.1 – *Graphical representation of computational modeling of synaptic plasticity.* A presynaptic neuron is linked to a postsynaptic neuron with a certain weight w_{ij} . Computational models (*black box*) provide synaptic rules giving a synaptic weight change Δw_{ij} with inputs given by pre- and postsynaptic neurons: during wake, tonic firing pattern is observed while during sleep, neurons show burst firing.

The plasticity between a neuron j to a neuron i is mathematically represented by a modification of weight Δw_{ij} , w_{ij} giving the efficiency of the connections between the two neurons.

4.1 Rate-based

One of the simplest model types in line with Hebb's principle ("Who fire together, wire together") [Hebb, 1949] consists of assuming that the rate of pre (ρ_j) and postsynaptic (ρ_i) neurons determine the magnitude and sign of plasticity. Hebbian plasticity has two main aspects [Gerstner et al., 2014]:

1. *locality*: Δw_{ij} can only depend on local variables at the homosynaptic site. In the case of firing rate-based models, it means the post and presynaptic rate only. We can thus deduce a general equation for the synaptic weight change:

$$\Delta w_{ij} = F(w_{ij}; \rho_i, \rho_j) \quad (4.1)$$

2. *simultaneousness*: the pre- and postsynaptic neurons have to be active at the same time to induce synaptic weight change. The function F can be deduced by expanding F in a Taylor series about $\rho_i = \rho_j = 0$:

$$\begin{aligned} \frac{d}{dt} w_{ij} = & c_0(w_{ij}) + c_1^{\text{pre}}(w_{ij}) \rho_j + c_1^{\text{post}}(w_{ij}) \rho_i + c_2^{\text{pre}}(w_{ij}) \rho_j^2 \\ & + c_2^{\text{post}}(w_{ij}) \rho_i^2 + c_{11}^{\text{corr}}(w_{ij}) \rho_i \rho_j + \mathcal{O}(\nu^3) \end{aligned} \quad (4.2)$$

The c_{11}^{corr} term is the term involving both the pre- and postsynaptic neurons and is thus needed to implement Hebbian's learning rule. Note that $c_{11}^{\text{corr}} > 0$ is necessary to state that the simultaneous activity of pre- and postsynaptic neurons strengthens the synapse. Else, it would be anti-Hebbian.

Different rules have been defined by the previous formalism. As an example, Oja's rule [Oja, 1982] takes $c_{11}^{\text{corr}} = \gamma > 0$ and $c_2^{\text{post}} = -\gamma \Delta w_{ij}$ and the other parameters = 0. It gives:

$$\frac{d}{dt} w_{ij} = \gamma [\rho_i \rho_j - w_{ij} \rho_i^2] \quad (4.3)$$

It has previously been introduced that the Hebbian rule alone is unstable since it only allows potentiation of synapses and leads to saturation, a possibility for decreasing synaptic weights should be implemented. Oja's rule normalises the weights to

$$\sum_j w_{ij}^2 = 1 \quad (4.4)$$

such as competition between synapses is implied.

Another known example is the Bienenstock-Cooper-Munro (*BCM*) rule that considers a non-linear function ϕ and an adaptative threshold ρ_θ as a function of post-synaptic neuron firing rate ρ_i [Bienenstock et al., 1982]:

$$\frac{d}{dt} w_{ij} = \phi(\rho_i - \rho_\theta) \rho_j \quad (4.5)$$

If the postsynaptic neuron fires at the same time as the presynaptic neuron at a low (resp. high) frequency $\rho_i < \rho_\theta$ (resp. , $\rho_i > \rho_\theta$) the efficiency of synapses activated by the presynaptic neuron is decreased (resp. increased) (see FIGURE 4.2). To avoid stability issues, ρ_θ is a function of the average postsynaptic rate. This can be interpreted as

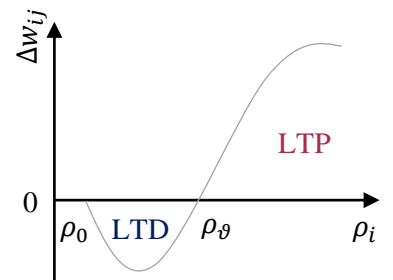


Figure 4.2 – *Bienenstock-Cooper-Munro (BCM) rule.* adapted from [Gerstner et al., 2014]

metaplasticity since the threshold is adaptative, meaning the plasticity rule itself has plastic properties.

4.2 Spike timing-based

4.2.1 Classical STDP: Pair-based model

Standard STDP (*spike timing-dependent plasticity*) modeling relies on fitting the model parameters with experimental data found by induction protocols explained in SECTION 3.3.2. [Bi and Poo, 2001, Van Rossum et al., 2000] fitted the experimental curve obtained in [Bi and Poo, 1998] (FIGURE 3.9 with two exponentials and the synaptic change (Δw) is assumed to be approximated by the following equations:

$$\Delta w(\Delta t) = \begin{cases} A_+ \exp(-\Delta t/\tau_+) & \Delta t > 0 \\ -A_- \exp(\Delta t/\tau_-) & \Delta t < 0 \end{cases} \quad (4.6)$$

where $A_+ > 0$, $A_- < 0$ and Δt representing the delay between the postsynaptic and presynaptic spikes, *i.e.* $\Delta t > 0$ for a pre-post pair and $\Delta t < 0$ for a post-pre pair. In this equation, A_+ (*resp.* A_-) represents the maximal (*resp.* minimal) amount of potentiation (*resp.* depression) when $\Delta t < 0$ (*resp.* $\Delta t > 0$). Note that this equation is not able to explain data from GABA-ergic neurons in hippocampal culture nor neocortex layer-4 spiny stellates, for example (see FIGURE 3.10). Thus, when fitting model parameters, attention should be driven to the physiological area that is supposed to be modeled.

A simple way to take into account the contribution of each spike is to consider that each pre- or postsynaptic spike leaves a trace decaying exponentially and that, each time the neuron spikes this trace is incremented by one. Those traces are used to low-pass filter the spikes and give dynamics to the system so it is more physiological. For example, at the presynaptic site, the trace can represent the decaying amount of neurotransmitters in the synaptic cleft, and the postsynaptic trace the calcium influx into the postsynaptic cell. However, spike timing models do not require those biophysical interpretations. Let's denote x_j the trace left by the presynaptic neuron j and t_j^f its spike timings. Similarly, let's denote y_i the trace left by the postsynaptic neuron i and t_i^f its spike timings [Morrison et al., 2008, Abbott and Nelson, 2000]. As explained above, the dynamics of those local variables can be written in the following way:

$$\frac{dx_j}{dt} = -\frac{x_j}{\tau_x} + \sum_{t_j^f} \delta(t - t_j^f) \quad (4.7)$$

$$\frac{dy_i}{dt} = -\frac{y_i}{\tau_y} + \sum_{t_i^f} \delta(t - t_i^f) \quad (4.8)$$

As illustrated in FIGURE 4.3, when the postsynaptic neuron spikes at t_j^f , the synaptic strength is decreased proportionally to the value of the postsynaptic trace y_i at this time t_i^f . Similarly, when the postsynaptic neuron spikes, the synaptic strength increases proportionally to the trace x_j .

$$\begin{aligned} \Delta w_{ij}^+(t_i^f) &= A_+ x_j(t_i^f) \\ \Delta w_{ij}^-(t_j^f) &= A_- y_i(t_j^f) \end{aligned} \quad (4.9)$$

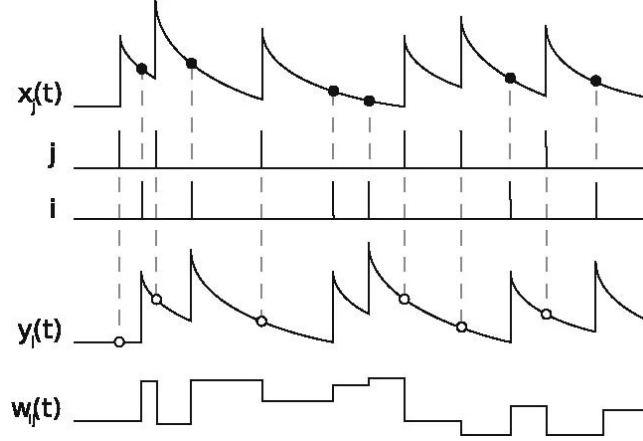


Figure 4.3 – *Implementation of STDP by trace variables.* The presynaptic neuron j leaves a trace $x_j(t)$ decaying exponentially and incremented at each presynaptic spike. Similarly, the postsynaptic neuron i leaves a trace $y_i(t)$ decaying exponentially and incremented at each postsynaptic spike. The weight between the two neurons w_{ij} updates at each spike: on one hand, when the presynaptic neuron spikes at a time t , the update is proportionally to the trace left by the postsynaptic neuron, $y_i(t)$ (empty circles), representing the post-pre pairing depression. On the other hand, when a postsynaptic spike occurs at a time t the weight update is proportional to the value of $x_j(t)$ (filled circles) giving the amount of potentiation of a pre-post pair [Morrison et al., 2008].

All-to-all models versus nearest-neighbour

In the spike-dependent model explained above, at each spike time, all previous spikes contribute to an increase or decrease of the synaptic weight. Thus, this is called *all-to-all* spike interaction. However, considering only the nearest spike is also a possibility and is called *nearest-neighbour* interaction. In other words, the low-pass filtered version of the spikes (the traces) cannot go above a certain value and are not cumulative in such a way that only the most recent spike has an influence, see FIGURE 4.4.

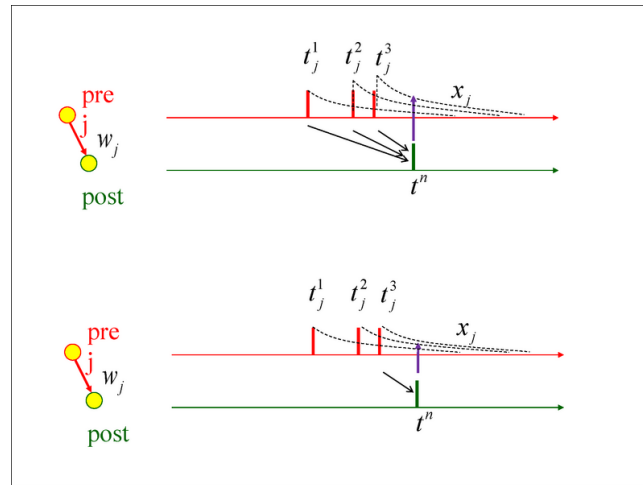


Figure 4.4 – *All-to-all (top) vs nearest neighbours interactions (bottom) in a pair-based model.* **(up)** all previous spikes interact with the postsynaptic spike. The trace variable x_j accumulates. **(bottom)** only the previous presynaptic spike interacts with the postsynaptic spike at t^n . The trace variable x_j corresponds only to the low-pass filtered version of the latest presynaptic spike [Sjöström and Gerstner, 2010].

Hard and soft bounds

The weight parameter should be bounded between $w^{min} < w_{ij} < w^{max}$ in order to keep biological interpretation. On one hand, as the synaptic weight can be interpreted as the amount of EPSP/EPSC induced by a presynaptic neuron, there should be a maximal value. Indeed, at a certain point, there is a biological saturation, for example, due to the postsynaptic calcium concentration that cannot be infinite [Petersen et al., 1998]. On the other hand, a negative synaptic weight would be equivalent to change the direction of the applied current and it would not mathematically make sense.

Implementation of bounds is illustrated in FIGURE 4.5 and can be modeled by using :

- *Hard bounds:* The update rule of w_{ij} is used as it is defined until a w^{max} or w^{min} is reached, and then the update stops at this value.
- *Soft bounds:* The parameters of the models are weight-dependent. For instance, the pair-based rule can be linearly bounded using

$$A_+(w_j) = (w^{max} - w_j) \eta_+ \quad \text{and} \quad A_-(w_j) = w_j \eta_- \quad (4.10)$$

with η_+ and η_- positive constant such as the weight update will keep w_{ij} in between the bounds [Sjöström and Gerstner, 2010].

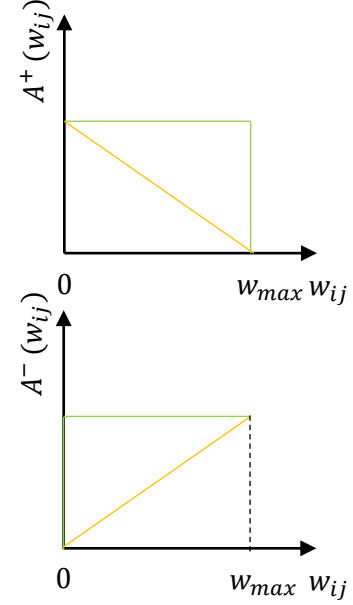


Figure 4.5 – *Hard bounds and soft bounds.* Illustration of hard bounds (green) and linear soft bounds (yellow). The potentiation (resp. depression) parameters (A_+) (resp. A_-) decreases (resp. increase) as w_{ij} increases in such a way that w_{ij} never reach the maximal and minimum bounds. (*adapted from [Sjöström and Gerstner, 2010]*)

STDP conclusions and limitations

[Babadi and Abbott, 2016] compare different models at a population level in terms of stability and competition: Standard *STDP* (pair-based) model, *Triplet* model, *Suppression* model, and *NMDA*-based model (a type of biophysical model not investigated in this review). Regarding the pair-based model, this paper concludes that STDP implemented with hard bounds only allows partial stability and Hebbian competition while implementing soft bounds permits obtaining stability but the (Hebbian) competition is lower.

Even if they have the ability to reproduce spike timing protocols, general STDP with no further amelioration failed to explain several experiments such as frequency dependence of spike timing protocols [Sjöström et al., 2001] or triplets and quadruplets protocols [Froemke and Dan, 2002, Wang et al., 2005]. Indeed, it shows that increasing the frequency of the pre-post or post-pre pair in the protocol leads to more potentiation in the cortex. Triplets experiments such as induction of "post-pre-post" or "post-pre-post" firing as well as quadruplets experiments failed to be represented by the pair-based model due to its symmetry [Pfister and Gerstner, 2006, Graupner et al., 2016].

4.2.2 Triplet models

Suppression model

As triplet experimental protocols were demonstrated, [Froemke and Dan, 2002] suggest adapting classical STDP with factors representing the efficiency of successive action potentials. Indeed, as it was explained in SECTION 3.1, the effect of two successive spikes are not simply cumulative, there can be a vesicle depletion effect. In other words, this model suppresses the effect of the previous presynaptic (*resp.* postsynaptic) spike to the second presynaptic (*resp.* postsynaptic) spike in each spike pair. In order to take this short-term plasticity event into account, an efficiency factor for the neuron i is defined as follows:

$$\epsilon_i = 1 - e^{-(t_i - t_{i-1})/\tau_s} \quad (4.11)$$

i.e. the efficacy ($\epsilon \in [0; 1]$) is minimal after each spike, and it increases exponentially back to 1 with a time constant τ_s . The final learning rule is

$$\Delta w_{ij} = \epsilon_i^{pre} \epsilon_j^{post} F(\Delta t) \quad (4.12)$$

where $F(\Delta t)$ is the standard pair-based equations in EQUATION 4.6.

Common triplet model

A more common approach to explain several experiments such as frequency dependence of spike timing protocols [Sjöström et al., 2001] or triplets and quadruplets protocols [Wang et al., 2005] is the general triplet model. Introduced by [Pfister and Gerstner, 2006] triplet models are also based on spike times.

Similarly to the pair-based model, it is implemented by local variables. However, a presynaptic spike is modeled by two different quantities r_1 and r_2 who are low-passed filtered traces of the spike but with different time constants, respectively τ_+ and τ_x . Namely, τ_+ is smaller than τ_x , *i.e.* the trace r_1 decays on a faster time-scale than the trace r_2 . Similarly, a postsynaptic spikes is associated to two different traces σ_1 and σ_2 with respectively the time constant τ_- and τ_y and $\tau_- < \tau_y$. It gives:

$$\begin{aligned} \frac{dr_1(t)}{dt} &= -\frac{r_1(t)}{\tau_+} & \text{if } t = t^{pre} & \text{ then } r_1 \rightarrow r_1 + 1 \\ \frac{dr_2(t)}{dt} &= -\frac{r_2(t)}{\tau_x} & \text{if } t = t^{pre} & \text{ then } r_2 \rightarrow r_2 + 1 \\ \frac{d\sigma_1(t)}{dt} &= -\frac{\sigma_1(t)}{\tau_-} & \text{if } t = t^{post} & \text{ then } \sigma_1 \rightarrow \sigma_1 + 1 \\ \frac{d\sigma_2(t)}{dt} &= -\frac{\sigma_2(t)}{\tau_y} & \text{if } t = t^{post} & \text{ then } \sigma_2 \rightarrow \sigma_2 + 1 \end{aligned} \quad (4.13)$$

where t_{pre} (*resp.* t_{post}) is the timing of a presynaptic spike (*resp.* postsynaptic). The full model implemented by [Pfister and Gerstner, 2006] takes into account weight change due to pre-post (with the constant A_2^+ , inducing potentiation) or post-pre pairs (with the constant A_2^- , inducing depression) (similar to classical pair-based model). The improvement over the classic pair-based model is that triplet of spikes are also considered. Thanks to previously introduced traces σ_2 and r_2 pre-post-pre triplets are treated (associated with the constant A_3^- , inducing depression) as well as post-pre-post triplets (associated with the constant A_3^+ , inducing potentiation) (see FIGURE 4.6). Weight change goes as follows:

$$w(t) \rightarrow w(t) - o_1(t) [A_2^- + A_3^- r_2(t - \epsilon)] \quad \text{if } t = t^{pre} \quad (4.14)$$

$$w(t) \rightarrow w(t) + r_1(t) [A_2^+ + A_3^+ \sigma_2(t - \epsilon)] \quad \text{if } t = t^{post} \quad (4.15)$$

It has been shown that this model can be mapped to the BCM rule that is a rate-based model explaining the selectivity of the postsynaptic neurons [Gjorgjieva et al., 2011]. Moreover, the triplet

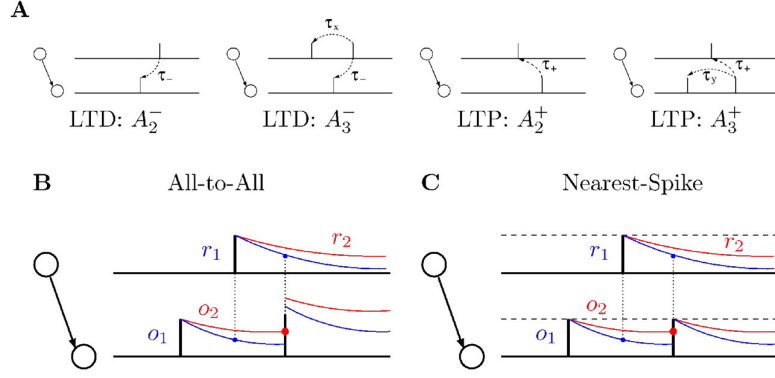


Figure 4.6 – *Implementation of Triplet model by trace variables.* [Pfister and Gerstner, 2006]

model further generalises it since it is also based on spike timing and adds spatiotemporal correlations in inputs.

Limitations

On one hand, [Babadi and Abbott, 2016] investigations on the triplet model show partial stability and only Hebbian competition for a limited range of parameters. On the other hand, the suppression model shows anti-Hebbian competition and stability when the average weight is high. Comparison with standard pair-based model and a biophysical model (NMDAR-based model) demonstrates that only the biophysical model allows coexistence of Hebbian and anti-Hebbian competition depending on the parameters, as well as stability.

[Graupner et al., 2016] introduces soft bounds in [Pfister and Gerstner, 2006] model. It shows that considering irregular firing patterns (*in vivo-like*), synaptic changes induced by AP timing can be equivalently induced by firing rate modification. This questions the predominant emphasise of precise spike timing protocols on their own as opposed to more natural patterns.

Moreover, this model shows no proof to be able to explain other experiments such as voltage experiments since it does not include any postsynaptic membrane potential variable and only recalls on spike timing.

4.2.3 Voltage-based models

This kind of models aims to be able to reproduce voltage-clamp experiments. Particularly, [Clopath et al., 2010] design a spike timing-based model taking into account the presynaptic voltage. The synaptic weight evolves as follows:

$$\frac{d}{dt}w_{ji} = -A_{LTD}X_i(t)[u_-(t) - \theta_-]_+ + A_{LTP}[u(t) - \theta_+]_+x_i(t)[u_+(t) - \theta_-]_+ \quad (4.16)$$

where

- A_{LTD} and A_{LTP} are respectively depression and potentiation constant.
- $x_i(t)$ is the trace of the presynaptic spike following

$$\tau_x \frac{dx_i(t)}{dt} = -x_i(t) + X_i(t) \quad (4.17)$$

- u is the postsynaptic voltage,

- u_+ and u_- are postsynaptic voltage traces with two different time constants ($\tau_+ > \tau_-$) following:

$$\tau_{+/-} \frac{du_{+/-}(t)}{dt} = -u_{+/-}(t) + u(t) \quad (4.18)$$

- θ_+ and θ_- are voltage threshold: respectively the action potential threshold and the equilibrium potential
- $X_i(t) = \sum_n \delta(t - t_n^i)$, t_n^i the presynaptic spike times.
- $[x]$ means that any value $x < 0$ equals 0

The equation is graphically explained in FIGURE 4.7. LTP is triggered if the postsynaptic voltage (u) is above the action potential threshold θ_+ and the low-pass filtered potential u_+ is above the threshold θ_- . The amount of potentiation is proportionally to $A_{LTP}x_i$. On the contrary, LTD is triggered if the low-pass filtered potential u_- is above the threshold potential θ_- at a presynaptic spike-time t^i and the synaptic weight is decreased by an amount proportionally to A_{LTD} .

Additionally to being able to reproduce a large variety of experimental protocols ([Sjöström et al., 2001, Artola et al., 1990, Nevian and Sakmann, 2006]), [Clopath et al., 2010] show the development of connectivity patterns and localised receptive fields. Indeed, bidirectionnality in the connections and clusters appears under rate coding procedure (neuron stimulated by different rate patterns). However, temporal coding (neurons firing successively) leads to unilateral connections.

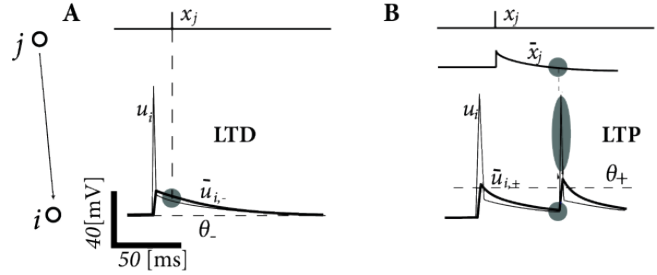


Figure 4.7 – Illustration of voltage-dependent plasticity modeled by [Clopath et al., 2010] **A.** LTD is triggered at the spike time of the presynaptic neuron j if the trace $\bar{u}_{i,-}$ is above θ_- . **B.** LTP is triggered at the spike time of the postsynaptic neuron i if the membrane potential u is above the threshold θ_+ and the trace $\bar{u}_{i,+}$ is above θ_- . The amount of potentiation is proportionally to the trace $\bar{x}_j(t)$ [Gerstner et al., 2014].

4.2.4 Three-factor rule

STDP alone is too simple to explain every aspect of plasticity. Experimental studies have more recently investigated the interaction of neuromodulation and STDP, by controlling the spike timing of the pre- and postsynaptic neurons together with neuromodulators [Seol et al., 2007, Zhang et al., 2009]. For instance, higher acetylcholine concentrations induce LTD while dopamine would lead to stronger LTP and a flip from LTD to LTP compared to standard STDP protocols [Frémaux and Gerstner, 2015]. Different neuromodulators applied at the same time interact to give even more diversified results, see examples in FIGURE 4.8. Those interactions are very complex and there is so much experimental data that it is nearly impossible to fit computational plasticity models containing all the experimental results [Frémaux and Gerstner, 2015]. Thus, it is more realistic to build a mathematical framework than a very precise model. The introduction of a "three-factor rule" that blends pre- and postsynaptic spike timing together with neuromodulation would be generally written as follows [Frémaux and Gerstner, 2015]:

$$\dot{w} = f(M, pre, post) \quad (4.19)$$

with \dot{w} the synaptic weight change, M the impact of neuromodulation and pre , $post$ the activity of pre- and postsynaptic cells.

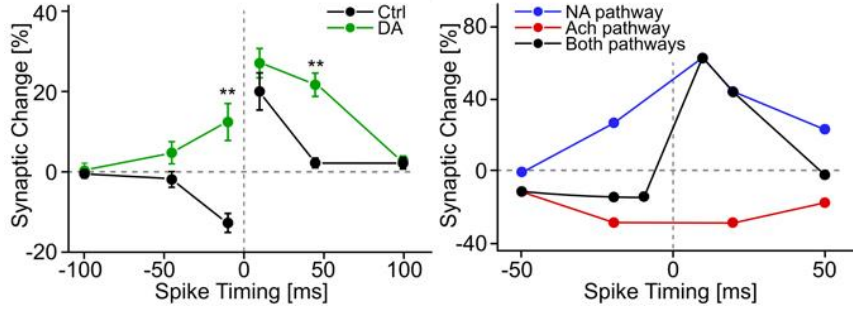


Figure 4.8 – *Effects of neuromodulators on STDP window. (left) Effect of dopamine in the hippocampus. (right) Effect of activation of noradrenaline and acetylcholine pathways in the visual cortex. (taken from [Frémaux and Gerstner, 2015])*

Other components could be pertinent to investigate as third factor in the three-factor rule such as nitric oxide (NO), brain-derived neurotrophic factor ($BDNF$), GABA or even astrocytes that all have been demonstrated to have the ability to modulate STDP [Foncelle et al., 2018].

Computational investigations on this topic are starting. [Pedrosa and Clopath, 2017] use a simple neuron model with four different learning rules corresponding to the impact on the STDP curve of different neuromodulators, represented in FIGURE 4.9. Computationally observing the impact of those rules with different settings can deepens the understanding of neuromodulatory effects on plasticity modulation. Applying the four different rules to see the impact on receptive field adaptation, [Pedrosa and Clopath, 2017] find that:

- upregulation of *learning rate* yields sharpening of receptive field,
- upregulation of *neuronal activity* yields either sharpening or broadening of the receptive field.

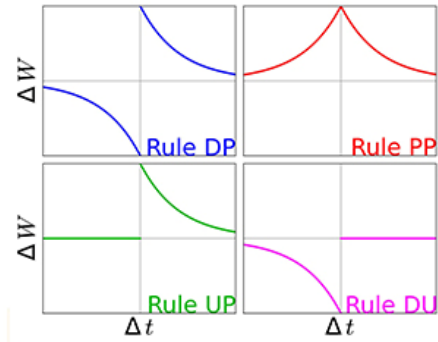


Figure 4.9 – *Four different STDP curves used by [Pedrosa and Clopath, 2017]. (blue) DP: depression-potential. Observed in the visual cortex ($Ach + NE$) and the dorsal striatum (DA). (red) PP: potentiation-potential. Observed in the visual cortex (NE) and hippocampus (DA). (green) UP : unchanged-potential. Observed in the amygdala (DA) (pink) DU: depression-unchanged. Observed in the prefrontal cortex (nicotine).*

4.2.5 Combination of models

In real-life experiments, plasticity occurs at many different time-scales. As previously introduced in CHAPTER 3, short-term and long-term plasticity coexist. Additionally, to allow stability in Hebbian plasticity, homeostasis is often required. Homeostatic plasticity refers to compensatory processes at various scales (spatial and temporal) allowing stabilisation of neural firing rate. Indeed, stability of neuronal activity seems to be maintained by homeostatic processes acting dynamically in order to adjust the strength of synaptic connections [Turrigiano and Nelson, 2004]. Often, it is modeled by synaptic scaling, *i.e.* all synaptic connections are divided by the same value, keeping the overall weights stable while maintaining the ratio between the different connections. This mathematical trick takes only a few seconds to happen, while it has been shown that the homeostasis process *in vivo* takes hours or even days [Zenke and Gerstner, 2017]. Consequently, implementing a combination of various plasticity rules occurring at different time scales is a relevant approach to better represent natural plasticity conditions. Different modeling methods at different time-scales can be implemented such as:

- **Short-term plasticity:** synaptic receptors (g , and particularly g_{AMPA}) can vary depending on various parameters such as short-term plasticity and weight [Zenke et al., 2015]:

$$\frac{dg}{dt} = F(X_{ST}, w_{ij}) \quad (4.20)$$

where $X_{ST}(t)$ is used to model short-term (ST) variables. It represents resources parameters that are depleted after an action potential and recover back to their initial value, schematically following:

$$\frac{X_{ST}(t)}{dt} = \frac{1 - X_{ST}}{\tau_{ST}} \quad (4.21)$$

- **Homeostasis:** In order to take into consideration homeostasis (*i.e.* process maintaining stability) synaptic scaling can be implemented to normalise all the synaptic weights at once, for example [Nere et al., 2012, Turrigiano and Nelson, 2004]:

$$w_{ij} = \frac{w_{ij}}{w_{max}} \quad (4.22)$$

But as previously explained, it does not match up to *in vivo* homeostatic process taking way more time to happen. Homeostatic regulation of LTD / LTP can be implemented by down-scaling the values of $A_+(t) / A_-(t)$ (in the specific case of pair-based model) with a really slow temporal dynamics ($\tau_h \gg 0$).

- **Heterosynaptic plasticity:** Within the same postsynaptic neuron, plasticity can also occur at synapses that were not active. This can provide competition and stabilisation of synaptic weights [Chistiakova et al., 2014]. Mainly, release of Ca^{2+} in one synapse can trigger change in the neighbouring synapses [Chen et al., 2013, Bannon et al., 2017].
- **Metaplasticity:** as introduced by [Bienenstock et al., 1982], plasticity itself is plastic and is not one specific fixed rule [Benuskova and Abraham, 2007, Yger and Gilson, 2015].
- ...

Excitatory synapses exhibiting different plasticity mechanisms at different time scales: short-term plasticity, STDP, heterosynaptic plasticity (plasticity induced by cooperativity at unstimulated synapses

of an excited postsynaptic neuron), and transmitter-induced plasticity in addition to consolidation and homeostasis have been implemented to allow stability [Zenke et al., 2015]. This model performs the development of different assemblies and memory recall of those different clusters. It shows that physiological rules based on synaptic plasticity can be able to classify and recall data in a Machine Learning way. In addition, the implementation of slow homeostatic processes have shown to facilitate the learning phase.

Going further

While models complexify, gain insights into stability mechanisms and are able to perform memory tasks, sleeping mechanisms are still on hold. As it is known that *in vivo* memory formation happens during sleep, it seems logical to investigate modeling approaches mimicking or involving sleep.

4.2.6 Sleep adaptation

Sleep can be implemented computationnaly in various ways. A popular opinion is based on SHY (*Synaptic Homeostasis Hypothesis of sleep*) which states that sleep decreases synaptic connections to optimise energy consumption, avoid cellular stress and connection saturation [Tononi and Cirelli, 2014]. Following this hypothesis, sleep is thus induced by a change in the learning rule during the sleep phase (no potentiation occurs).

[González-Rueda et al., 2018] make this assumption to implement a rule that would differ from waking to sleep. On one hand, a standard STDP is used during wake and sleep DOWN-states. On the other hand, an UP-mediated learning rule is implemented which down-scales the synaptic weight during UP-states of SWS. Using this change of learning rule, weaker synapses are depressed during sleep while synapses with higher connections are protected and preserved. Additionnaly, the signal-to-noise ratio is improved and information is stored throughout several wake/sleep cycles (see FIGURE 4.10).

Following the same hypothesis, [Nere et al., 2012] implement sleep-like phase which down-scale the synaptic weight and depression-only sleeping phase occurs. However, trusting the idea that bursts are highly energetic events and should contain useful information, Burst-STDP is implemented during waking such as only potentiation is happening. Additionally, neuromodulation effect is added by using reward-based learning principle. This model is able to perform object recognition and motion anticipation tasks in a highly structured neural network for a digital neuromorphic hardware design purpose. One year later, [Nere et al., 2013] follow the same hypothesis and provides computational proof of the beneficial effects of sleep using only depression during this period. Consolidation of declarative and procedural memories, gist extraction, and the integration of new with old memories are achieved.

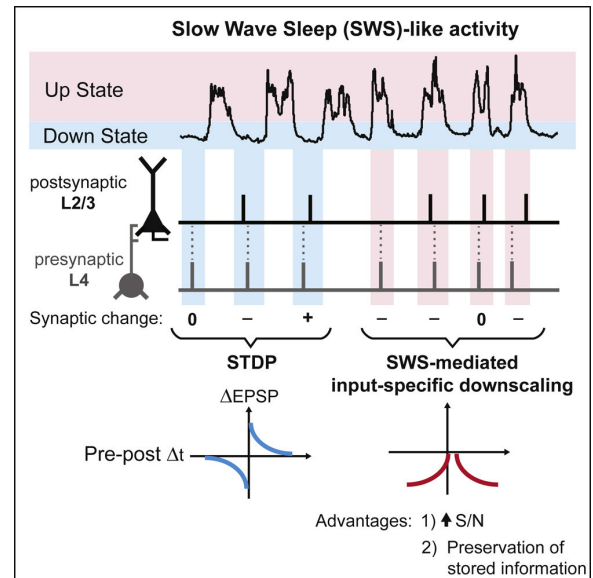


Figure 4.10 – Graphical summary of [González-Rueda et al., 2018]. Synaptic rule changes according to UP and DOWN states in sleep.

Nevertheless, SHY is based on the different neuromodulators concentration during the different brain states but those concentrations are far from being binary as a function of the state. Moreover, the effects of sleep-wake regulated neuromodulators are not consistent with the fact that STDP would reverse [Puentes-Mestril and Aton, 2017].

Using the knowledge that acetylcholine levels are different in sleep and waking states, [Fink et al., 2013] add a slow K^+ conductance to modulate the different acetylcholine levels in waking (high *Ach*) and sleep (low *Ach*) states. It shows high synchronous network activity during sleep and the weights are either up or down-scaled to extreme values.

Finally, [Capone et al., 2019] implements a thalamocortical loop and shows how sleep UP-states during slow oscillations improve classification task (recognition of MNIST digits). The protocol used is the following: a training phase implemented with STDP, a retrieval phase during which neurons are reactivated, a sleep phase with STDP induced manually by non-specific Poisson noise (700Hz) and increase in spike frequency adaptation. Finally during the post-sleep phase, the classification accuracy is better and groups of neurons coding for the same digits are strengthened.

4.2.7 Burst

As introduced in SECTION 2, SWS implies bursting firing pattern at the cellular level in the cortex. Consequently, finding a learning rule compatible with this bursting mode and allowing memory formation could be investigated.

Thus far, the impact on synaptic weight of bursting firing pattern as wake/sleep switch mechanism has rarely been studied. However, bursting patterns have been investigated in other scenarios.

[Gjorgjieva et al., 2009] introduced *burst-timing-dependent plasticity*, a synaptic rule dependent of the timing in between bursts but temporally symmetric and with a bigger time-scale compared to classical STDP. The suggested rule has proven segregation of retinal inputs during the development (relying on bursting) while classical STDP rule did not give satisfying results.

With an experimental protocol, [Delattre et al., 2015] investigate the effects on timed bursts (high frequency spikes) on STDP. Experimental results showed some flips from LTP to LTD or LTD to LTP depending on the exact timing of the bursts. This gave rise to the notion of *Network timing-dependent plasticity* (*NTDP*) where local STDP of individual synaptic pathways is regulated by the timing of synchronous bursts generated by the network. Making the hypothesis that the flip from LTP to LTD is due to the depletion of critical resources needed for LTP, they implement a resource-dependent regulation of STDP.

4.3 Modeling specifications

All modeling assumptions of the mentioned models are summarised in TABLE 4.1 and the FIGURE 4.11 includes all abbreviations used. As it can be seen, models are mainly implemented using less or more complex integrate-and-fire neuron models [Gjorgjieva et al., 2009, Delattre et al., 2015, Clopath et al., 2010, Zenke et al., 2015, González-Rueda et al., 2018]. In this case, the weight between two neurons is usually defined by a simple abstract value that is not taken into account in the strengthening of the connection between the neurons. However, [Zenke et al., 2015] use an IF model with spike-frequency adaptation in which the synaptic weight value is actually used to modulate the AMPA conductance efficiency. [Pedrosa and Clopath, 2017, Nere et al., 2012, Nere et al., 2013] use an IF model in which w modulate a synaptic current I_{syn} .

For their triplet or suppression model, [Pfister and Gerstner, 2006, Gjorgjieva et al., 2011, Froemke and Dan, 2002] only use the spike timing (event-based modeling) to fully model the neurons without differential equation.

[Fink et al., 2013] uses a conductance-based model in which the weight is associated to a synaptic current from a presynaptic neuron to a postsynaptic neuron.

Synaptic rule	Neuron model	Network Shape	Protocol
STDP Suppression-model	C Conductance-based	S 2-9 neurons	Hippocampus H
Triplet Burst-STDP	EB Event-based	M Medium 10-100	H1 [Wang et al. , 2005]
BTDP Combination	Integrate-and-fire	L Large 100-1000	H2 [Ngezahayo et al., 2000]
Voltage UP-mediated	LIF Leaky	XL Extra Large > 1000	Cortex C
NMOD Resource-dependent STDP (r-STDP)	IF Non-Linear	FW Feedforward	C1 [Sjöström et al. , 2001]
			C2 [Froemke et al., 2001]
			C3 [Artola et al. , 1990]
			Thalamus (retina)
			R [Lee et al. , 2002]

Definition w	Memory task	Sleep Switch
w Abstract weight	A Associativity	Manually induced
Isyn Weight on synaptic current	R Retinal response	Conductance change
S EPSP strength	D Development	Synaptic rule change
CS Conductance strength		

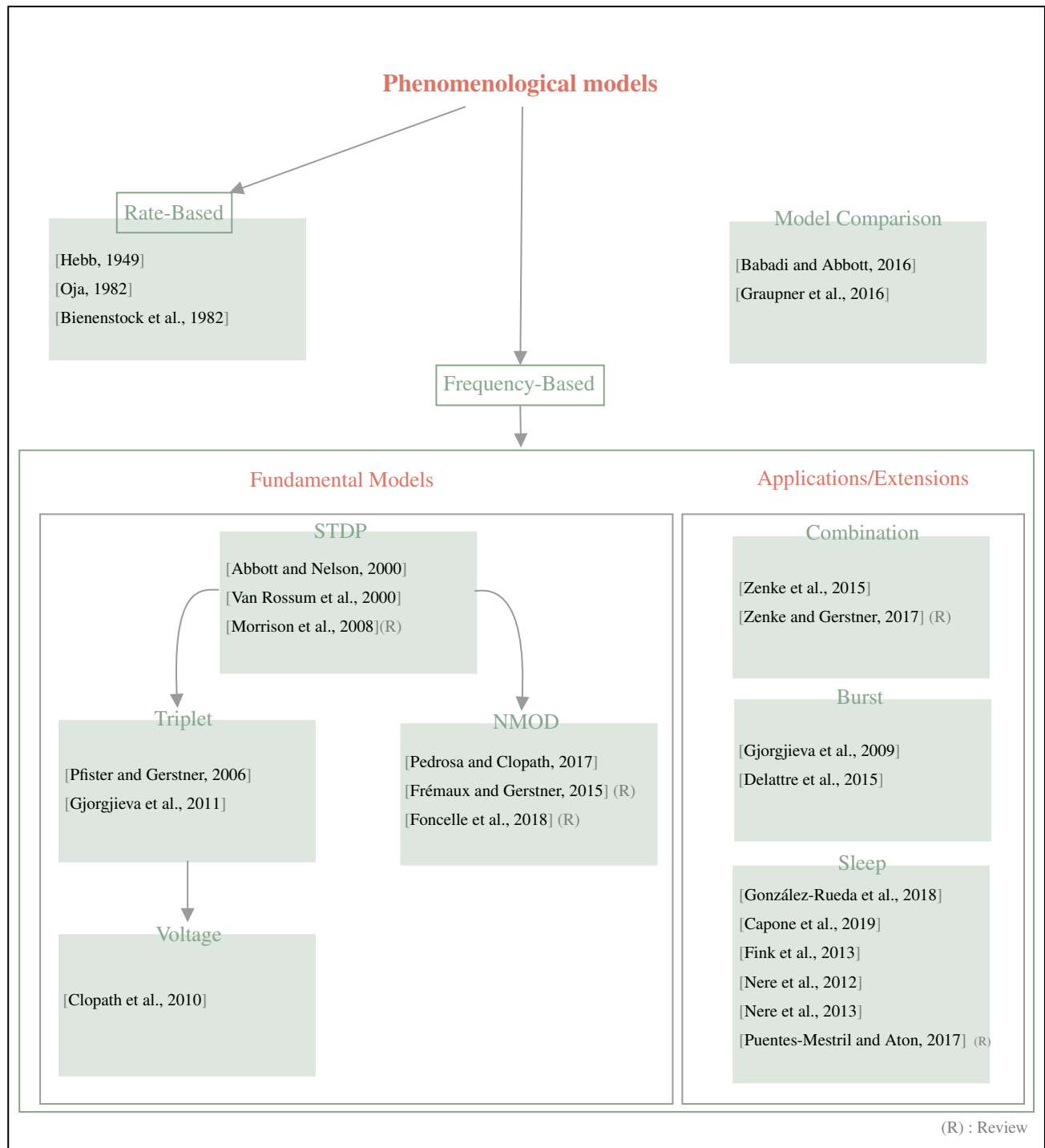
Figure 4.11 – *Abbreviations of modeling specifications used in TABLE 4.1*

Table 4.1 – *Computational phenomenological models of synaptic plasticity*. List of the different computational models used for synaptic plasticity. Displayed with authors and years, the name of the synaptic rule, the neuron model, the network size, the definition of w , the protocol used for parameters fitting, the memory task, the switch mechanism and a short description. Separated by (a) Wake and (b) Sleep. NS means *Not stated* and ND *Not Determined*.

	Authors	Synaptic rule	Neuron Model	Network Size	Definition w	Protocol	Memory task	Switch	Brief Summary
(a) Wake	[Gjorgjieva et al., 2009]	BTDP	IF	M FW	w	R	D	—	Introduction burst-timing-dependent plasticity to overcome STDP limitations and explain the segregations of ON/OFF retinal inputs during development.
	[Pfister and Gerstner, 2006]	Triplet	EB	S FW	w	C1 H1	/	—	Introduction of the Triplet model to overcome STDP limitations. The authors provide proof that the model reproduces more experimental protocols compared to classical STDP.
	[Delattre et al., 2015]	r-STDP	IF	L	w	C	/	—	The standard STDP curve is altered by application of network-generated bursts. A resource-dependant STDP may explain those results.
	[Zenke et al., 2015]	Combination	IF	XL	CS	NS	A	—	Implementation of synaptic plasticity with combination of models at various time scale. An associative task is performed and the model is to recall memories.
	[Clopath et al., 2010]	Voltage	IF	M	w	C1 C3 H2	A	—	Voltage-dependent STDP model able to reproduce a large panel of experimental data. Connectivity reflecting neural coding in a neuron network is shown.
	[Froemke and Dan, 2002]	Suppression	EB	S	w	C2	/	—	Experimental triplet protocol explained by a suppression model using short-term dependent plasticity principles.
	[Gjorgjieva et al., 2011]	Triplet	EB	M	EPSP	C1 H1	R	—	Triplet model (spike-timing based) can be rewritten to generalize the BCM model (rate-based)
	[Pedrosa and Clopath, 2017]	NMOD	LIF	M	I_{syn}	NS	D	—	Investigation of four different model with different STDP. Each represents the impact of different neuromodulators. The computational study examines the receptive field formation and adaptation by different.
(b) Sleep	[González-Rueda et al., 2018]	UP-mediated	LIF	S FW	w	C	/	synaptic rule change	Following SHY hypothesis, use of a standard STDP during wake and an UP-mediated learning rule during sleep which down-scale the synaptic weight during up-states of SWS. This allows preservation of biggest synaptic weights and depression of the others.
	[Fink et al., 2013]	STDP	C	L	I_{syn}	NS	/	conductance change	Addition of a slow K^+ conductance to model the different <i>Ach</i> levels in waking and sleep states. High synchronous network activity during sleep is shown and sleep period either depresses or potentiates to extreme values the different weights.
	[Capone et al., 2019]	STDP	IF	L	w	NS	A	manually induced	Implementation of a thalamocortical loop and reproduction of slow oscillations sleep to improve classification accuracy (digits recognition).
	[Nere et al., 2012]	Burst-STDP	LIF	L	I_{syn}	NS	A	synaptic scaling	Following SHY, sleep-like phase down-scale the synaptic weight (depression only). Making the assumptions that bursts are highly energetic events and should contain useful information, Burst-STDP is implemented during waking such as only potentiation occurs. Neuromodulation effect is added by using reward-based learning principle. The model is able to perform object recognition and motion anticipation tasks.
	[Nere et al., 2013]	Burst-STDP	IF	L	I_{syn}	NS	A	synaptic scaling	Similarly to the previous article, sleep-like phase down-scale the synaptic weight following <i>SHY</i> hypothesis. The model is able to explain the beneficial effects of sleep on various tasks: the consolidation of both procedural and declarative memories, on gist extraction, and on the integration of new memories with old ones .

4.4 Summary

Literature Review of Phenomenological Models of Plasticity



Part III

Computational study

Chapter 5

Integration of synaptic rule in a switching network: validation in *tonic* mode

After reviewing different types of models from the literature, some of them were implemented in a conductance-based model. As the ultimate goal of this project is to test the compatibility of plasticity rules with memory consolidation during sleep, a switching network able to switch from tonic to burst is needed. This conductance-based circuit therefore allows a better physiological representation. An *ECI* circuit of three neurons was used: one excitatory cortical (E) neuron connected to a cortical neuron (C) (with *AMPA* connection) as well as an inhibitory neuron (I) sending inhibitory connections to the two other cells (with *GABA_A* and *GABA_B* connections), see FIGURE 5.1 (A). The latter sets the pace of the circuit. Indeed, a high-frequency tonic rhythm puts the two others in silent mode, while a burst in the inhibitory neuron drives the whole circuit in bursting mode. Thus, the switch is obtained by hyperpolarising *I* only with an artificial current $I_{app,I}$. In this chapter, in order to recreate spike timing-based protocols, pulse currents were applied to the pre- and postsynaptic neurons in such a way that spikes were initiated at a given frequency with a given delay $\Delta t = t_{post} - t_{pre}$ (FIGURE 5.1 (B)).

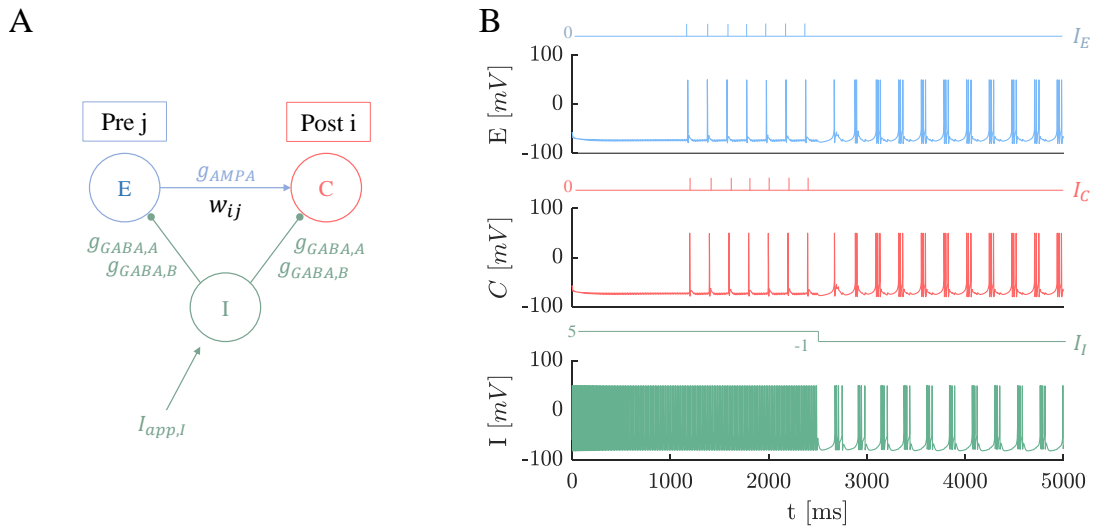


Figure 5.1 – *ECI circuit and achievable firing patterns*. **A.** Schematic representation of the ECI circuit, showing excitatory connection from cell E to cell C and inhibitory connections from cell I to cells E and C. **B.** Time course of the membrane voltage [mV] of the ECI circuit and the applied currents [nA] showing three firing patterns for cells E-C (top and middle): silent mode thanks to inhibition from cell I (bottom) which fires at high-frequency, tonic mode at a given frequency with $\Delta t = t_{post} - t_{pre} = 20[ms]$ and bursting mode in all cells driven by hyperpolarisation of cell I.

The connection between E (pre) and C (post) is where the plasticity will take place and be investigated during both tonic and bursting mode (next chapter) thanks to the switching network. As previously seen in the CHAPTER 4, different plasticity types are observed. In this model, the plasticity modulates the efficiency of the *AMPA* receptor from the cortical cell, controlling the strength of the connection in-between cells E and C. For more details on the conductance-based modeling, see APPENDIX C.

5.1 Model integration in conductance-based circuit (ECI)

Three models taken from the literature review will be further investigated:

- The *pair-based model* from [Abbott and Nelson, 2000] and reproduced by [Graupner et al., 2016].
- The *triplet model* from [Pfister and Gerstner, 2006] and also reproduced by [Graupner et al., 2016].
- The *voltage-dependent model* from [Clopath et al., 2010].

First, all those learning rules are implemented in-between the pre- (E) and postsynaptic (C) cells in the switching ECI circuit.

5.1.1 Pair-based model from [Abbott and Nelson, 2000, Graupner et al., 2016]

As already introduced in CHAPTER 4, pair-based model can be implemented thanks to the following equations:

$$\frac{dx_j}{dt} = -\frac{x_j}{\tau_x} + \sum_{t_j^f} \delta(t - t_j^f) \quad (5.1)$$

$$\frac{dy_i}{dt} = -\frac{y_i}{\tau_y} + \sum_{t_i^f} \delta(t - t_i^f) \quad (5.2)$$

representing the trace from presynaptic spikes (x_j) and postsynaptic spikes (y_i) with dynamics τ_x , τ_y and t_j^f , t_i^f respectively the timings of a pre- and postsynaptic spike. Then, synaptic weight changes following:

$$\begin{aligned} \Delta w_{ij}^+ (t_i^f) &= A_+ x_j (t_i^f) \\ \Delta w_{ij}^- (t_j^f) &= A_- y_i (t_j^f) \end{aligned} \quad (5.3)$$

where $A_+ > 0$, $A_- < 0$.

In this chapter, the synaptic weight will be either hard or soft-bounded such that $w \in [0 : 1]$.

The conversion from integrate-and-fire to conductance-based neuron model was simply put forth by defining a spike at time t when the cell membrane voltage $U(t)$ crosses a threshold taken as $0[mV]$, *i.e.* $U(t) > 0[mV]$ and $U(t-1) < 0[mV]$.

Parameters used as well as resolution of the different differential equations (voltage, traces, weight) can be found in APPENDIX D.

5.1.2 Triplet model from [Pfister and Gerstner, 2006, Graupner et al., 2016]

The following equations were used to implement the triplet model:

$$\begin{aligned}
\frac{dr_1(t)}{dt} &= -\frac{r_1(t)}{\tau_+} & \text{if } t = t^{\text{pre}} & \text{ then } r_1 \rightarrow r_1 + 1 \\
\frac{dr_2(t)}{dt} &= -\frac{r_2(t)}{\tau_x} & \text{if } t = t^{\text{pre}} & \text{ then } r_2 \rightarrow r_2 + 1 \\
\frac{d\sigma_1(t)}{dt} &= -\frac{\sigma_1(t)}{\tau_-} & \text{if } t = t^{\text{post}} & \text{ then } \sigma_1 \rightarrow \sigma_1 + 1 \\
\frac{d\sigma_2(t)}{dt} &= -\frac{\sigma_2(t)}{\tau_y} & \text{if } t = t^{\text{post}} & \text{ then } \sigma_2 \rightarrow \sigma_2 + 1
\end{aligned} \tag{5.4}$$

where t_{pre} (*resp.* t_{post}) is the timing of a presynaptic spike (*resp.* postsynaptic). Weight change goes as follows:

$$w(t) \rightarrow w(t) - o_1(t) [A_2^- + A_3^- r_2(t - \epsilon)] \text{ if } t = t^{\text{pre}} \tag{5.5}$$

$$w(t) \rightarrow w(t) + r_1(t) [A_2^+ + A_3^+ o_2(t - \epsilon)] \text{ if } t = t^{\text{post}} \tag{5.6}$$

The difference between [Pfister and Gerstner, 2006] and [Graupner et al., 2016] models is that the latter fits the model parameters implementing *soft bounds* ($w \in [0 : 1]$) while [Pfister and Gerstner, 2006] model is not bounded. However, in this thesis, hard bounds are added to stay in physiological range. Note that [Pfister and Gerstner, 2006] found that their model was able to reproduce experimental data with fewer parameters, calling it *minimal models*. In the following sections, minimal models will be used. All parameter sets can be found in APPENDIX D.

Similarly to the pair-based model, the conversion from simplistic integrate-and-fire to conductance-based neuron model was realised by defining spike timing when the membrane voltage $U(t)$ crosses a threshold ($0[mV]$) *i.e.* $U(t) > 0[mV]$ and $U(t - 1) < 0[mV]$.

Parameters used as well as illustration of temporal evolution can be found in APPENDIX D.

5.1.3 Voltage-dependent model [Clopath et al., 2010]

In the voltage-dependent model, weight change goes as follows:

$$\frac{d}{dt} w_{ji} = -A_{\text{LTD}} X_i(t) [\bar{u}_-(t) - \theta_-]_+ + A_{\text{LTP}} [u(t) - \theta_+]_+ x_i(t) [\bar{u}_+(t) - \theta_-]_+ \tag{5.7}$$

The voltage-based plasticity rule from [Clopath et al., 2010] failed to be converted into the conductance-based model.

First, the threshold values θ_+ and θ_- were originally taken as respectively the integrate-and-fire firing threshold and resting membrane potential (θ and u_{rest} in SECTION 2.3.2). In a more physiological model such as conductance-based model, such exact values cannot be known in advance since it depends on the neuronal type, the afferent connections, etc. Moreover, [Clopath et al., 2010] voltage-dependent model increases the synaptic strength w_{ij} when the membrane potential is above the threshold θ_+ . While for a non-linear integrate-and-fire model this corresponds to an infinitely small period of time, the dynamic of a physiological action potential reproduced by a conductance-based model is much slower.

For those reasons, the fitted parameters (accurate for an IF model) are unlikely to lead to satisfying results in a conductance-based model.

5.2 Experiments

Two plasticity rules were successfully implemented in this conductance-based model:

- The classical *pair-based* model from [Abbott and Nelson, 2000].
- The *Triplet* model from [Pfister and Gerstner, 2006] (*hard-bounded*) and the one from [Graupner et al., 2016] (*soft-bounded*).

To clarify the reading, papers corresponding to experimental protocols on which model parameters are fitted are indicated with \circ . Moreover, TABLE 5.1 summarises which experimental protocols the different models have been fitted on as well as the corresponding brain areas.

Model	Author	Fitted on experimental protocol \circ
Pair-based	[Abbott and Nelson, 2000]	[Bi and Poo, 1998] \circ (H)
	[Graupner et al., 2016]	[Bi and Poo, 1998] \circ (H)
Triplet	[Pfister and Gerstner, 2006]	[Wang et al., 2005] \circ (H) [Sjöström et al., 2001] \circ (C)
	[Graupner et al., 2016]	[Sjöström et al., 2001] \circ (C)

Table 5.1 – *Summary of different models that will be further investigated.* The circ (\circ) is for experimental protocols and (H) stands for hippocampus, (C) for cortex.

The following sections show the successful (or not) implementation of those plasticity rules by reproduction of experimental protocols based on spike timing (introduced in SECTION 3.3): STDP protocol as well as the behaviour with variability in the firing pattern and frequency dependence of STDP protocol.

5.2.1 Reproduction of STDP protocol

As already introduced in SECTION 3.3, spike timing-dependent plasticity was observed following protocols during which the precise timings of pre- and postsynaptic spikes were controlled [Bi and Poo, 1998] \circ . The experimental results show asymmetric potentiation and depression in the hippocampus. Significant potentiation was induced when a postsynaptic spike followed a presynaptic spike within a time window of 20[ms], whereas significant depression was observed when the presynaptic spike followed a postsynaptic spike within a window of 20[ms]. The first experiment realised on the ECI circuit (summarised in FIGURE 5.2) was to reproduce the STDP curve by introducing the different plasticity rules in-between pre and postsynaptic neurons. When parameters from the hippocampus were available, the repetition of pairings were realised following the experimental protocol, *i.e.* 60 pairings for each Δt at a frequency of 1 [Hz].

1 Reproduction of STDP protocol

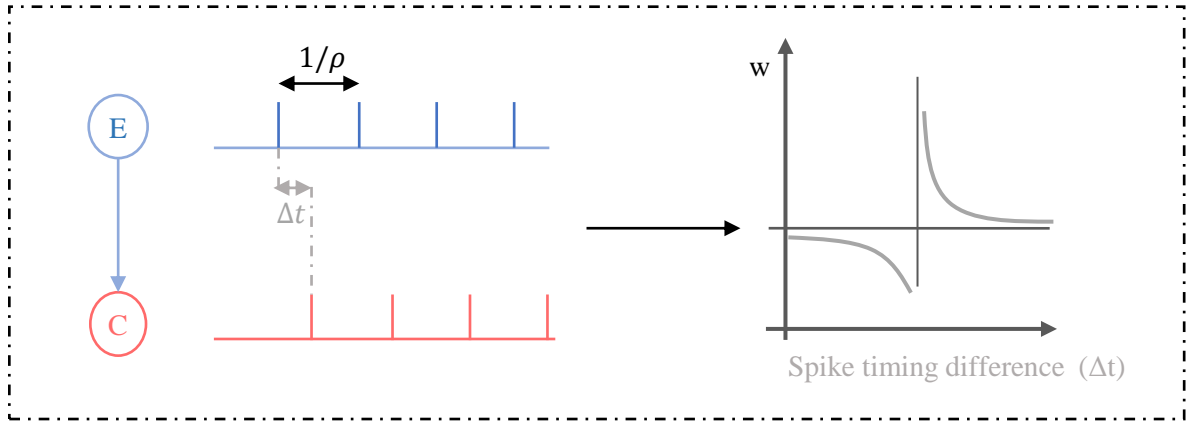


Figure 5.2 – *First experiment on plasticity rules.* Pairings at a given frequency were realised with $\Delta t = t_{post} - t_{pre}$ in order to reproduce the classical STDP curve. For each Δt , 60 pairings were realised and the percentage of w change was computed following $\frac{w_f - w_0}{w_0} * 100$.

Pair-based

This plasticity rule was first put forth by [Bi and Poo, 2001] after their well-known experimental spike timing-based protocol [Bi and Poo, 1998] ◦ described above. [Bi and Poo, 2001] provided a model fitting the exponential parameters from EQUATION 4.6 on those experimental data.

FIGURE 5.3 shows the reproduction of [Abbott and Nelson, 2000] model (implemented with traces from EQUATION 5.1) together with experimental results. As expected, the model reproduces the experimental trend. This proves that the model was implemented correctly.

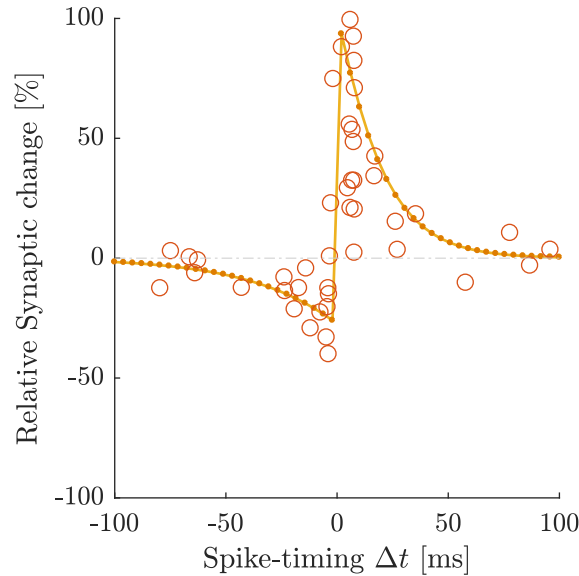


Figure 5.3 – *Reproduction of STDP curve for the pair-based model.* Large open circles represent experimental data while small filled circles are the computational data obtained following the experimental protocol from [Bi and Poo, 1998] ◦, *i.e.* 60 pairings repeated at 1 [Hz].

Triplet model

The same approach as pair-based model is taken concerning triplet models: verification of experimental results is first realised by reproducing STDP protocol.

As already stated in TABLE 5.1, the parameters from [Pfister and Gerstner, 2006] were fitted for two different protocols:

- [Sjöström et al., 2001] ◦ showing the frequency dependence of STDP in the visual (C).
- [Wang et al., 2005] ◦ demonstrating the effects of triplets and quadruplets experiments in the *hippocampus* (H).

Since experimental results from [Bi and Poo, 1998] ◦ (STDP protocol) were obtained in the hippocampus, the set of parameters used is the one corresponding to this brain region. As can be seen from FIGURE 5.4 (A), [Pfister and Gerstner, 2006] model fitted on [Wang et al., 2005] ◦ (H) is able to reproduce experimental results from [Bi and Poo, 1998] ◦, *i.e.* pairing for different time differences $\Delta t = t_{post} - t_{pre}$ at 1[Hz].

The parameters from [Graupner et al., 2016] triplet model were only fitted on cortical data. Thus, it makes no sense to reproduce the protocol observed on the hippocampus and expect to get the same result. Indeed, as it will be developed in the next section, [Sjöström et al., 2001] ◦ (C) observed that the amount of potentiation and depression in the cortex varies in function of the frequency. However, FIGURE 5.4 (B) shows, as an example, that the trend is preserved for a frequency of 10[Hz].

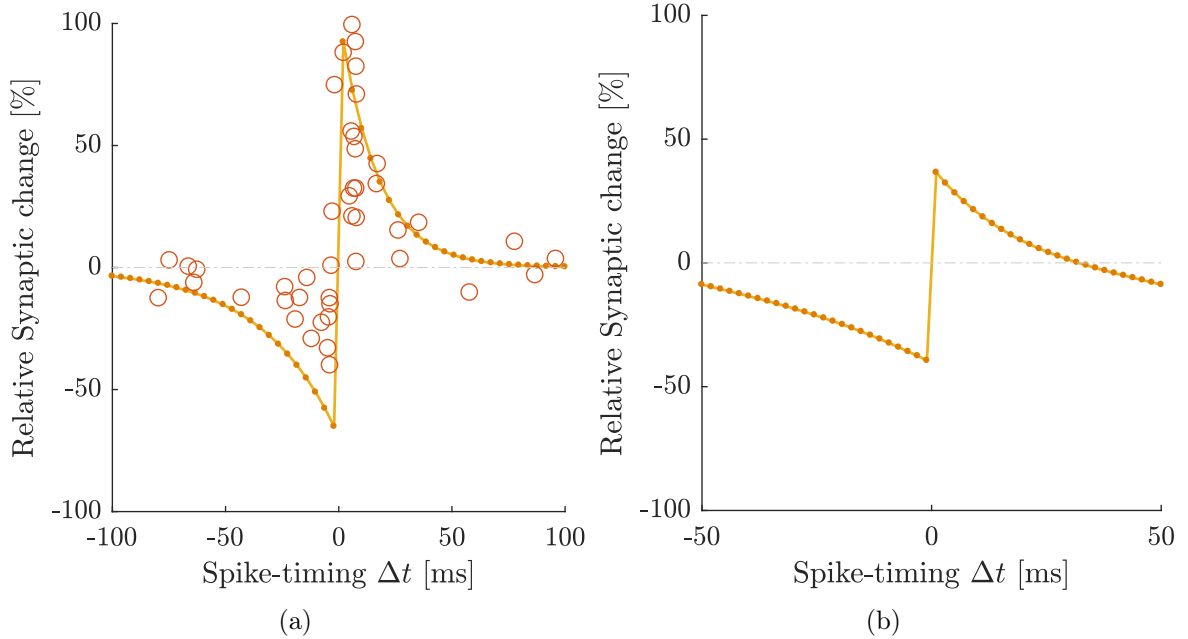


Figure 5.4 – *Reproduction of STDP curve for the triplet model from (a) [Pfister and Gerstner, 2006]: open circles represent experimental data from [Bi and Poo, 1998] ◦, filled circles the computational data in the ECI network obtained following the experimental protocol from [Bi and Poo, 1998] ◦ (60 pairings at 1[Hz]). (b) [Graupner et al., 2016]: filled circles are the computational data obtained with 60 pairings repeated at 10 [Hz]. No experimental data is shown since [Bi and Poo, 1998] ◦ experiment is realised in the hippocampus and [Graupner et al., 2016] parameters are for the cortex.*

Note that the curve seems to be shifted since depression is observed for high values of $\Delta t > 0$. This feature will be explained in SECTION 5.2.2.

5.2.2 Adding variability

2 Adding variability to STDP protocol

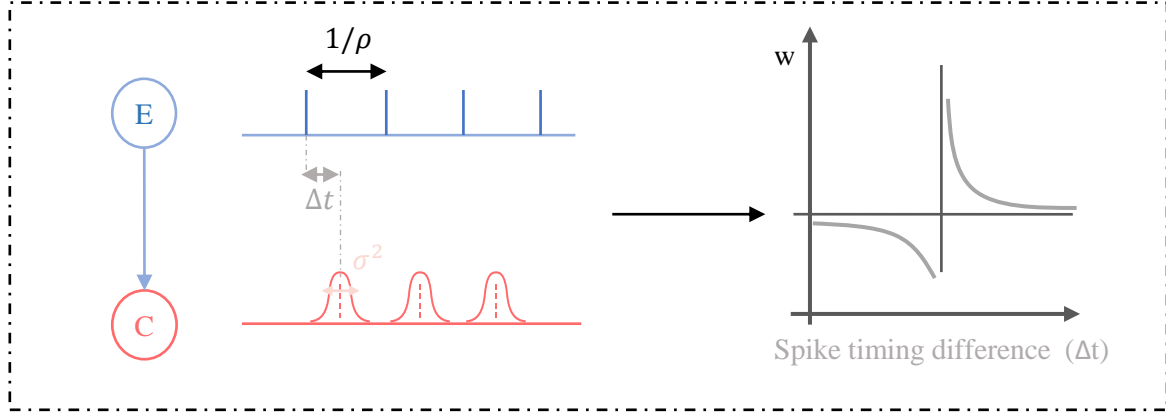


Figure 5.5 – *Second experiment on plasticity rules*. In order to see the impact of firing variability on the STDP curve, pairings were simulated with a presynaptic spike firing at given frequency (20 [Hz]) and postsynaptic spike firing following a Gaussian distribution with $\Delta t = t_{\text{post}} - t_{\text{pre}}$: $\Delta t \sim \mathcal{N}(\mu, \sigma)$, $\mu = \Delta t$, $\sigma \in [0.1 : 10]$. For each σ and each Δt , 60 pairings were realised and the percentage of w change was computed following $\frac{w_f - w_0}{w_0} * 100$.

In vivo firing patterns are far from being as regular [Softky and Koch, 1993]. Here, the plasticity rule was tested by adding variability to the firing pattern. The presynaptic neuron was firing at a given frequency of 20[Hz] but irregularity in the delay of the postsynaptic neuron was added. Taking the period $T = \frac{1}{f}$ and $n = 1, 2, 3, \dots$ the n^{th} -paired presynaptic spike, the firing time of the postsynaptic cell ($n * T + \Delta t$) was randomly computed, Δt following a Normal distribution

$$\Delta t \sim \mathcal{N}(\mu, \sigma)$$

where $\mu = \Delta t$ is the mean of the Normal distribution and $\sigma \in [0.1 : 10]$ the standard deviation.

FIGURE 5.5 summarises this experiment. For each σ value, the STDP curve was reproduced and for each Δt , 60 pairings were realised. Parameters from cortical data were used for the triplet models.

Pair-based

As can be observed from FIGURE 5.7 small Gaussian mean ($\mu = \Delta t$) were sensitive to variations of σ while for higher values of μ the impact was less important. This seems logical since increasing the Gaussian width for small Δt increases the probability of shifting positive Δt (pre-post pairs) to negative values (post-pre pairs) and inversely. An illustration of the different Normal distributions for a small $\mu = \Delta t$ is shown in FIGURE 5.6. In addition, the window for small values of $|\Delta t|$ is the one in which biggest synaptic change occurs, while for bigger $|\Delta t|$ the change is much lower.

Interestingly, increasing the Gaussian width does not only decreases the maximum of potentiation and depression but shifts them to higher values of $|\Delta t|$ (see FIGURE 5.7). The maximum depression and potentiation values can be found in TABLE 5.2. Some values are outliers of the main trend but this is due to the fact that the protocol only considers 60 pairings for each Δt . Some noise thus appears in the data.

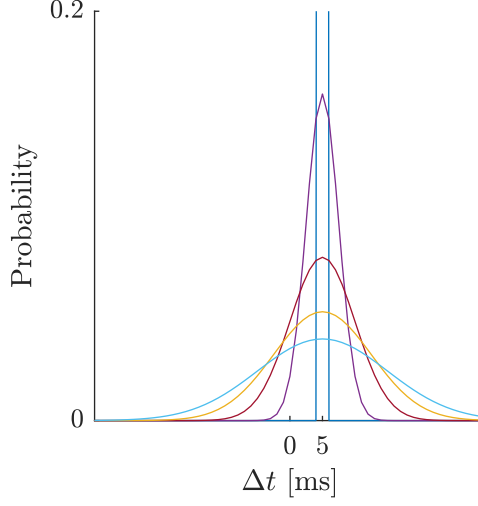


Figure 5.6 – *Different Gaussian distribution centered in $\mu = 5$, for 5 values of $\sigma \in [0.1 : 2.45 : 10]$. Increasing σ leads, in increasing order, to the curves represented in : blue, purple, red, yellow and light blue curves. For small μ such as this one, increasing the σ results in increasing the probability of having $\Delta t < 0$, resulting in depression. In the same way, small $\mu < 0$ would result in a non-zero probability of having $\Delta t > 0$, resulting in potentiation.*

std	0.1	2.5	5	7.5	10	std	0.1	2.5	5	7.5	10
minimum [%]	-67.8	-56.7	-44.8	-35.0	-26.7	maximum [%]	83.4	59.6	42.6	33.1	22.8
peak timing [ms]	-2.55	-6.63	-9.69	-13.77	-10.71	peak timing [ms]	2.55	4.59	7.65	9.69	11.73

Table 5.2 – *Maximum (potentiation) and minimum (depression) of the STDP curve for the pair-based model with variability. Increasing the variance decreases the values and shifts the extrema to higher $|\Delta t|$.*

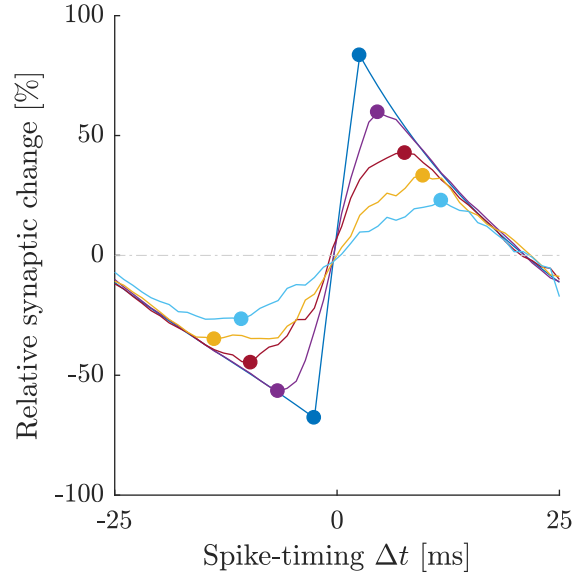


Figure 5.7 – *STDP curve with firing variability for the pair-based model. For each curve and each Δt , 60 pairings were repeated at 20 [Hz]. Postsynaptic neuron fires with a time difference Δt with probability following a Normal distribution: $\Delta t \sim \mathcal{N}(\mu, \sigma)$ where $\mu = \Delta t$ and $\sigma \in [0.1 : 10]$. The different σ are the different curves: blue, purple, red, yellow and light blue curves (increasing σ in this particular order).*

Note that for value of approximately $\Delta t > 20$, the relative synaptic change goes under 0 (FIGURE 5.7), which is not observed for experimental protocols at 1[Hz] as it can be seen from FIGURE 5.3. Since the model is implemented by traces decaying exponentially, it seems logical that for high frequencies like this one, the trace from one spike is not completely restored to its initial value when another spike appears. Indeed, the value of τ_+ (relative to the exponential decrease of the trace x for the presynaptic spike) is lower than τ_- (relative to the exponential decrease of the trace y for the postsynaptic spike), *i.e.* the presynaptic trace decays faster than the postsynaptic one. This results in more depression than potentiation. It can be illustrated in FIGURE 5.8 taking only τ_+ and τ_- . The same effect is observed for the triplet model (FIGURE 5.4 AND 5.9): using the minimal model, potentiation is proportional to σ_2 (τ_y) and r_1 (τ_+) and depression to σ_1 (τ_-). Thus, when Δt is higher, pre-post-pre triplets have less impact because $\tau_+ \ll \tau_-$ leading to more depression. Illustration is shown in FIGURE 5.8 taking the three traces into account.

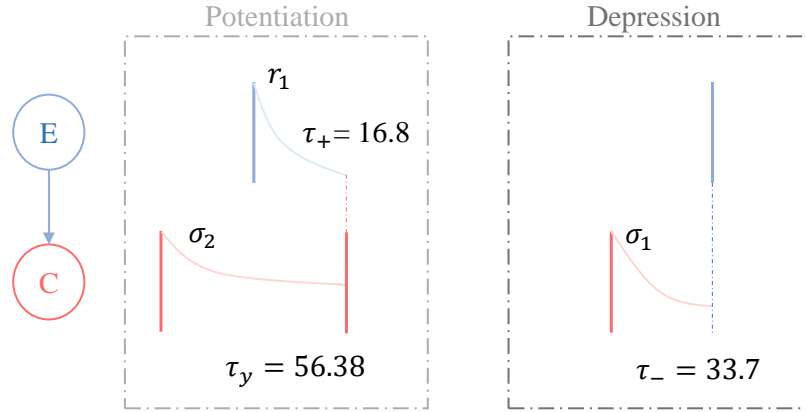


Figure 5.8 – Scheme illustrating that less potentiation is observed for the triplet model (high Δt). Amount of potentiation is proportional to r_1 , σ_1 and depression to σ . r_1 decays faster and for high value of Δt , the potentiation amount is way lower.

Triplet

Similarly to pair-based model, increasing the variance decreases and shifts the maximum of depression and potentiation (see FIGURE 5.9). The maximum values from [Pfister and Gerstner, 2006] are much higher because hard bounds are applied.

std	0.1	2.5	5	7.5	10	std	0.1	2.5	5	7.5	10
minimum [%]	-40.4	-34.1	-28.9	-25.5	-19.7	maximum [%]	31.8	23.7	17	9.6	3.6
peak timing [ms]	-2.55	-5.61	-6.63	-9.69	-13.77	peak timing [ms]	2.55	4.59	8.67	9.69	15.81

Table 5.3 – Maximum (potentiation) and minimum (depression) of the STDP curve for the [Graupner et al., 2016] triplet model with variability. Increasing the variance decreases the values and shifts the extrema to higher $|\Delta t|$.

std	0.1	2.5	5	7.5	10	std	0.1	2.5	5	7.5	10
	●	●	●	●	●		●	●	●	●	●
minimum [%]	-90.9	-73.7	-58.3	-48.2	-41.2	maximum [%]	98.0	80.7	59.8	44.1	25.3
peak timing [ms]	-2.55	-5.61	-9.69	-13.77	-12.75	peak timing [ms]	2.55	4.59	7.65	9.69	5.61

Table 5.4 – *Maximum (potentiation) and minimum (depression) of the STDP curve for [Pfister and Gerstner, 2006] triplet model with variability.* Increasing the variance decreases the values and shifts the extrema to higher $|\Delta t|$.

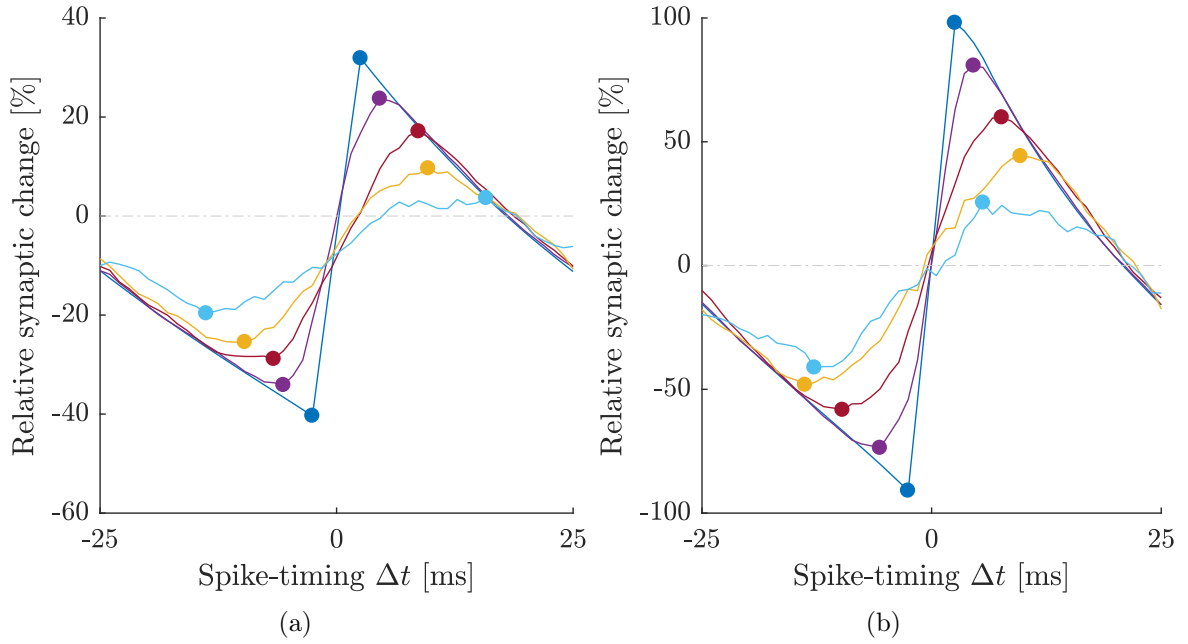


Figure 5.9 – *STDP curve with firing variability for the triplet model from (a) [Graupner et al., 2016] (b) [Pfister and Gerstner, 2006].* For each curve and each Δt , 60 pairings were repeated at 20 [Hz]. Postsynaptic neuron fires with a time difference Δt with probability following a Normal distribution: $\Delta t \sim \mathcal{N}(\mu, \sigma)$ where $\mu = \Delta t$ and $\sigma \in [0.1 : 10]$. The different σ are the different curves: blue, purple, red, yellow and light blue curves (increasing σ in this particular order).

5.2.3 Reproduction of frequency effect on STDP protocol

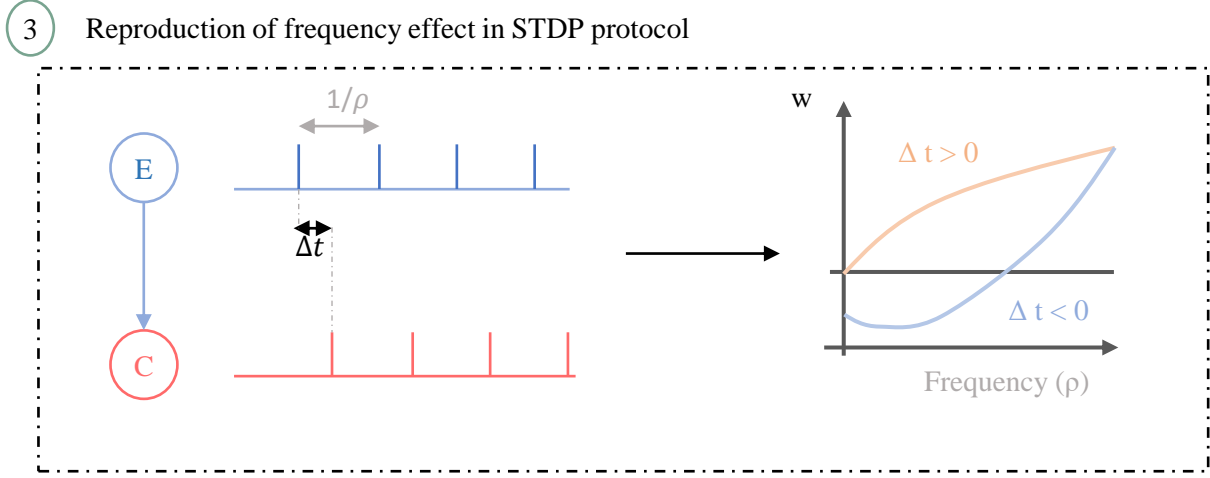


Figure 5.10 – *Third experiment on plasticity rules*. For $\Delta t = 10$ and $\Delta t = -10$, 60 pairings were realised and the percentage of w change was computed following $\frac{w_f - w_0}{w_0} * 100$.

[Sjöström et al., 2001] ◦ show that spike timing protocol results in different synaptic changes as a function of the spiking rate in the cortex. In other words, for a given Δt , the result of a spike timing protocol is different, meaning that the STDP curve varies as a function of the pairing frequency. The results of [Sjöström et al., 2001] ◦ suggest that

- amount of potentiation increases with frequency, even for $\Delta t < 0$.
- at very low frequencies, no potentiation is observed.

The curves originating from the different models in FIGURE 5.11 (in a IF model) are reproduced in the conductance-based circuit (ECI) in FIGURES 5.12 AND 5.13 by following the experiment illustrated in FIGURE 5.10. On those figures, two distinct protocols will be represented (which are summarised in TABLE 5.5):

- The exact experimental protocol followed by [Sjöström et al., 2001] ◦ (grey). In this original protocol, presynaptic spikes are paired with postsynaptic spikes advanced by $\Delta t = 10ms$ or delayed by $\Delta t = -10ms$. For $\rho = 0.1Hz$, 50 pairs were induced while for $\rho > 0.1Hz$ 5 pairings followed by time breaks were repeated 15 times.
- Authors protocols differing as depending on the model, see description of the protocols on each section (orange).

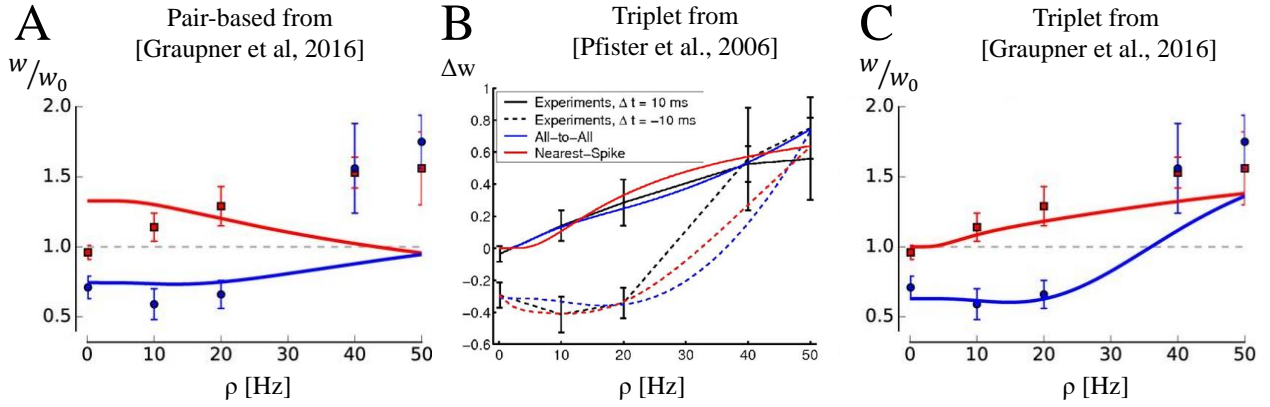


Figure 5.11 – *Original curves of different models simulating the frequency effect of STDP with IF spiking neurons.* **A.** Pair-based model from [Graupner et al., 2016] **B.** Triplet model from [Pfister and Gerstner, 2006] **C.** Triplet model from [Graupner et al., 2016].

Author	Author protocol	Experimental protocol from [Sjöström et al., 2001] ◦
Graupner 2016 (pair-based)	No matter the frequency, 75 pairings	For $\rho > 0.1$ [Hz] : 5 * 15 pairings separated by time breaks. For $\rho = 0.1$ [Hz]: 50 pairings without break
Graupner 2016 (triplet)		
Pfister 2006 (triplet)	No matter the frequency, 60 pairings	

Table 5.5 – *Summary of protocols.* Authors computational protocols are compared with the experimental protocol followed by [Sjöström et al., 2001] ◦.

Pair-based

As can be seen in FIGURE 5.12, the classical pair-based model fails to reproduce such results. First, even at very low frequency, when a postsynaptic spike follows a presynaptic spike, the amount of potentiation is never equal to 0 because the only potentiation term depends on A^+ . This value cannot be negative since it fits STDP results from [Bi and Poo, 1998]. Second, increasing the frequency means that pre-post pairs are getting closer. Thus, the postsynaptic spike of one pair is approaching the presynaptic spike of the next one and it induces depression (as a new post-pre pair). This is opposite to experimental results.

The orange curves reproduce results from [Graupner et al., 2016] using the pair-based model with soft bounds, simulating 75 pairings without time breaks and no matter the frequency. This difference does not drastically change the trend of the curves if applied to the exact protocol (grey).

Note that [Graupner et al., 2016] implement soft bounds in the pair-based model but use model parameters from [Bi and Poo, 2001] which is not implemented with soft bounds.

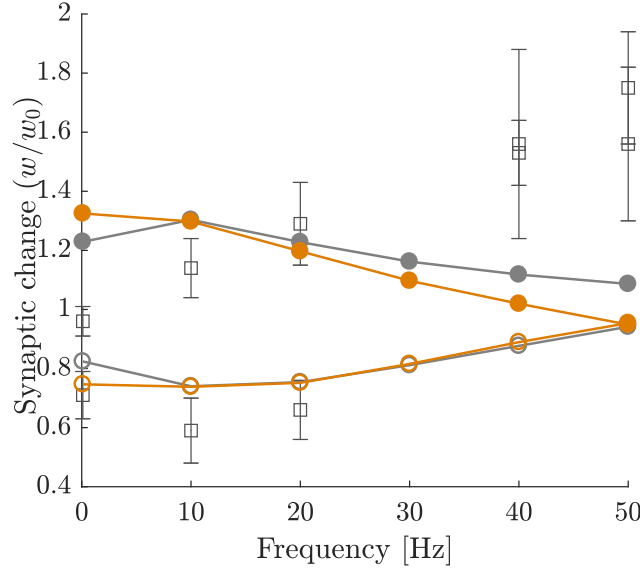


Figure 5.12 – Reproduction of pair-based protocol at different frequencies [Sjöström et al., 2001] using pair-based model. Filled circles $\Delta t = t_{post} - t_{pre} = +10ms$ and unfilled circles $\Delta t = -10ms$ (grey). Following the exact protocol by [Sjöström et al., 2001], i.e. for $\rho > 0.1Hz$ 15 repetitions of 5 pairings followed by breaks and for $\rho = 0.1Hz$ 50 pairings without a break. (orange) following method by [Graupner et al., 2016], i.e. each for each frequency 75 pairings without a break. Grey squares represent experimental data plus standard deviation.

Triplet

Conversely, triplet models from [Pfister and Gerstner, 2006] and [Graupner et al., 2016] are able to reproduce the experimental observation from [Sjöström et al., 2001] o. First, setting A_2^+ (*i.e.* the potentiation term linked to a pre-post pair) to a low value enables the absence of potentiation at low frequency. In the minimal model, A_2^+ is even set to 0. Then, increase of potentiation with frequency is achieved because the potentiation parameter A_3^+ has a bigger impact than the depression term A_3^- . The synaptic weight changes for both models as a function of the frequency are shown in FIGURE 5.13. As for the pair-based model, the orange curve reproduces the authors' results while the grey curve is obtained after following the exact protocol.

On one hand, [Pfister and Gerstner, 2006] simulate 60 pairings no matter the frequency and without a break. On the other hand, [Graupner et al., 2016] use a similar method but with 75 pairings (TABLE 5.5). However, using the fitted parameters to reproduce the exact protocol (grey curves) the results are much different, especially for [Pfister and Gerstner, 2006] model. Indeed, since exponentially decaying traces are used to implement the synaptic weight change, making time breaks in between sets of pairings makes a difference. The traces have thus the time to decay and differences are expected. Consequently, the models do not fit the exact experimental data.

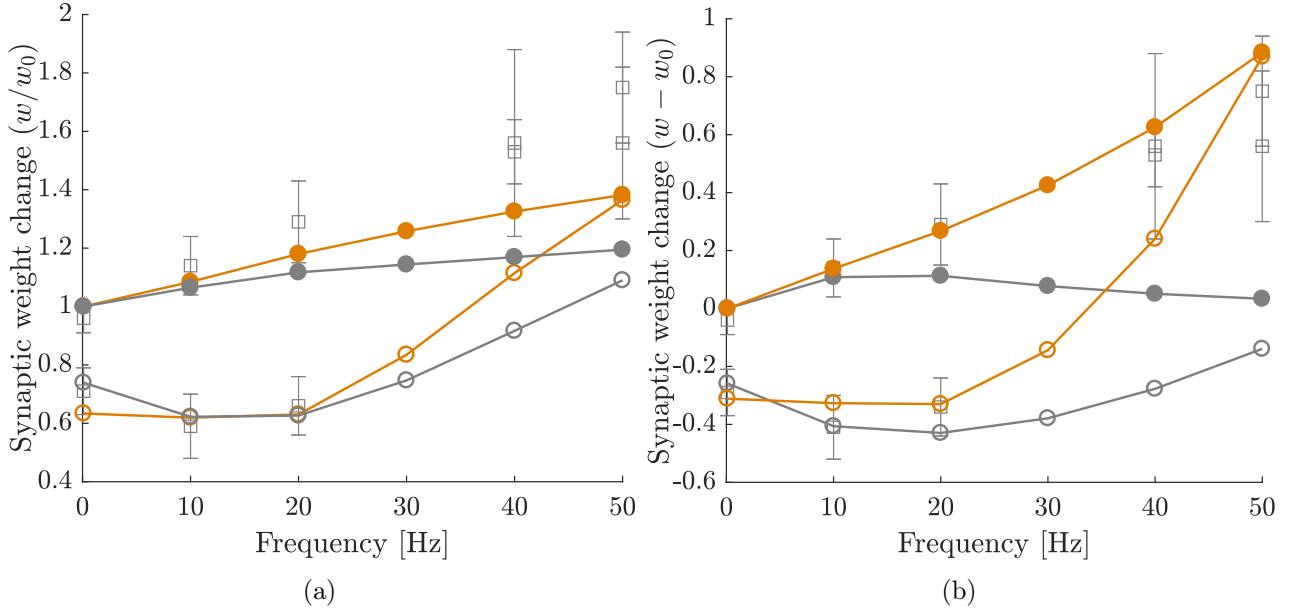


Figure 5.13 – Reproduction of pair-based protocol at different frequencies [Sjöström et al., 2001] o using triplet model from (a) [Graupner et al., 2016] (b) [Pfister and Gerstner, 2006]. Filled circles $\Delta t = t_{post} - t_{pre} = +10ms$ and unfilled circles $\Delta t = -10ms$ (grey) Following the exact protocol by [Sjöström et al., 2001] o, *i.e.* for $\rho > 0.1Hz$ 15 repetitions of 5 pairings followed by breaks and for $\rho = 0.1Hz$ 50 pairings without a break. (orange) following method by [Graupner et al., 2016], *i.e.* each for each frequency 75 pairings without a break or by [Pfister and Gerstner, 2006] 60 pairings without a break. The convention of the original papers are taken for the y-axis to exactly reproduce the curves. Grey squares represent experimental data plus standard deviation.

5.3 Summary

CONTRIBUTIONS

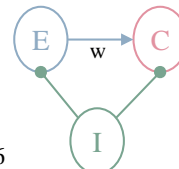
1 From integrate-and-fire to conductance-based model

Classical pair-based



Triplet model:

- Pfister et al., 2006
- Graupner et al., 2016



Voltage-based model

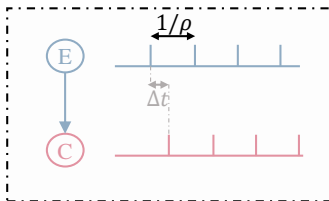
- Clopath et al., 2010

No straightforward application in conductance-based model

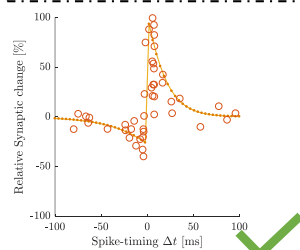


2 Experiments

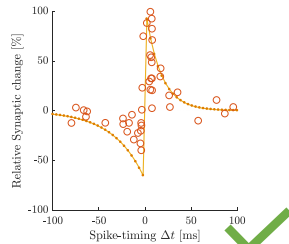
1 STDP protocol



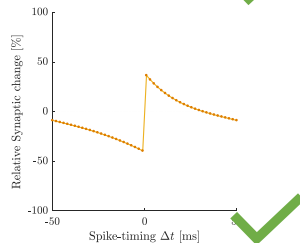
Pair-based



Triplet from [Pfister et al. 2006]

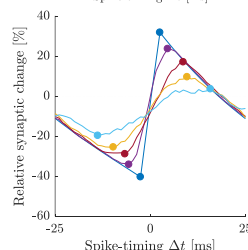
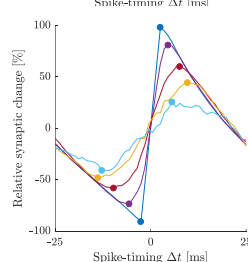
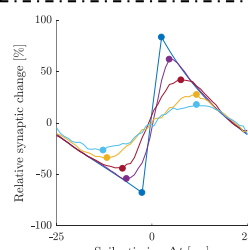
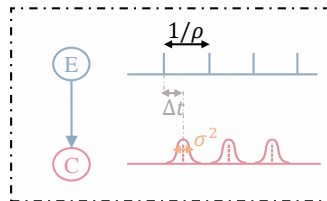


Triplet from [Graupner et al. 2016]



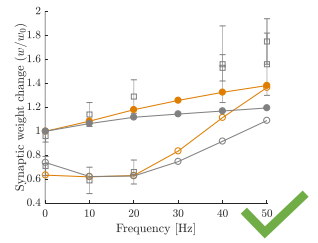
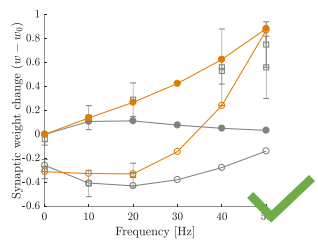
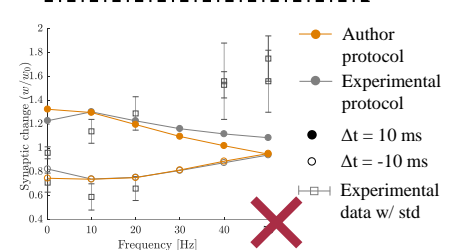
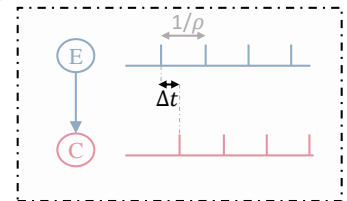
- Successful model reproduction.
- Only pair-based model and [Pfister et al., 2006] triplet were fitted for the hippocampus (experimental data).

2 STDP protocol w/ variability



Maximum of potentiation and depression shifted and decreased with increasing variability

3 Frequency effect



- Only triplet model is able to reproduce frequency effect.
- Authors did not fit their models on the exact exp. protocol.

Chapter 6

Compatibility of plasticity rules with memory consolidation during sleep in *bursting* mode

As memory consolidation occurs during sleep, it is of obvious interest to find a learning rule that is compatible with sleep firing pattern, *i.e.* bursting. Now that learning rules taken from the literature have been reproduced in a switching circuit, let us investigate their behaviour when neurons show burst firing. Two hypotheses can be expected:

- *SHY*, already introduced in SECTION 4.2.6: learned memories during wake (resulting in bigger weights) are preserved during sleep while smaller weights are depressed [Tononi and Cirelli, 2014].
- *Active system consolidation* : learned memories during wake (resulting in bigger weights) are replayed during sleep and thus consolidated while smaller weights are depressed [Klinzing et al., 2019, Feld and Born, 2017].

Thus, this chapter finds out if the implemented learning rules are compatible with one of those hypotheses of memory consolidation during sleep, *i.e.* during a period of burst (illustration in FIGURE 6.1).

The same ECI circuit is used. Note that, compared to usually used IF neuron model, the conductance-based neuron model implemented is a powerful tool to constrain bursts to behave like physiological ones. In order to reproduce different sleep rhythms, different hyperpolarisation steps have been applied to the inhibitory cell $I_{app,I} \in [-3.9 : 0.1 : -4.7]$ (nA). This results in different burst patterns in cells E-C with different parameters:

- Intraburst frequency (*IBF*): $IBF \in [42.4 : 69.2][Hz]$
- Interburst period (*PER*): $PER \in [198 : 333][ms]$
- Spikes-per-burst (*SPB*): $SPB \in [2 : 3]$

Those values are the same regardless of w_0 . Exact parameters values for each $I_{app,I}$ can be found on APPENDIX E.1.

To mimic the situation in which new information has been learned during the day, different initial weights ($w_0 \in [0 : 1.]$) are taken to imitate the different memory levels after the waking state. Then, the different sleep rhythms are induced by applying different hyperpolarisation steps $I_{app,I}$ on cell I. The final value of w after a sleep (*i.e.* bursting) period is extracted to check whether or not the model

is able to consolidate memory during sleep. This protocol is first applied in a *perfect world* in which the pre- and postsynaptic cells are identical. The bursting ability from the pre- and postsynaptic cells are similar and have always the same properties for every $I_{app,I}$. Then, this protocol is applied in a *realistic world* in order to mimic variability between neurons by adding 1% of variability into intrinsic conductances (g_{ions}) of the two neurons. The pair-based and triplet models are evaluated applying both hard and soft bounds.

Pre- and postsynaptic neurons are connected through an *AMPA* conductance (see APPENDIX C):

$$g_{AMPA} = g_{EC} * w$$

While the synaptic weight w can be seen as the *efficiency* of the receptors, differences between weak ($g_{EC} = 0.01$) and strong ($g_{EC} = 0.5$) *AMPA* conductances is evaluated, *i.e.* synapses with respectively low and high *connectivity*.

6.1 In a perfect world

The computational experiment is illustrated in FIGURE 6.1.

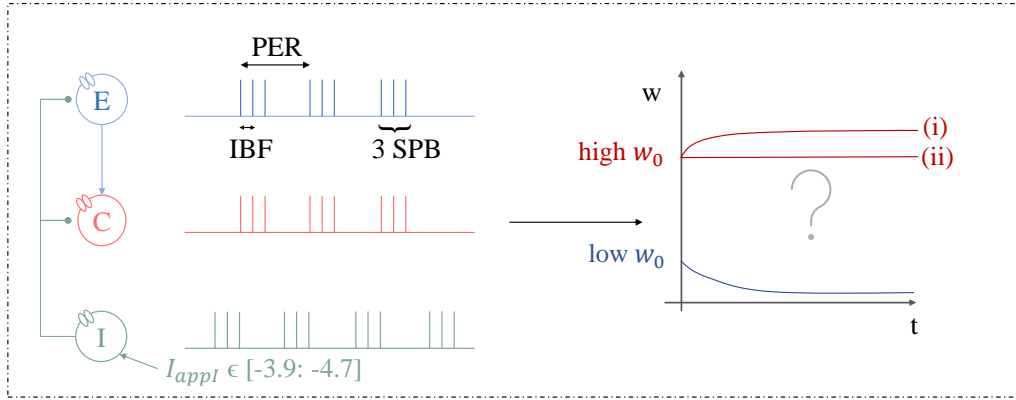


Figure 6.1 – *Computational experiment: plasticity rules tested in bursting activity.* Different $I_{app,I}$ are applied to the inhibitory cell, driving the whole circuit in bursting mode with different bursting features (intraburst frequency *IBF*, interburst period (*PER*), spikes per burst *SPB*) mimicking different potential sleep patterns. The impact of a bursting (*i.e.* sleep) period on the synaptic weights is evaluated to investigate whether or not the different models can reproduce one memory consolidation hypothesis, *i.e.* (i) *Active system consolidation*: big weights are potentiated and small weight depressed (ii) *SHY*: big weight are preserved while small weights are depressed.

General results

FIGURE 6.2 summarises the different temporal evolution for both *hard* (*HB*) and *soft* (*SB*) bounds applied to the *pair-based* and *triplet* models and for low and high connectivities (g_{EC}). The analysis of the different cases will be investigated here under.

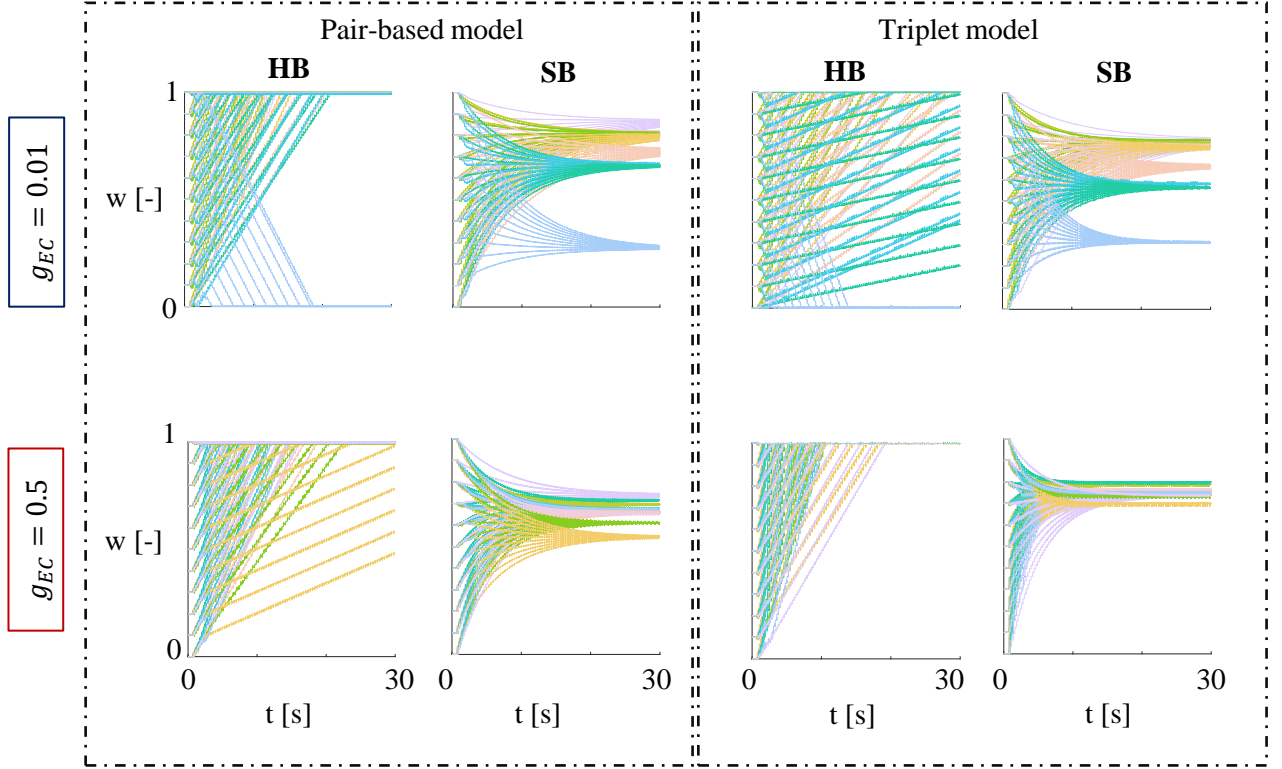


Figure 6.2 – Temporal evolution of the weight values (w) for both pair-based and triplet models implemented with hard (HB) and soft bounds (SB) and for different connectivity strengths (g_{EC}). Different colors represent the different $I_{app,I}$ values.

6.1.1 Synapse with low connectivity

Pair-based model

FIGURE 6.2 (TOP, LEFT) exposes the temporal evolution of the synaptic weights (w) for the *pair-based model* implemented with hard and soft bounds and for low connectivity, *i.e.* $g_{EC} = 0.01$. As a reminder, hard bounds are added by imposing a maximum and minimum value that can not be exceeded, as implemented in [Pfister and Gerstner, 2006] triplet model. By contrasts, soft bounds are obtained adding a weight dependence to the potentiation and depression parameters (see SECTION 4.2.1), as implemented by [Graupner et al., 2016] triplet model:

$$A_+(w) = (w^{max} - w) \eta_+ \quad \text{and} \quad A_-(w) = w \eta_-$$

Using the same model but changing only the bound has drastic consequences:

- **Hard bounds:** The weights all go to extreme values with a rate depending on $I_{app,I}$ regardless the initial value of w_0 (at the beginning of the sleep stage). In FIGURE 6.2, lines of the same colors correspond to a given $I_{app,I}$. One can observe that the lines are parallels meaning that the rates are similar regardless of w_0 and thus w_F will be identical.
- **Soft bounds:** The weights reach a steady-state value depending on $I_{app,I}$ in-between the two extrema. This seems logical given the definition of soft bounds: the closer the weight to $w_{max} = 1$ (*resp.* $w_{min} = 0$), the more preponderant depression (*resp.* potentiation).

In both cases, the value taken by $I_{app,I}$ determines the final value of w . Those values are summarised in TABLE 6.1. Consequently, it means that small weights as well as big weights have exactly the same behaviour during sleep. After a bursting period, the synaptic weights resulting from learning during the day are all reset to the same value. As this model was already flawed in *tonic mode*, it is definitively not a plasticity rule compatible with the hypothesis of memory consolidation during sleep.

$I_{app,I}[nA]$	-4.7	-4.6	-4.5	-4.4	-4.3	-4.2	-4.1	-4.0	-3.9
HB	1	1	1	1	1	1	1	0	1
SB	0.813	0.723	0.794	0.805	0.808	0.66	0.66	0.28	0.86

Table 6.1 – *Final value of the weight depending on $I_{app,I}$ for the pair-based model with (HB) hard bounds (SB) soft bounds, no matter the value of w_0 .*

Triplet model

The exact same protocols have been applied to the triplet model from both [Pfister and Gerstner, 2006] (hard bounds) and [Graupner et al., 2016] (soft bounds). The results are surprising: the behaviour of the models in bursting mode are strangely similar to the behavior of the pair-based model with hard and soft bounds, see FIGURE 6.2 (TOP, RIGHT) and TABLE 6.2:

- **Hard bounds [Pfister and Gerstner, 2006]:** The weights also evolve towards extreme values with a rate depending on $I_{app,I}$. However, after 30 [s] the final value has not always been reached yet compared to the pair-based model. This makes sense considering that [Pfister and Gerstner, 2006] triplet’s potentiation parameter (A_3^+) is smaller than the potentiation parameter of the pair-based model.
- **Soft bounds [Graupner et al., 2016]:** The weights stabilise to a fixed point depending on $I_{app,I}$ in-between the two extrema. The stabilisation is faster than for the pair-based model because [Graupner et al., 2016] have chosen bigger potentiation and depression parameters. (A_+^3 and A_-^2). The steady-states values are also varying from one model to another because of those different parameters.

$I_{app,I}[nA]$	-4.7	-4.6	-4.5	-4.4	-4.3	-4.2	-4.1	-4.0	-3.9
HB	1	0.92	1	1	1	0.67	0.77	0	1
SB	0.76	0.66	0.75	0.77	0.78	0.56	0.58	0.3	0.77

Table 6.2 – *Final value of the weight depending on $I_{app,I}$ for the triplet model with (HB) hard bounds [Pfister and Gerstner, 2006] (SB) soft bounds [Graupner et al., 2016], regardless of the value of w_0 .*

Furthermore, one can wonder why for the pair-based (*resp.* triplet) models with hard bounds (FIGURES 6.2 (TOP, LEFT), *resp.* (TOP, RIGHT)) only one value of $I_{app,I}$ decreases all the weights to 0 (*resp.* smaller values) while all the other reach the maximum weight (*resp.* higher values). As shown in FIGURE 6.3 (example for the triplet model), an hyperpolarisation step of $I_{app,I} = -4.2[nA]$ leads to potentiation while the only value leading to depression is $I_{app,I} = -4[nA]$. This is due to the fact that the presynaptic spikes are slightly delayed or advanced, respectively. A similar conclusion can be drawn for the pair-based model and reveals robustness-deficiency of the models since they are highly sensitive to very small variability. As the applied current corresponds to modulations to switch in sleeping mode, it shows variability *in vivo*. Thus, since a small variation leads to completely different synaptic weights, it is not compatible with more realistic situations. A same weight will be either completely depressed or either completely potentiated with a slightly different sleeping mode.

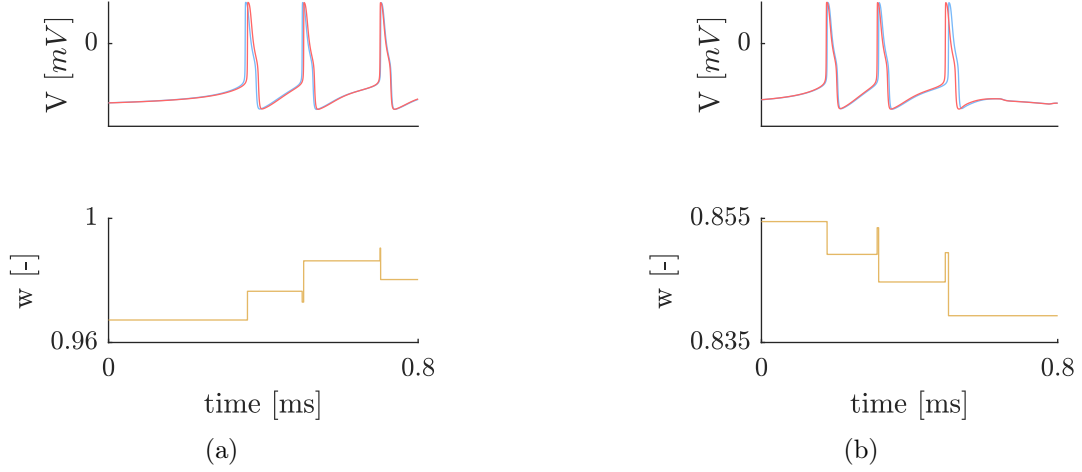


Figure 6.3 – *Robustness deficiency of triplet model*. Presynaptic (blue) and postsynaptic (pink) bursts for different $I_{app,I}$ (a) $I_{app,I} = -4.2$ [nA], resulting in potentiation because the postsynaptic burst is slightly delayed while for (b) $I_{app,I} = -4$ [nA], resulting in depression because the postsynaptic burst is slightly advanced.

6.1.2 Synapse with high connectivity

Pair-based model and triplet model: General Conclusions

FIGURE 6.2 (BOTTOM, LEFT) and (BOTTOM, RIGHT) expose the temporal evolution of the synaptic weights (w) for the *pair-based model* and *triplet model*, respectively. Here under we look at the consequences of having bigger connectivity, *i.e.* $g_{EC} = 0.5$. When compared to the previous section with smaller connectivity, the conclusions are similar for both models:

- **Hard bounds:** The weights all evolve towards the maximum value without exception. Indeed, since the connectivity between the pre-(E) and postsynaptic (C) neurons is higher, the activity of the cell E drives the activity of the cell C and more spikes are initiated in the bursts, see FIGURE 6.4. Indeed, g_{EC} represents conductance relative to the synaptic current. Consequently, while a low g_{EC} value will only induce a EPSP in the postsynaptic cell, an higher value like $g_{EC} = 0.5$ will allow spike generation in the postsynaptic neuron. Those spikes will add up to the intrinsic bursting ability. This bursting ability is independent of the pre-post connectivity because it is driven by the activity of the inhibitory cell (I). If the connectivity is higher, the activity of the cell C is simultaneously driven by the inhibitory cell as well as the spikes induced by the excitatory cell and the pre-post connectivity.

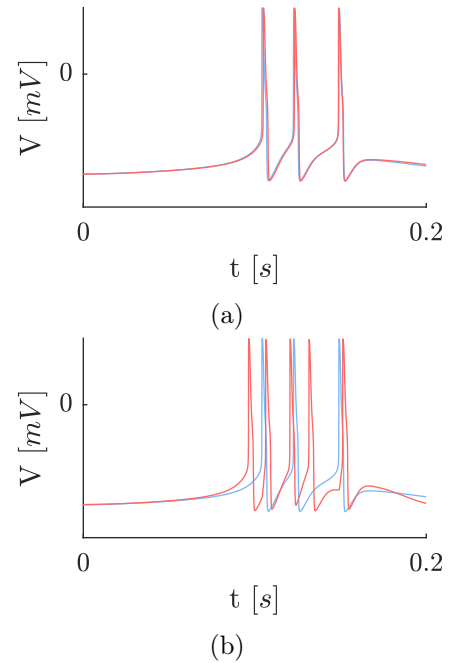


Figure 6.4 – *Burst difference with (a) low ($g_{EC} = 0.01$) and (b) high ($g_{EC} = 0.5$) connectivity* (a) Presynaptic (blue) and postsynaptic (pink) bursts are similar while (b) presynaptic burst induces new spikes in the postsynaptic burst. ($I_{app,I} = -4.5$ [nA]).

- **Soft bounds:** The weights also reach a steady-state value depending on $I_{app,I}$ in-between the two extrema, still due to the effect of the soft bounds. However, since post-synaptic bursts are composed of more spikes, the steady-state value is different and is reached faster than for a low connectivity ($g_{EC} = 0.01$).

6.2 In a realistic world

Even if the previous simulations are not conclusive, they lack an important realistic dimension: the firing patterns *in-vivo* are far from being that regular and variability in-between neurons is required to obtain more realistic and physiological patterns. Thus, in this section, 1% variability is added to the ionic conductances of the conductance-based model such as the three neurons from the circuit are not exactly the same anymore, meaning that the bursting patterns will slightly differ from one simulation to another. Ten circuits are simulated in which g_{ion} values are varying by 1%, *i.e.* $g_{ion} \in [g_{ion} - 1\% g_{ion}; g_{ion} + 1\% g_{ion}]$. For example, g_{Na} initially equals to 170 so each circuit will be built by randomly picking a value of g_{Na} in $[169.3; 171.7] [mS/cm^2]$ (see FIGURE 6.5).

As already shown in FIGURE 6.3, the lack of robustness of the models have been demonstrated, so only $n = 10$ is sufficient to draw conclusions. Once again, low and high connectivity have been evaluated.

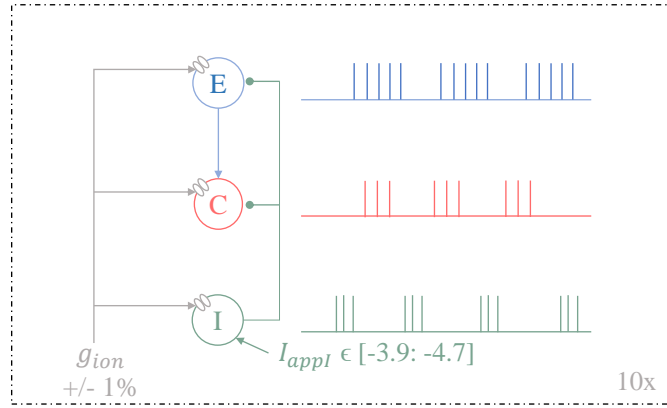


Figure 6.5 – *Computation experiment to test plasticity rules in bursting activity with variability added in ionic conductances g_{ion} .* Different $I_{app,I}$ are applied to the inhibitory cell, driving the whole circuit in bursting mode. Variability in intrinsic conductances g_{ion} is added mimicking more physiological neurons and 10 circuit are simulated.

For each $I_{app,I}$ and each w_0 , the mean over the 10 simulations is taken such as in FIGURE 6.6. The mean hides the behaviour of w that can be extreme ($w \rightarrow 1$, $w \rightarrow 0$) from one simulation to another.

General results

FIGURE 6.7 summarises the different temporal evolution for both hard (*HB*) and soft (*SB*) bounds applied to the pair-based and triplet models and for low and high connectivity (g_{EC}). FIGURE 6.8 summarises the different mean final weights for the different models, bounds, connectivity as well as their standard deviation. The analysis of the different cases will be investigated here under.

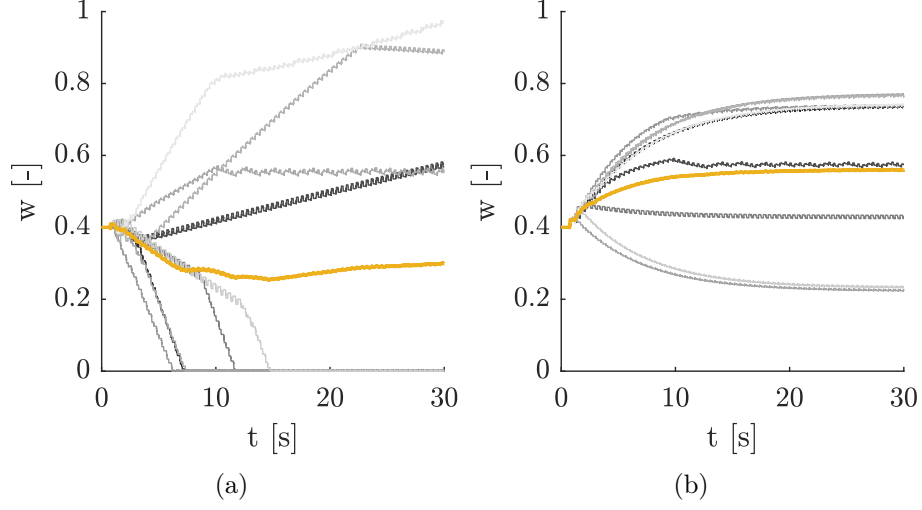


Figure 6.6 – Time courses for one $I_{app,I}$ and $w_0 = 0.4$ of w for the 10 different set of ionic conductances values (shade of grey) and the mean of those 10 curves (orange). Example for the triplet model from (a) [Pfister and Gerstner, 2006], hard bounds (b) [Graupner et al., 2016], soft bounds.

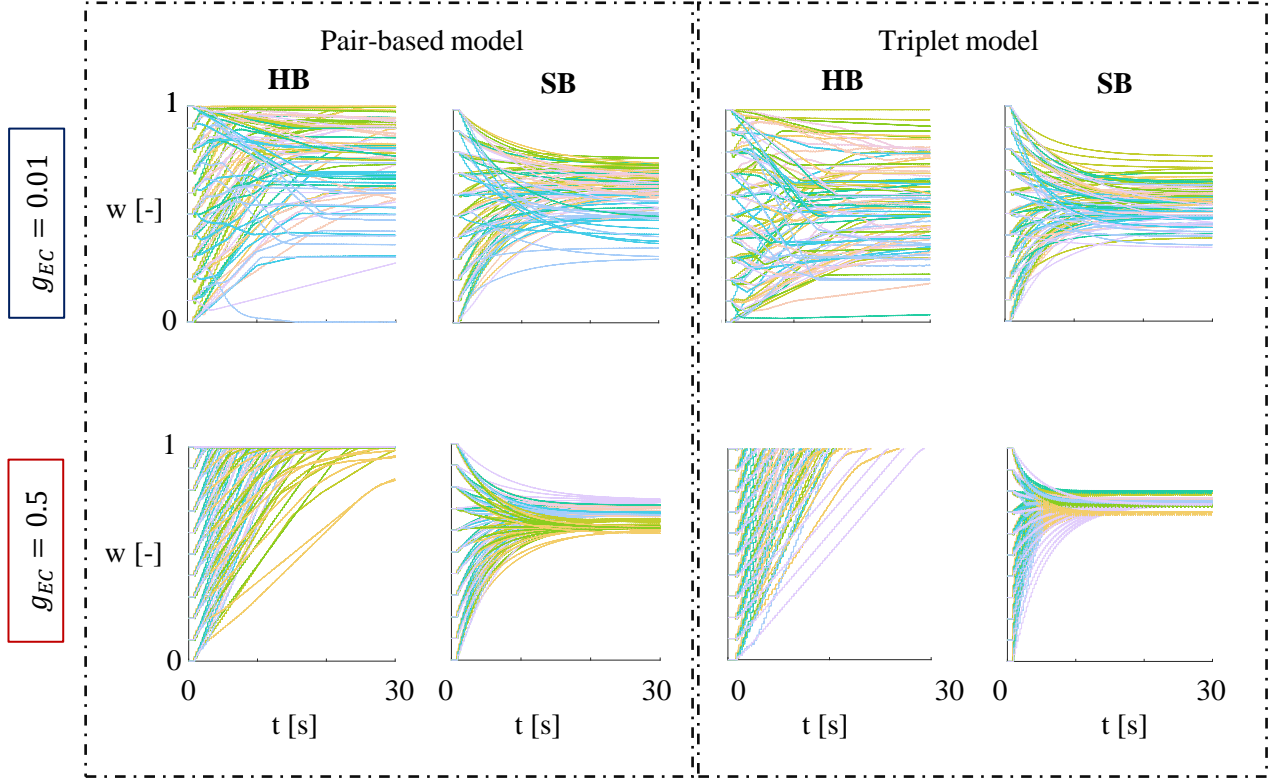


Figure 6.7 – Temporal evolution of the mean final value ($\text{mean}(w_F)$) for both pair-based and triplet models implemented with hard (HB) and soft bounds (SB) and for different connectivity strengths (g_{EC}). In a realistic world, i.e. $n=10$ different circuit are taken with 1% variability added between the different cell conductances. Different colors represent the different $I_{app,I}$ values.

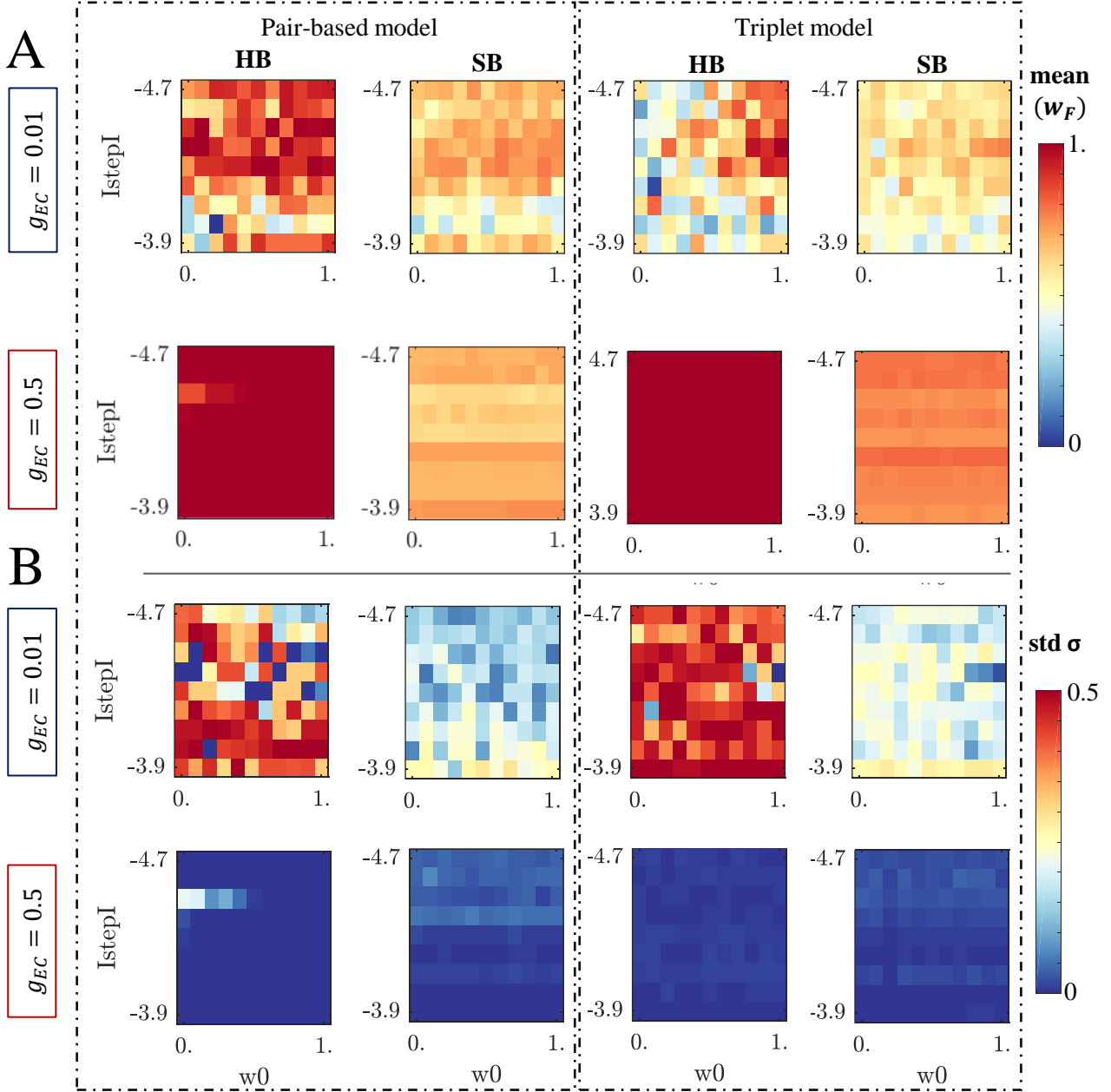


Figure 6.8 – Mean final value ($\text{mean}(w_F)$) and standard deviation (std) for both pair-based and triplet models implemented with hard and soft bounds and for different connectivity strengths (g_{EC}). **A.** $\text{mean}(w_F)$: For both models, low connectivity ($g_{EC} = 0.01$) results in more heterogeneous final weights (top). High connectivity ($g_{EC} = 0.5$) results in homogeneous final values, around 0.8 for the soft bounds (SB) and 1 for the hard bounds (HB) (bottom). **B.** std : For all models, low connectivity ($g_{EC} = 0.01$) results in very high standard deviation for the hard bounds (around 0.5) and smaller for the soft bounds (around 0.25) (top). However, high connectivity ($g_{EC} = 0.5$) results in almost no standard deviation (bottom).

6.2.1 Synapse with low connectivity

Pair-based and Triplet Models: General Conclusions

Once again, similar conclusion can be drawn for the pair-based model and the triplet model with hard and soft bounds and $g_{EC} = 0.01$. TABLE 6.4 indicates the resulting figures for the two models tested

with the two types of bounds.

Temporal evolution		mean(w_F)	std w_F
Pair-based	Triplet	Pair-based & Triplet	
HB	FIGURE 6.2 A	FIGURE 6.2 A	FIGURE 6.8 A
SB	(TOP, LEFT)	(TOP, RIGHT)	(TOP, LEFT) (TOP, RIGHT)

Table 6.3 – Results obtained for the different plasticity rules with hard and soft bounds after a bursting period for a low connectivity ($g_{EC} = 0.01$). (HB) hard bounds and (SB) for soft bounds, w_F final weight when 1% variability is added.

- **Hard bounds:** adding variability makes the models very fragile. Indeed, for both pair-based and triplet models, the standard deviation can be very high (up to 0.5, see FIGURE 6.8 B) *i.e.* from one simulation to another, the weights can either be potentiated or depressed towards one of the extrema. The mean of synaptic weight is thus in-between the minimum (0) and the maximum (1).
- **Soft bounds:** as in the previous section, the synaptic weights are all converging towards the same range of values. The standard deviation is lower than for hard bounds which makes sense since the soft bounds force the weight to evolve toward the same direction, away from the extrema. Thus, the final values are less spread compared to the hard bounds which stops the final values to the extrema.

6.2.2 Synapse with high connectivity

Pair-based and Triplet Models: General Conclusions

Looking now at the consequences of having a bigger connectivity between pre- and postsynaptic cells ($g_{EC} = 0.5$), similar conclusion can once more be drawn for the pair-based model and the triplet model with hard and soft bounds. TABLE 6.4 indicates the resulting figures for the two models tested with the two types of bounds.

Temporal evolution		mean(w_F)	std w_F
Pair-based	Triplet	Pair-based & Triplet	
HB	FIGURE 6.2 A	FIGURE 6.2 A	FIGURE 6.8 A
SB	(BOTTOM, LEFT)	(BOTTOM, RIGHT)	(BOTTOM, LEFT) (BOTTOM, RIGHT)

Table 6.4 – Results obtained for the different plasticity rules with hard and soft bounds after a bursting period for an high connectivity ($g_{EC} = 0.5$). (HB) hard bounds, (SB) for soft bounds, mean(w_F) for mean final weight when 1% variability is added.

- **Hard bounds:** adding variability do not change the results at all when g_{EC} is high. Indeed, for both pair-based and triplet models, the standard deviation is this time equals to 0 *i.e.* all weights are all the time potentiated to the maximum value (*i.e.* the maximum weight) because of the better coordination of the bursts. As previously observed, when the connectivity is higher, bursts of the postsynaptic cell are composed of more spikes resulting in more potentiation.
- **Soft bounds:** as in the previous sections, soft bounds force the synaptic weights to converge towards the same range of values. However, the steady-state values are reached faster and at higher final values. The standard deviation is also much lower. Once again, this is due to the better coordination of the pre-post spikes.

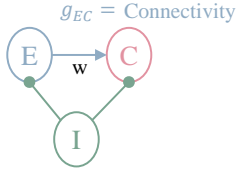
6.3 Summary and conclusion

The main conclusion highlights the varying behaviour between the different bounds: on one hand, the same model implemented with *soft bounds* always converge to a steady-state value, regardless of the initial weight. On the other hand, under an implementation with *hard bounds*, the weights reach the extremes values. Absolutely no conclusion can be drawn from both the pair-based and the triplet models concerning memory consolidation during sleep.

The plasticity rules behaviours during a bursting period gives different results as a function of g_{EC} :

- *Low connectivity*: the models are less robust and the results are *heterogeneous*. The standard deviation is high because the behaviour of the model varies from one simulation to another.
- *High connectivity*: if the bursts are more correlated, the models all lead to more potentiation in a homogeneous way, regardless of the values of w_0 or $I_{app,I}$ (standard deviation low).

CONTRIBUTIONS

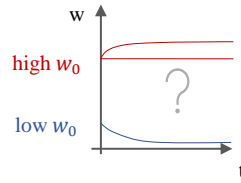
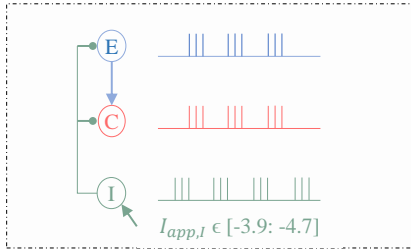


Δw

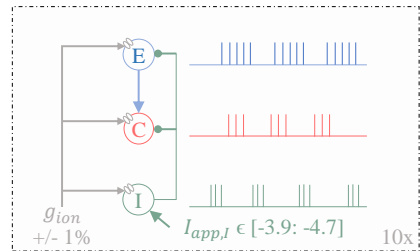
Pair-based model
Triplet model

hard bounds (HB)
soft bounds (SB)

1 In a perfect world



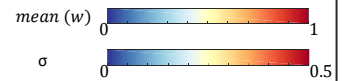
2 In a realistic world



		HB	SB
Low connectivity $g_{EC} = 0.01$	w_F	Extrema	Steady-state value
High connectivity $g_{EC} = 0.5$	w_F	Maxima	Steady-state value

↗ Convergence
↗ Potentiation

		HB	SB
Low connectivity $g_{EC} = 0.01$	$mean w_F$	Heterogeneous 	Around steady state
	σ	Very high 	Medium
High connectivity $g_{EC} = 0.5$	$mean w_F$	Homogenous $\rightarrow w_{max}$ 	Around steady state
	σ	Very low $\rightarrow 0$ 	Very low $\rightarrow 0$



- Sleeping period resets all the weights to the same value
- Triplet and pair-based models have the same behaviour whether they have *hard* or *soft* bounds.
- Higher connectivity induces faster convergence and more potentiation

Both models are **not** compatible with memory consolidation

Part IV

Conclusions and Perspectives

Chapter 7

Conclusion and perspectives

7.1 Thesis summary

This thesis aimed to understand synaptic plasticity in the context of memory consolidation during sleep, using phenomenological models. The following elements have been highlighted:

- *What are the neuronal features that can be modeled and how can they be modeled?* (CHAPTER 2)
Mainly, neuronal features can be modeled thanks to *integrate-and-fire* models, reproducing the spiking aspect of neurons or thanks to *conductance-based* models providing more physiological representation. In particular, *bursting* firing pattern arising during sleep can be better depicted by conductance-based models as well as the switch from tonic firing (*wake*) to burst firing (*sleep*).
- *What is synaptic plasticity and how can it be modeled?* (CHAPTERS 3 AND 4)
Synaptic plasticity has been well documented and occurs at different time scales, either at the pre- or postsynaptic sites. Different factors driving plasticity have been discovered thanks to experimental protocols: the *frequency*, the *voltage* of the postsynaptic cell and the *spike timing*. A literature review has been realised to clarify and classify different computational *phenomenological* models that aim to reproduce experimental protocols and/or to perform a memory task and/or to validate a sleep hypothesis.
- *Are the models existing from the literature compatible not only with learning during the day...* (CHAPTER 5)
Three phenomenological models have been implemented in a conductance-based switching 3-cells network:
 - *Pair-based* model from [Abbott and Nelson, 2000, Graupner et al., 2016] has been successfully implemented.
 - *Triplet* model from [Pfister and Gerstner, 2006, Graupner et al., 2016] has been successfully implemented
 - *Voltage-based* model from [Clopath et al., 2010] failed to be implemented in the circuit. This highlights the possible difficulties to adapt a model from a simple spiking neuron model such as an *IF* to a more complex and physiological one as well as its lack of robustness.

In the first two models, experimental protocols of spike timing-dependent plasticity (*hippocampus*) as well as the frequency dependence of STDP (*cortex*) have been reproduced in *tonic* mode. Reproduction of those experimental results showed their successful implementation and highlighted the flaws of the pair-based model to not being able to reproduce the frequency effect.

Moreover, this thesis reveals that the parameters fitting of the authors do not strictly follow the experimental protocols.

- ... but also with the theory of memory consolidation during sleep (CHAPTER 6)?

The same model implemented in *tonic* mode (*pair-based*, *triplet*) have been tested in *burst* firing to investigate whether or not they could potentially be compatible with memory consolidation during sleep. Additionally to the fact that both models are robust-deficient and are not compatible with memory consolidation, the bounds (either *hard* or *soft* bounds) applied on both models completely determine the outcome. Indeed, the same model with either hard or soft bounds gives different results:

- Hard bounds: Initial weights acquired during learning all saturate to extreme values.
- Soft bounds: Initial weights acquired during learning stabilise at a fixed point in-between the extrema.

Additionally, a slightly different behaviour is observed when the connectivity strength between the pre- and postsynaptic cell is changed:

- Low connectivity: the models are less robust and the results are *heterogeneous*.
- High connectivity: the bursting ability of the postsynaptic cell is enhanced by the presynaptic activity since action potential are induced by a higher synaptic current. The bursts are consequently more correlated and the models all potentiate in a more homogeneous way, regardless of the values of w_0 or I_{appI} .

In any case, as each of the initial weight evolves towards one value, the models are not compatible with memory consolidation during sleep since sleep would reset all the connections and not keep their differences.

7.2 Perspectives

7.2.1 A variety of models

As it has been reviewed, a large amount of models are already implemented and could be potential candidates for memory consolidation during sleep. A first alternative could be to add more timescales to the plasticity and combine different models [Zenke et al., 2015, Zenke and Gerstner, 2017].

However, even if only two models have been tested in this thesis, classical phenomenological models showed difficulties in their implementation in more physiological neuron models (like [Clopath et al., 2010] model that failed to be implemented). Thus, considering *biophysical models* of plasticity could be an interesting alternative to better represent the molecular processes.

In this thesis, only efficiency of the conductance was considered as a mechanism of plasticity. In CHAPTER 3, different mechanisms have been summarised, such as presynaptic plasticity, the number of receptors or, at a longer timescale, spine formation and protein synthesis. All those processes could be put together.

7.2.2 The importance of neuromodulation

STDP coupled with neuromodulation

As it has been briefly introduced in PART II, a variety of neurotransmitters or other neuronal components has the ability to shape, stabilise or modulate classical STDP. Considering only two factors (pre- and postsynaptic neurons) is restrictive compared to the large variety of experimental results. Adding those components as a third factor to the learning rules is called neo-Hebbian plasticity and could explain the different STDP patterns recorded in the different areas (see FIGURE 3.10). In [Fink et al., 2013], modeling of different acetylcholine levels are added in a conductance-based model thanks to an additional K^+ conductance. Indeed, the increase of concentration of this neuromodulator is thought to lead to the closure of specialized K^+ currents in cortical and thalamic neurons inducing the shift from sleep to waking. Reducing this conductance would depolarise the neurons towards firing threshold and increase the excitability of the cells [Zagha and McCormick, 2014]. Adding this dimension in the conductance-based would be of special interest to reproduce neuromodulatory effects.

Synaptic Homeostasis Hypothesis of Sleep (SHY)

- **Concept**

One of the hypothesis that could result from the different neuromodulatory states is a change in the STDP kernel.

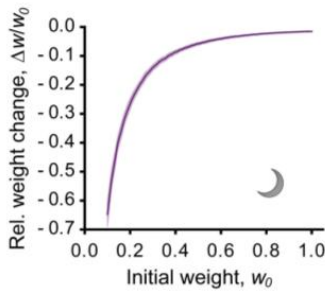


Figure 7.1 – *Computational results from [González-Rueda et al., 2018] proving memory consolidation using SHY hypothesis. Bigger weights are preserved while smaller weights are depressed.*

As stated in the SECTION 4.2.6, *SHY* hypothesis ([Tononi and Cirelli, 2014]) states that during sleep, thanks to those different neuromodulatory effects, connections are down-scaled in such a way that bigger weights are preserved and smaller weights depressed (see FIGURE 7.1) and improving the *signal-to-noise* ratio [González-Rueda et al., 2018].

Consequently, it would be of interest to investigate whether or not this hypothesis is also compatible with bursting firing mode during sleep. To test this hypothesis, preliminary computations have been performed using [González-Rueda et al., 2018] UP-mediated learning rule in the *ECI* circuit, *i.e.* in a physiological conductance-based neuron model able to switch. This rule only enables depression to occur during sleep UP-states (see details on modeling in APPENDIX D.4).

- **Implementation in the conductance-based ECI circuit**

A similar protocol than in CHAPTER 6 is followed:

1. Starting with different initial weights and for different initial AMPA conductances (g_{EC}) representing the level of connectivity between the pre- (E) and postsynaptic (C) cells:

$$g_{AMPA} = g_{EC} * w$$

This allows to see the impact of w in different situation, the cells being more or less connected. A bursting period is applied in a *perfect* world, *i.e.* the pre- (j) and postsynaptic (i) cells are exactly alike.

2. Starting once again with different initial weights and g_{EC} , a bursting period is applied in a *realistic* world, *i.e.* the pre- and postsynaptic neurons have slightly different ionic conductances (differing from 5%).

• Results

In a *perfect* world, similar results than [González-Rueda et al., 2018] (*IF* neuron model) are obtained with the physiological circuit. FIGURE 7.2 (A) shows for one connectivity value ($g_{EC} = 0.3$) the relative weight change for each initial weight value $w_0 \in [0.1 : 0.9]$. The trend is similar to the one obtained by [González-Rueda et al., 2018] in FIGURE 7.1. However, here the conclusion is binary FIGURE 7.2 (A): "*big*" weights are preserved (no relative weight change) while "*small*" weight are completely depressed (relative weight change = -1).

FIGURE 7.2 (B) shows the behaviour for the different g_{EC} values. One can observe that the notion of "*small*" and "*big*" weights is different from one conductance (g_{EC}) value to another. Indeed, increasing g_{EC} shifts to smaller values the minimum initial weight that is preserved during sleep. Given the definition of the excitability conductance $g_{AMPA} = g_{EC} * w$, it makes sense that increasing (g_{EC}) has a similar effect than increasing w_{ij} . Nevertheless, this allows to take into consideration various initial conditions. For values of $g_{EC} \leq 0.2$, all weights are depressed and this dichotomous behaviour is not observed.

In a *realistic* world (FIGURE 7.2 C), the results are similar. The weights are also either depressed or either potentiated in a binary way and the standard deviation is low for $g_{EC} > 0.2$, meaning that this model is at first glance robust (note that only $n = 5$ simulations have been run) and that *SHY* hypothesis could be a potential explanation of memory consolidation.

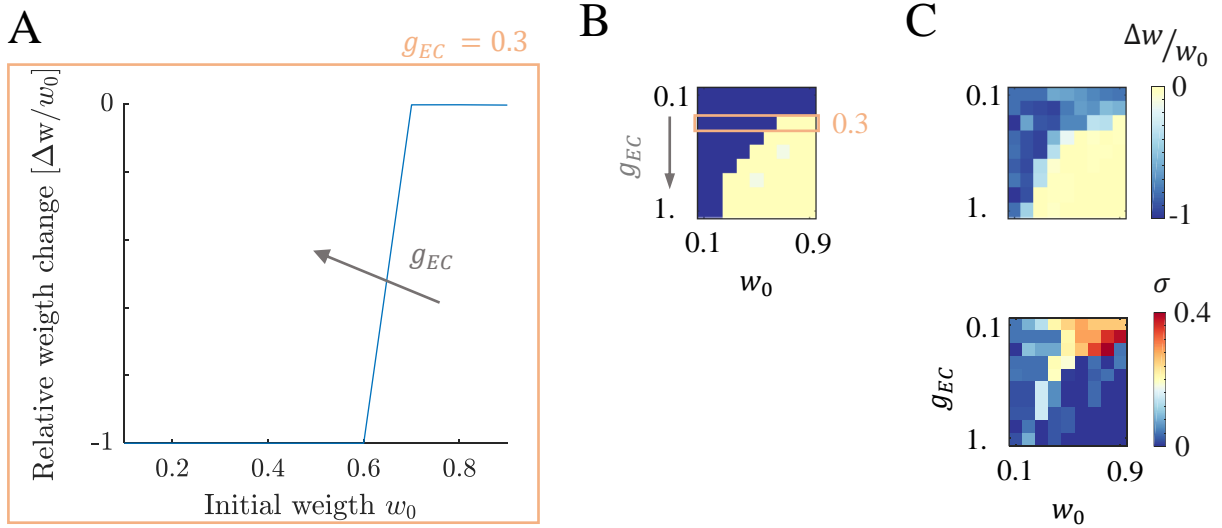


Figure 7.2 – *Implementation of SHY hypothesis in the ECI circuit.* **A.** Relative synaptic weight change ($\Delta w/w_0$) for different initial weights (w_0) and one AMPA conductances ($g_{EC} = 0.3$) using UP-mediated learning rule from [González-Rueda et al., 2018]. Increasing g_{EC} shifts the curve to the left, in such a way that smaller initial weights are preserved (*i.e.* weights for which relative weight change = 0). **B.** In a perfect world (cells E, C are the same), bigger weights are preserved (yellow) and smaller weights are depressed (blue). Increasing g_{EC} increases the amount of preserved weights. The line relative to $g_{EC} = 0.3$ is highlighted referring to the preceding graph. **C.** In a realistic world (cells E, C different) the same behaviour is observed and the standard deviation is low for $g_{EC} > 0.2$ ($n = 5$). For all simulations, the relative weight change is taken after $T = 1000$ [s].

Learning during the day

Finally, it is important to take into account the context of learning. Indeed, learning is often due to a rewarding information or a surprise/novelty [Frémaux and Gerstner, 2015]. STDP alone would miss

that crucial information for learning selectivity.

In reward learning, the actual delivery of reward by neuromodulators occurs later than the rewarding action, a phenomenon known as the *temporal credit assignment problem*. It therefore raises a question of how the reward is integrated at the synapse. Do neuromodulators shape existing plasticity or do they allow plasticity expression? The concept of eligibility traces has been raised, representing tags set by Hebbian plasticity and transformed later by neuromodulation [Ziegler et al., 2015, Seibt and Frank, 2019, Frémaux and Gerstner, 2015, Foncelle et al., 2018].

Appendix A

Neurophysiology basis

A.1 Action potential mechanism

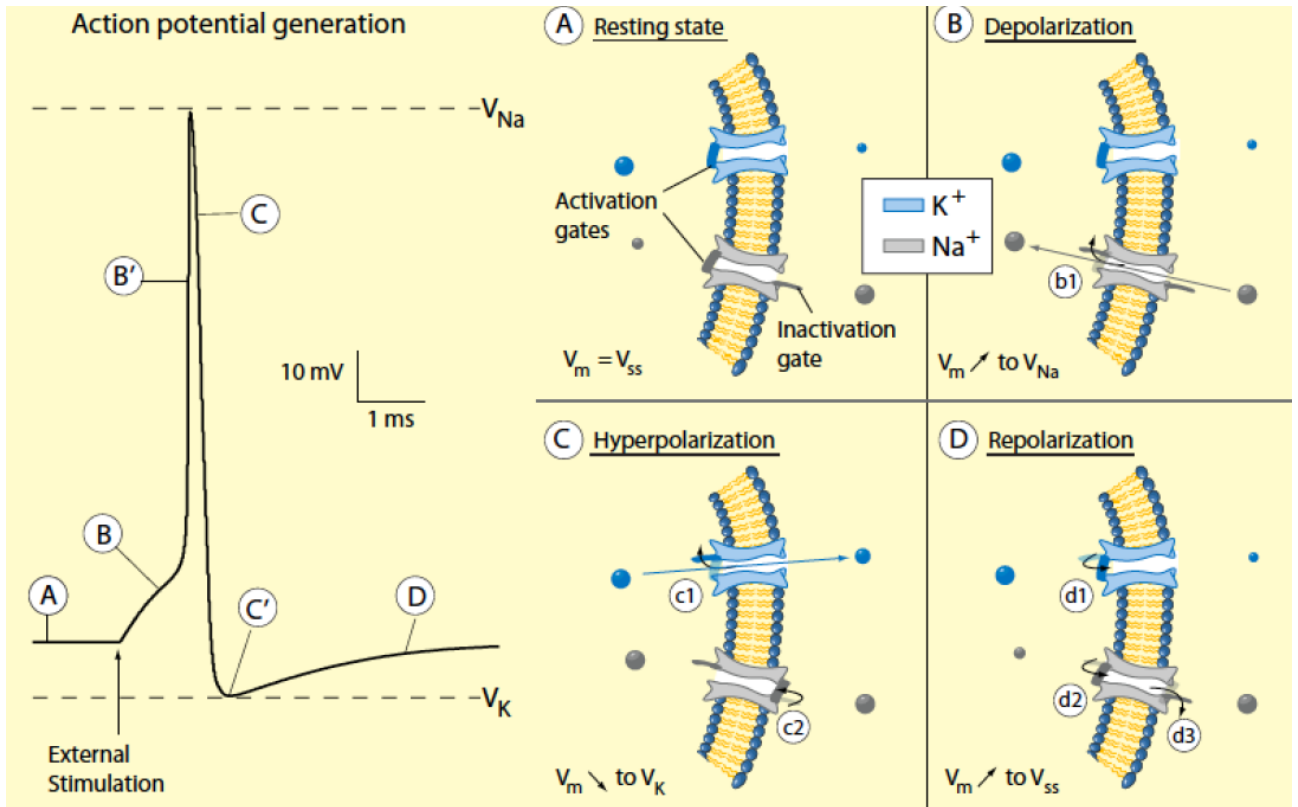


Figure A.1 – Action potential mechanism. **(left)** *Action potential generation*. Time evolution of the membrane potential for an external stimulation. **(right)** *Ionic channels dynamics*. (A) Resting-state. V_m is around -70 [mV]. Activation gates are closed but the inactivation sodium gate is open. (B) After external stimulation, the membrane voltage increases. (B') If it reaches a certain threshold, activation sodium gate opens(voltage-dependent) and the membrane is strongly depolarised almost to the sodium Nernst potential. (C) Potassium activation gate opens and sodium inactivation gate closes because they have a slower dynamics than the sodium activation gate. Potassium goes out of the cell. (C') The membrane is hyperpolarised and reach the potassium Nernst potential. (D) The membrane potential recovers its steady-state value and the gates go back to their initial position. [Jacquerie, 2018]

Neurons communicate between each other thanks to the propagation of signals through the axon towards synapses. The movement of ions (mainly sodium and potassium) through voltage-dependent

channels described in the previous section is at the core of the mechanism of the action potential generation. It can be described in four steps, as it can be seen in FIGURE A.1:

1. **At rest**, the membrane is hyperpolarised (-70mV) as the cell is slightly more permeable to potassium than sodium.
2. **Depolarisation**: As an external stimulus is applied, two scenarios are possible:
 - The stimulus is not large enough to make the membrane potential reach its threshold value, *i.e.* the voltage at which the sodium voltage-gated channels will open. The cell thus recovers its resting state.
 - The stimulus is large enough for the membrane potential to reach its threshold value. The sodium channel is activated and consequently sodium rapidly flows into the cell, resulting in a strong depolarisation towards the Sodium Nernst potential.
3. **Hyperpolarisation**: The activation gate of the potassium channel has a slower dynamics and is opening and closing delayed compared to the sodium channel. While the depolarisation inactivates the sodium channel, potassium flows out of the cell resulting in the hyperpolarisation of the membrane at a slightly lower value than the resting state potential, reaching the potassium Nernst potential.
4. **Repolarisation**: The membrane potential recovers its resting-state value.

A.2 Nernst Potential of main ions

Ion	Nernst potential (mV)
Na^+	51
K^+	-97
Ca^{2+}	120
Cl^-	-42

Table A.1 – Nernst potentials of main ions across the membrane in human cells. $V_{\text{Nernst}} = \frac{RT}{zF} \ln \frac{[\text{ion}]_{\text{out}}}{[\text{ion}]_{\text{in}}}$ [Jacquerie, 2018].

Appendix B

Thalamus mechanisms during sleep

B.1 T-Type current

The bursting ability of the thalamic neurons that induces the sleep state is due to an additional ionic current in the membrane. It has been shown that, when the cell is hyperpolarised under a certain threshold, a calcium current can be measured. This current is called T-Type Calcium current or low-threshold Ca^{2+} current [Jacquerie, 2018].

Associated to this current, the T-type calcium channel possess one activation gate and one slower inactivation gate. The activation one opens when the cell is depolarised and the inactivation one when it hyperpolarises. Additionally to this current, another one leads to the bursting firing pattern in the thalamus: an hyperpolarisation activated cation current, I_H . The following mechanism describes the interaction between those different ionic current coupled to the classical sodium-potassium currents that leads to burst in a relay neuron FIGURE B.1 (B)):

- The relay neurons are inhibited by the TRN, leading to an hyperpolarisation and thus an opening of the inactivation gate of T-Type calcium channel.
- This hyperpolarisation induces the activation of the I_H current leading to a slow depolarisation.
- Around -65mV, the depolarisation leads to the opening of the activation gate of the T-Type calcium channel, allowing Calcium to freely enter the cell and depolarises the membrane. After reaching the threshold for classical action potentials (-55mV), this allows classical Na/K spiking mechanism to occur.
- After approximately 100ms, the T-type calcium channel inactivation occurs and the calcic current stops, leading to a hyperpolarisation. I_H also de-activates.
- The hyperpolarisation leads again to the same mechanism.

In a modeling point of view, the bursting firing pattern is thus simply simulated by adding ionic currents in the conductance-based model.

B.2 Spindles

The thalamus and notably the TRN thanks to their inhibitory connections influence the flow of information between the thalamus and the cerebral cortex. Particularly, during the transition from wake to Slow-wave-sleep, a phenomenon called *spindles* occurs and is induced by thalamic rhythms. Spindles are fast 7-14 *Hz* oscillations separated by 3-10 *s*. They are the result of rhythmic (7-14 *Hz*)

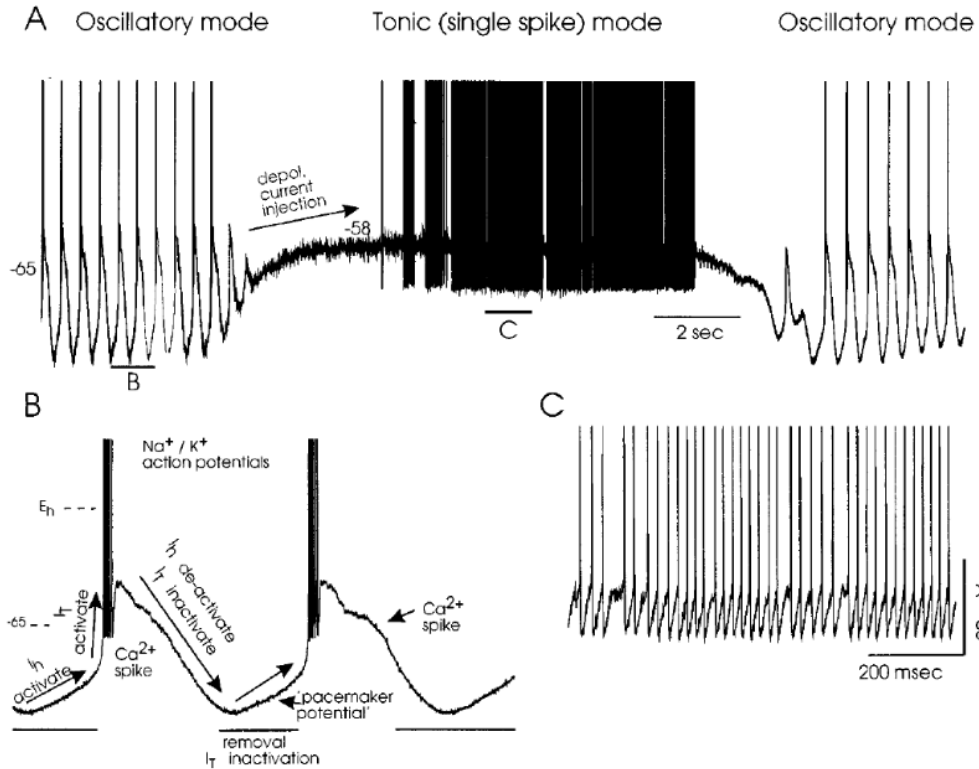


Figure B.1 – *Thalamocortical neurons recordings* **A.** Oscillatory mode (bursting mode) appears when the cell is hyperpolarised. A depolarisation current injection switch the cell in tonic mode. **B.** Bursting mechanism and the underlying ionic current dynamics involved. **C.** Tonic discharge. [McCormick and Bal, 1997]

bursts in the TRN generated by T-Type Ca^{2+} spikes. Those bursts inhibits thalamocortical cells and give rise to rhythmic IPSPs. The hyperpolarisation thus leads to the mechanism described in 2.2.3. On one hand, the relay neurons sends excitatory inputs to cortical neurons the bursts leads to EPSPs in pyramidal cells and results in EEG spindles. On the other hand, the excitatory inputs sent in the TRN facilitates their rhythmic oscillations [Steriade et al., 1993] [McCormick and Bal, 1997].

Appendix C

Conductance-based model

All computations were performed using Julia programming language. A conductance-based model is used and follows the equation from [Drion et al., 2018]:

$$C_m \dot{V}_m = -I_{Na} - I_K - I_{CaT} - I_{K,Ca} - I_H - I_{leak} + I_{app} \quad (C.1)$$

- $I_{leak} = \bar{g}_{leak} (V - V_{leak})$ is a leaky current,
- $I_{Na} = \bar{g}_{Na} m_{Na}^3 h_{Na} (V - V_{Na})$ is a transient sodium current,
- $I_{Ca,T} = \bar{g}_{Ca,T} m_{Ca,T}^3 h_{Ca,T} (V - V_{Ca})$ is a T-type calcium current,
- $I_{K,D} = \bar{g}_{K,D} m_{K,D}^4 (V - V_K)$ is a delayed-recctifier potassium current,
- $I_{K,Ca} = \bar{g}_{K,Ca} m_{K,Ca}([Ca]) (V - V_{Ca})$ is a calcium-activated potassium current,
- $I_H = \bar{g}_H m_H (V - V_H)$ is an hyperpolarisation-activated cation current,
- I_{app} an externally applied current.

where m represents activation variable and h inactivation variable. Thus, it leads to the following equation, with parameters values summarised in TABLE C.1:

$$C_m \dot{V}_m = -\bar{g}_{Na} m_{Na}^3 h_{Na} (V_m - V_{Na}) - \bar{g}_{K,D} m_{K,D}^4 (V_m - V_K) - \bar{g}_{Ca,T} m_{Ca,T}^3 h_{Ca,T} (V_m - V_{Ca}) - \bar{g}_{K,Ca} m_{K,Ca}([Ca]) (V_m - V_K) - \bar{g}_H m_H (V_m - V_H) - \bar{g}_{leak} (V_m - V_{leak}) + I_{app} \quad (C.2)$$

Model parameters			
C_m	1	g_L	0.055
V_{Na}	50	g_{Na}	170
V_K	-85	g_{Kd}	40
V_{Ca}	120	g_H	0.01
V_L	-55	$g_{K,Ca}$	4
V_H	20	$g_{Ca,T}$	0.55
K_d	170	$k1$	1e-1
		$k2$	0.1e-1

Table C.1 – Conductance-based model parameters. **Left.** global parameters. **Rigth.** cell parameters, identicals for each cell of the ECI circuit. Potentials are in [mV], conductances in [mS/cm^2] and capacitance in [$/cm^2$]

The activation (m) and inactivation (h) variables dynamics of the voltage-gated channels are modeled using the following equations:

$$m_{X,\infty} = \frac{1}{1 + \exp((V + A)/B)} \quad \tau_X = A - \frac{B}{1 + \exp((V + D)/E)} \quad (\text{C.3})$$

The parameters for the different channels are summarised in the following table:

Param.	A	B	Param.	A	B	D	E
$m_{Na,\infty}$	35.5	- 5.29	$\tau_{m_{Na}}$	1.32	1.26	120	-25
$h_{Na,\infty}$	48.9	5.18	$\tau_{h_{Na}}$	$(0.67/(1 + \exp((V + 62.9)/-10.0))) * (1.5 + 1/(1 + \exp((V + 34.9)/3.6)))$			
$m_{Kd,\infty}$	12.3	-11.8	$\tau_{m_{Kd}}$.2	6.4	28.3	-19.2
$m_{CaT,\infty}$	67.1	-7.2	$\tau_{m_{CaT}}$	21.7	21.3	68.1	-20.5
$h_{CaT,\infty}$	80.1	5.5	$\tau_{h_{CaT}}$	410	179.6	55.	-16.9
$m_{H,\infty}$	80.	6.	τ_{m_H}	272.	-1149.	42.2	-8.73

C.1 Connection between cells

Excitatory connection

$$I_{AMPA} = g_{AMPA} * s_{AMPA} * (V - 0) \quad (\text{C.4})$$

where s_{AMPA} is a *AMPA* gate whose dynamics depends on the presynaptic potential V_{Pre} :

$$\dot{s}_{AMPA} = 1.1\tau_m(V_{Pre}) * (1 - s_{AMPA}) - 0.19 * s_{AMPA}$$

Inhibitory connection connection

$$I_{GABA_A} = g_{GABA_A} * s_{GABA_A} * (V - V_{Cl}) \quad (\text{C.5})$$

$$I_{GABA_B} = g_{GABA_B} * s_{GABA_B} * (V - V_K) \quad (\text{C.6})$$

where s_{GABA_A} s_{GABA_B} are $GABA_{A,B}$ gates whose dynamics depend on the presynaptic potential V_{Pre} :

$$\dot{s}_{GABA_A} = 0.53\tau_m(V_{Pre}) * (1 - s_{GABA_A}) - 0.19 * s_{GABA_A}$$

$$\dot{s}_{GABA_B} = 0.016\tau_m(V_{Pre}) * (1 - s_{GABA_B}) - 0.0047 * s_{AMPA}$$

and

$$\tau_m(V_{Pre}) = \frac{1}{(1 + \exp(-(V_{Pre} - 2)/5))}$$

Plasticity implementation

In the ECI circuit, plasticity occurs between cell E and cell C and changes the AMPA conductance.

$$g_{EC} = g_{EC}^- * w \quad (\text{C.7})$$

where g_{EC} is g_{AMPA} between cell E and cell C and g_{EC}^- is a constant multiplied by the synaptic weight w . In CHAPTER 5, very small connectivity $g_{EC} = 0.01$ is taken such as no spike is initiated from pre- to postsynaptic cell.

Appendix D

Plasticity rules and computational details

D.1 Pair-based model

Parameters used

A_+	A_-	τ_+	τ_-
0.0096	0.0053	16.8	33.7

Table D.1 – Pair-based parameters from [Bi and Poo, 2001]

Time course illustration

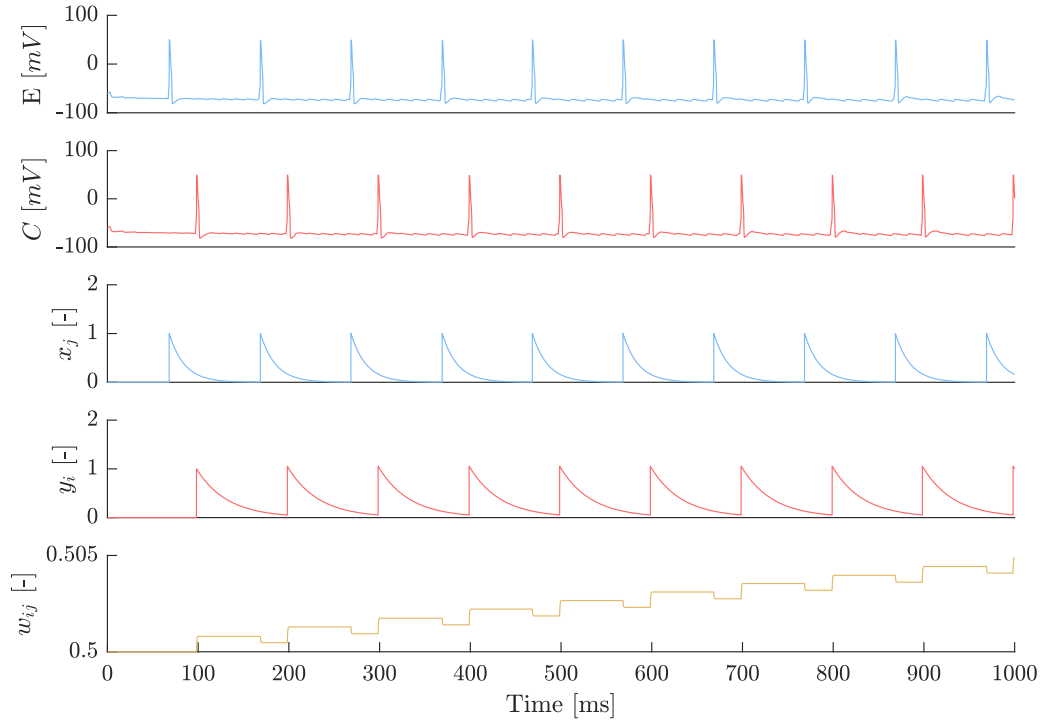


Figure D.1 – Temporal evolution of pre- (E) and postsynaptic (C) voltage, spikes traces (x_j (pre), y_i (post)), and weight change. $\Delta_t = 30[ms]$ and $\rho = 10[Hz]$

D.2 Triplet model

Parameters used

	Model	A_2^+	A_3^+	A_2^-	A_3^-	τ_x	τ_y
(C)	Full model	$5e^{-10}$	$6.2e^{-3}$	$7e^{-3}$	$2.3e^{-4}$	101	125
	Minimal model	0	$6.5e^{-3}$	$7.1e^{-3}$	0		114
(H)	Full model	$6.1e^{-3}$	$6.7e^{-3}$	$1.6e^{-3}$	$1.4e^{-3}$	946	27
	Minimal model	$5.3e^{-3}$	$8e^{-3}$	$3.5e^{-3}$	0		40

Table D.2 – Triplet parameters from [Pfister and Gerstner, 2006]. Fitted on [Sjöström et al., 2001] (C) and [Wang et al., 2005] (H). $\tau_+ = 16.8$ and $\tau_- = 33.7$ were always the same

	Model	A_2^+	A_3^+	A_2^-	A_3^-	τ_x	τ_y
(C)	Minimal model	0	0.0165746	0.00826477	0		56.38

Table D.3 – Triplet parameters from [Graupner et al., 2016]. Fitted on [Sjöström et al., 2001] (C). $\tau_+ = 16.8$ and $\tau_- = 33.7$ were the same as pair-based model.

Time course illustration

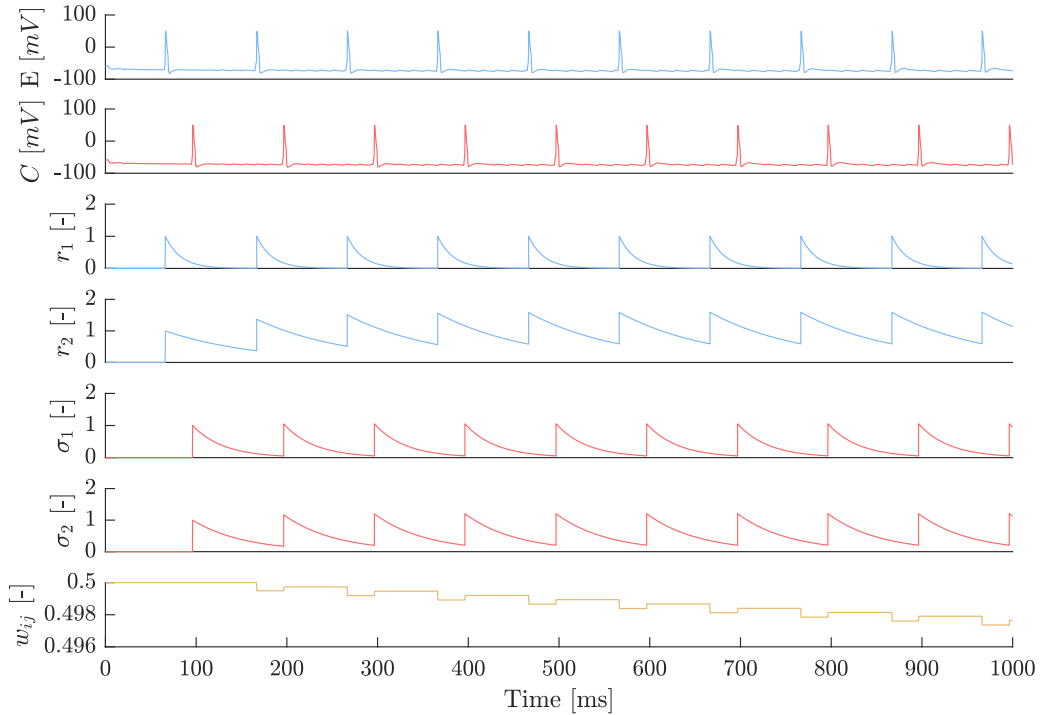


Figure D.2 – Temporal evolution of pre- (E) and postsynaptic (C) voltage, spikes traces (r_1 , r_2 (pre), σ_1 , σ_2 (post)), and weight change. $\Delta t = 30[ms]$ and $\rho = 10[Hz]$

D.3 Voltage-dependent model [Clopath et al., 2010]

Parameters used

Exper.	$\theta_-(mV)$	$\theta_+(mV)$	$A_{LTD} (mV)^{-1}$	$A_{LTP} (mV)^{-2}$	$\tau_x(ms)$	$\tau_-(ms)$	$\tau_+(ms)$
(C)	-70.6	-45.3	$14e^{-5}$	$8e^{-5}$	15	10	7
(H)	-41	-38	$38e^{-5}$	$2e^{-5}$	16		

Table D.4 – Voltage-dependent model parameters from [Clopath et al., 2010] for different protocols

D.4 UP-mediated learning rule from [González-Rueda et al., 2018]:

Following *SHY*, synaptic weights were updated such that presynaptic spikes alone led to depression while pre- action potential followed within 10 [ms] by a postsynaptic spike restored the previous weight. Thus, a presynaptic trace x_j was reset to 10 for every presynaptic spike and decayed linearly otherwise [González-Rueda et al., 2018]:

$$\begin{aligned} x_j &\rightarrow 10 \text{ if presynaptic neuron } j \text{ fires} \\ \tau \frac{dx_j}{dt} &= -1 \quad \text{otherwise,} \end{aligned} \quad (D.1)$$

where $\tau = 1[ms]$ and the weight is updated following:

$$\begin{aligned} w_j(t) &\rightarrow w_j(t) - A && \text{if } t = t^{\text{pre}} \\ w_j(t) &\rightarrow w_j(t) + A (x_j(t) > 0) && \text{if } t = t^{\text{post}} \end{aligned} \quad (D.2)$$

D.5 Dynamical evolution of the synaptic weight

In order to implement the synaptic weight change in a dynamical way, *i.e.* following:

$$w \rightarrow w + \Delta w$$

A differential equation is implemented:

$$\frac{dw}{dt} = \frac{(w + \Delta w) - w}{\tau_w} \quad (D.3)$$

with $\tau_w = 0.01$ in CHAPTER 5. For CHAPTER 6, the evolution is assumed instantaneous and $w = w + \Delta w$ is taken.

D.6 Variability in ionic conductances

The variability is added in the following way:

$$g_{ion} = g_{ion} * (1 - 2 * \gamma * (rand(1) - 0.5))$$

where, g_{ion} is the ionic conductance, γ the percentage of variability $\in [0 : 1]$ and $rand(1)$ is a random number $\in [0 : 1]$.

Appendix E

Supplementary results

E.1 Bursts parameters for the different simulations

In a perfect world, low connectivity ($g_{EC} = 0.01$)

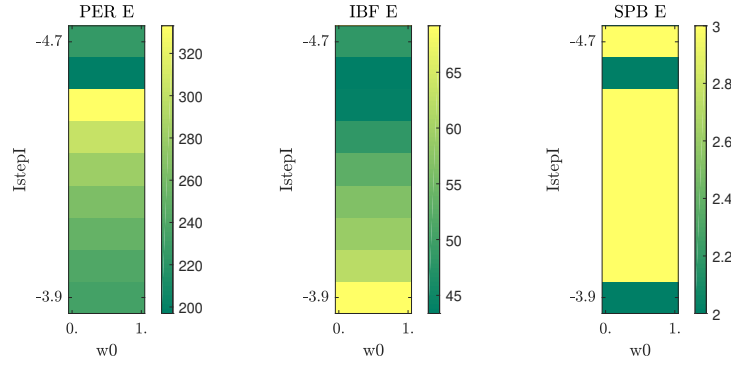


Figure E.1 – Burst parameters for the cell E when the connectivity is low ($g_{EC} = 0.01$) for the different $I_{step,I} = I_{app,I}$. The parameters are similar for cell C.

In a perfect world, high connectivity ($g_{EC} = 0.5$)

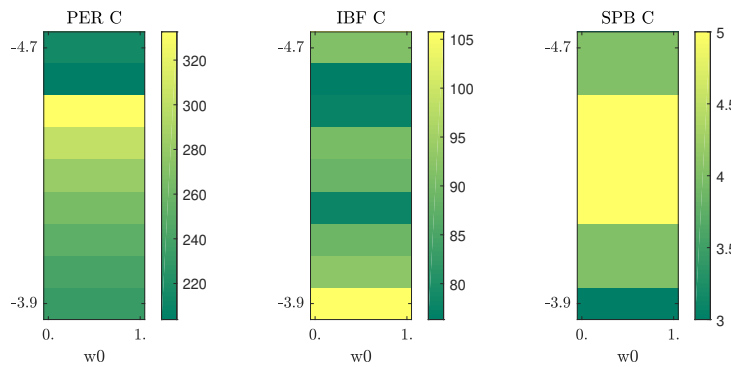


Figure E.2 – Burst parameters for the cell C when the connectivity is high ($g_{EC} = 0.5$) for the different $I_{step,I} = I_{app,I}$. More spike-per-bursts and intraburst frequency are expected in cell C compared to cell E (which has the same parameters than in FIGURE E.1).

Bibliography

- [Abbott and Nelson, 2000] Abbott, L. F. and Nelson, S. B. (2000). Synaptic plasticity: Taming the beast. *Nature Neuroscience*, 3(11s):1178–1183.
- [Artola et al., 1990] Artola, A., Bröcher, S., and Singer, W. (1990). Different voltage-dependent thresholds for inducing long-term depression and long-term potentiation in slices of rat visual cortex. *Nature*, 347(6288):69–72.
- [Babadi and Abbott, 2016] Babadi, B. and Abbott, L. F. (2016). Stability and Competition in Multi-spike Models of Spike-Timing Dependent Plasticity. *PLoS Computational Biology*, 12(3).
- [Bannon et al., 2017] Bannon, N. M., Chistiakova, M., Chen, J.-Y., Bazhenov, M., and Volgushev, M. (2017). Adenosine shifts plasticity regimes between associative and homeostatic by modulating heterosynaptic changes. *Journal of Neuroscience*, 37(6):1439–1452.
- [Benuskova and Abraham, 2007] Benuskova, L. and Abraham, W. C. (2007). StdP rule endowed with the bcm sliding threshold accounts for hippocampal heterosynaptic plasticity. *Journal of computational neuroscience*, 22(2):129–133.
- [Bi and Poo, 1998] Bi, G.-q. and Poo, M.-m. (1998). Synaptic modifications in cultured hippocampal neurons: dependence on spike timing, synaptic strength, and postsynaptic cell type. *Journal of neuroscience*, 18(24):10464–10472.
- [Bi and Poo, 2001] Bi, G.-q. and Poo, M.-m. (2001). Synaptic modification by correlated activity: Hebb’s postulate revisited. *Annual review of neuroscience*, 24(1):139–166.
- [Bienenstock et al., 1982] Bienenstock, E. L., Cooper, L. N., and Munro, P. W. (1982). Theory for the development of neuron selectivity: orientation specificity and binocular interaction in visual cortex. *Journal of Neuroscience*, 2(1):32–48.
- [Bliss and Lømo, 1973] Bliss, T. V. and Lømo, T. (1973). Long-lasting potentiation of synaptic transmission in the dentate area of the anaesthetized rabbit following stimulation of the perforant path. *The Journal of physiology*, 232(2):331–356.
- [Bosch and Hayashi, 2012] Bosch, M. and Hayashi, Y. (2012). Structural plasticity of dendritic spines. *Current opinion in neurobiology*, 22(3):383–388.
- [Capone et al., 2019] Capone, C., Pastorelli, E., Golosio, B., and Paolucci, P. S. (2019). Sleep-like slow oscillations improve visual classification through synaptic homeostasis and memory association in a thalamo-cortical model. *Scientific reports*, 9(1):1–11.
- [Caton, 1887] Caton, R. (1887). Researches on electrical phenomena of cerebral grey matter. *Ninth International Medical Congress*, 3:246.

- [Chen et al., 2013] Chen, J.-Y., Lonjers, P., Lee, C., Chistiakova, M., Volgushev, M., and Bazhenov, M. (2013). Heterosynaptic plasticity prevents runaway synaptic dynamics. *Journal of Neuroscience*, 33(40):15915–15929.
- [Chistiakova et al., 2014] Chistiakova, M., Bannon, N. M., Bazhenov, M., and Volgushev, M. (2014). Heterosynaptic plasticity: multiple mechanisms and multiple roles. *The Neuroscientist*, 20(5):483–498.
- [Citri and Malenka, 2008] Citri, A. and Malenka, R. C. (2008). Synaptic plasticity: Multiple forms, functions, and mechanisms. *Neuropsychopharmacology*, 33(1):18–41.
- [Clopath et al., 2010] Clopath, C., Büsing, L., Vasilaki, E., and Gerstner, W. (2010). Connectivity reflects coding: A model of voltage-based STDP with homeostasis. *Nature Neuroscience*, 13(3):344–352.
- [Cooper et al., 1979] Cooper, L. N., Liberman, F., and Oja, E. (1979). A theory for the acquisition and loss of neuron specificity in visual cortex. *Biological cybernetics*, 33(1):9–28.
- [De Vivo et al., 2017] De Vivo, L., Bellesi, M., Marshall, W., Bushong, E. A., Ellisman, M. H., Tononi, G., and Cirelli, C. (2017). Ultrastructural evidence for synaptic scaling across the wake/sleep cycle. *Science*, 355(6324):507–510.
- [Delattre et al., 2015] Delattre, V., Keller, D., Perich, M., Markram, H., and Muller, E. B. (2015). Network-timing-dependent plasticity. *Frontiers in Cellular Neuroscience*, 9(June):1–11.
- [Diekelmann and Born, 2010] Diekelmann, S. and Born, J. (2010). The memory function of sleep. *Nature Reviews Neuroscience*, 11(2):114–126.
- [Drion et al., 2018] Drion, G., Dethier, J., Franci, A., and Sepulchre, R. (2018). Switchable slow cellular conductances determine robustness and tunability of network states. *PLoS Computational Biology*, 14(4):1–20.
- [Dudek and Bear, 1995] Dudek, S. M. and Bear, M. F. (1995). Homosynaptic long-term depression in area ca1 of hippocampus and effects of n-methyl-d-aspartate receptor blockade. In *How We Learn; How We Remember: Toward An Understanding Of Brain And Neural Systems: Selected Papers of Leon N Cooper*, pages 200–204. World Scientific.
- [Feld and Born, 2017] Feld, G. B. and Born, J. (2017). Sculpting memory during sleep: concurrent consolidation and forgetting. *Current Opinion in Neurobiology*, 44:20–27.
- [Ferreira et al., 2017] Ferreira, J. S., Papouin, T., Ladépêche, L., Yao, A., Langlais, V. C., Bouchet, D., Dulong, J., Mothet, J.-P., Sacchi, S., Pollegioni, L., et al. (2017). Co-agonists differentially tune glun2b-nmda receptor trafficking at hippocampal synapses. *Elife*, 6:e25492.
- [Fink et al., 2013] Fink, C. G., Murphy, G. G., Zochowski, M., and Booth, V. (2013). A Dynamical Role for Acetylcholine in Synaptic Renormalization. *PLoS Computational Biology*, 9(3).
- [Foncelle et al., 2018] Foncelle, A., Mendes, A., Jędrzejewska-Szmek, J., Valtcheva, S., Berry, H., Blackwell, K. T., and Venance, L. (2018). Modulation of spike-timing dependent plasticity: towards the inclusion of a third factor in computational models. *Frontiers in Computational Neuroscience*, 12:49.
- [Franceschetti et al., 1995] Franceschetti, S., Guatteo, E., Panzica, F., Sancini, G., Wanke, E., and Avanzini, G. (1995). Ionic mechanisms underlying burst firing in pyramidal neurons: intracellular study in rat sensorimotor cortex. *Brain research*, 696(1-2):127–139.

- [Frémaux and Gerstner, 2015] Frémaux, N. and Gerstner, W. (2015). Neuromodulated spike-timing-dependent plasticity, and theory of three-factor learning rules. *Frontiers in Neural Circuits*, 9(JAN2016).
- [Froemke and Dan, 2002] Froemke, R. C. and Dan, Y. (2002). Spike-timing-dependent synaptic modification induced by natural spike trains. *Nature*, 416(6879):433–438.
- [Gerstner and Kistler, 2002] Gerstner, W. and Kistler, W. M. (2002). *Spiking neuron models: Single neurons, populations, plasticity*. Cambridge university press.
- [Gerstner et al., 2014] Gerstner, W., Kistler, W. M., Naud, R., and Paninski, L. (2014). *Neuronal dynamics: From single neurons to networks and models of cognition*. Cambridge University Press.
- [Gjorgjieva et al., 2011] Gjorgjieva, J., Clopath, C., Audet, J., and Pfister, J. P. (2011). A triplet spike-timing-dependent plasticity model generalizes the Bienenstock-Cooper-Munro rule to higher-order spatiotemporal correlations. *Proceedings of the National Academy of Sciences of the United States of America*, 108(48):19383–19388.
- [Gjorgjieva et al., 2009] Gjorgjieva, J., Toyozumi, T., and Egle, S. J. (2009). Burst-time-dependent plasticity robustly guides ON/OFF segregation in the lateral geniculate nucleus. *PLoS Computational Biology*, 5(12).
- [González-Rueda et al., 2018] González-Rueda, A., Pedrosa, V., Feord, R. C., Clopath, C., and Paulsen, O. (2018). Activity-Dependent Downscaling of Subthreshold Synaptic Inputs during Slow-Wave-Sleep-like Activity In Vivo. *Neuron*, 97(6):1244–1252.e5.
- [Graupner, 2017] Graupner, M. (2017). Synaptic Plasticity : Spike-timing dependent plasticity (STDP) Synaptic Plasticity : Spike-timing dependent plasticity (STDP). [Powerpoint Presentation].
- [Graupner et al., 2016] Graupner, M., Wallisch, P., and Ostojic, S. (2016). Natural firing patterns imply low sensitivity of synaptic plasticity to spike timing compared with firing rate. *Journal of Neuroscience*, 36(44):11238–11258.
- [Hebb, 1949] Hebb, D. O. (1949). The organization of behavior; a neuropsychological theory. *A Wiley Book in Clinical Psychology*, 62:78.
- [Heidelberg et al., 2014] Heidelberg, R., Shouval, H., Zucker, R. S., and Byrne, J. H. (2014). Synaptic Plasticity. In *From Molecules to Networks: An Introduction to Cellular and Molecular Neuroscience: Third Edition*, pages 533–561. Elsevier Inc.
- [Hodgkin and Huxley, 1952] Hodgkin, A. L. and Huxley, A. F. (1952). A quantitative description of membrane current and its application to conduction and excitation in nerve. *The Journal of physiology*, 117(4):500–544.
- [Jacquerie, 2018] Jacquerie, K. (2018). Sensitivity and robustness analysis of thalamic neuron models at the cellular and network levels.
- [Jenkins and Dallenbach, 1924] Jenkins, J. G. and Dallenbach, K. M. (1924). Obliviscence during sleep and waking. *The American Journal of Psychology*, 35(4):605–612.
- [Kandel et al., 2000] Kandel, E. R., Schwartz, J. H., Jessell, T. M., Siegelbaum, S., Hudspeth, A. J., and Mack, S. (2000). *Principles of neural science*, volume 4. McGraw-hill New York.

- [Killgore, 2010] Killgore, W. D. (2010). Effects of sleep deprivation on cognition. *Progress in brain research*, 185:105–129.
- [Klinzing et al., 2019] Klinzing, J. G., Niethard, N., and Born, J. (2019). Mechanisms of systems memory consolidation during sleep. *Nature Neuroscience*, 22(October).
- [Konorski, 1948] Konorski, J. (1948). Conditioned reflexes and neuron organization. *Cambridge University Press*.
- [Korb and Finkbeiner, 2011] Korb, E. and Finkbeiner, S. (2011). Arc in synaptic plasticity: from gene to behavior. *Trends in neurosciences*, 34(11):591–598.
- [Lapique, 1907] Lapique, L. (1907). Recherches quantitatives sur l’excitation électrique des nerfs traitée comme une polarisation. *Journal of Physiology and Pathology*, 9:620–635.
- [Markram et al., 1997] Markram, H., Lübke, J., Frotscher, M., and Sakmann, B. (1997). Regulation of synaptic efficacy by coincidence of postsynaptic aps and epsps. *Science*, 275(5297):213–215.
- [Martin and Morris, 2002] Martin, S. and Morris, R. (2002). New life in an old idea: the synaptic plasticity and memory hypothesis revisited. *Hippocampus*, 12(5):609–636.
- [Martin et al., 2000] Martin, S. J., Grimwood, P. D., and Morris, R. G. (2000). Synaptic plasticity and memory: an evaluation of the hypothesis. *Annual review of neuroscience*, 23(1):649–711.
- [McCormick and Bal, 1997] McCormick, D. A. and Bal, T. (1997). Sleep and arousal: Thalamocortical mechanisms. *Annual Review of Neuroscience*, 20:185–215.
- [Meriney and Fanselow, 2019] Meriney, S. D. and Fanselow, E. E. (2019). *Synaptic Transmission*. Elsevier Inc.
- [Morrison et al., 2008] Morrison, A., Diesmann, M., and Gerstner, W. (2008). Phenomenological models of synaptic plasticity based on spike timing. *Biological cybernetics*, 98(6):459–478.
- [Mulkey and Malenka, 1992] Mulkey, R. M. and Malenka, R. C. (1992). Mechanisms underlying induction of homosynaptic long-term depression in area ca1 of the hippocampus. *Neuron*, 9(5):967–975.
- [Nere et al., 2012] Nere, A., Olcese, U., Balduzzi, D., and Tononi, G. (2012). A neuromorphic architecture for object recognition and motion anticipation using burst-stdp. *PloS one*, 7(5):e36958.
- [Nere et al., 2013] Nere, A. T., Hashmi, A., Cirelli, C., and Tononi, G. (2013). Sleep-dependent synaptic down-selection (i): modeling the benefits of sleep on memory consolidation and integration. *Frontiers in neurology*, 4:143.
- [Nevian and Sakmann, 2006] Nevian, T. and Sakmann, B. (2006). Spine ca^{2+} signaling in spike-timing-dependent plasticity. *Journal of Neuroscience*, 26(43):11001–11013.
- [Ngezahayo et al., 2000] Ngezahayo, A., Schachner, M., and Artola, A. (2000). Synaptic activity modulates the induction of bidirectional synaptic changes in adult mouse hippocampus. *Journal of Neuroscience*, 20(7):2451–2458.
- [Oja, 1982] Oja, E. (1982). Simplified neuron model as a principal component analyzer. *Journal of mathematical biology*, 15(3):267–273.

- [Pedrosa and Clopath, 2017] Pedrosa, V. and Clopath, C. (2017). The role of neuromodulators in cortical plasticity: a computational perspective. *Frontiers in synaptic neuroscience*, 8:38.
- [Petersen et al., 1998] Petersen, C. C., Malenka, R. C., Nicoll, R. A., and Hopfield, J. J. (1998). All-or-none potentiation at ca3-ca1 synapses. *Proceedings of the National Academy of Sciences*, 95(8):4732–4737.
- [Pfister and Gerstner, 2006] Pfister, J. P. and Gerstner, W. (2006). Triplets of spikes in a model of spike timing-dependent plasticity. *Journal of Neuroscience*, 26(38):9673–9682.
- [Puentes-Mestril and Aton, 2017] Puentes-Mestril, C. and Aton, S. J. (2017). Linking network activity to synaptic plasticity during sleep: Hypotheses and recent data. *Frontiers in Neural Circuits*, 11(September):1–18.
- [Purves, 2004] Purves, D. (2004). *Neurosciences*, 3rd edition.
- [Ramón y Cajal, 1894] Ramón y Cajal, S. (1894). The croonian lecture.—la fine structure des centres nerveux. *Proceedings of the Royal Society of London*, 55(331-335):444–468.
- [Rennó-Costa et al., 2019] Rennó-Costa, C., da Silva, A. C. C., Blanco, W., and Ribeiro, S. (2019). Computational models of memory consolidation and long-term synaptic plasticity during sleep. *Neurobiology of Learning and Memory*, 160(January 2018):32–47.
- [Segal, 2005] Segal, M. (2005). Dendritic spines and long-term plasticity. *Nature Reviews Neuroscience*, 6(4):277–284.
- [Seibt and Frank, 2019] Seibt, J. and Frank, M. G. (2019). Primed to sleep: the dynamics of synaptic plasticity across brain states. *Frontiers in systems neuroscience*, 13:2.
- [Seol et al., 2007] Seol, G. H., Ziburkus, J., Huang, S., Song, L., Kim, I. T., Takamiya, K., Huganir, R. L., Lee, H.-K., and Kirkwood, A. (2007). Neuromodulators control the polarity of spike-timing-dependent synaptic plasticity. *Neuron*, 55(6):919–929.
- [Sjöström et al., 2001] Sjöström, P. J., Turrigiano, G. G., and Nelson, S. B. (2001). Rate, timing, and cooperativity jointly determine cortical synaptic plasticity. *Neuron*, 32(6):1149–1164.
- [Sjöström and Gerstner, 2010] Sjöström, J. and Gerstner, W. (2010). Spike-timing dependent plasticity. *Scholarpedia*, 5(2):1362. revision #184913.
- [Softky and Koch, 1993] Softky, W. R. and Koch, C. (1993). The highly irregular firing of cortical cells is inconsistent with temporal integration of random epsps. *Journal of neuroscience*, 13(1):334–350.
- [Steriade et al., 1993] Steriade, M., McCormick, D. A., and Sejnowski, T. J. (1993). Thalamocortical Oscillations in the Sleeping and Aroused Brain.
- [Stuchlik, 2014] Stuchlik, A. (2014). Dynamic learning and memory, synaptic plasticity and neurogenesis: an update. *Frontiers in behavioral neuroscience*, 8:106.
- [Takeuchi et al., 2014] Takeuchi, T., Duszkievicz, A. J., and Morris, R. G. (2014). The synaptic plasticity and memory hypothesis: encoding, storage and persistence. *Philosophical Transactions of the Royal Society B: Biological Sciences*, 369(1633):20130288.
- [Tononi and Cirelli, 2014] Tononi, G. and Cirelli, C. (2014). Sleep and the price of plasticity: from synaptic and cellular homeostasis to memory consolidation and integration. *Neuron*, 81(1):12–34.

- [Turrigiano and Nelson, 2004] Turrigiano, G. G. and Nelson, S. B. (2004). Homeostatic plasticity in the developing nervous system. *Nature reviews neuroscience*, 5(2):97–107.
- [Van Rossum et al., 2000] Van Rossum, M. C., Bi, G. Q., and Turrigiano, G. G. (2000). Stable hebbian learning from spike timing-dependent plasticity. *Journal of neuroscience*, 20(23):8812–8821.
- [Vorster and Born, 2015] Vorster, A. P. and Born, J. (2015). Sleep and memory in mammals, birds and invertebrates. *Neuroscience & Biobehavioral Reviews*, 50:103–119.
- [Wang et al., 2005] Wang, H.-X., Gerkin, R. C., Nauen, D. W., and Bi, G.-Q. (2005). Coactivation and timing-dependent integration of synaptic potentiation and depression. *Nature neuroscience*, 8(2):187–193.
- [Yang and Calakos, 2013] Yang, Y. and Calakos, N. (2013). Presynaptic long-term plasticity. *Frontiers in synaptic neuroscience*, 5:8.
- [Yger and Gilson, 2015] Yger, P. and Gilson, M. (2015). Models of metaplasticity: a review of concepts. *Frontiers in computational neuroscience*, 9:138.
- [Zagha and McCormick, 2014] Zagha, E. and McCormick, D. A. (2014). Neural control of brain state. *Current Opinion in Neurobiology*, 29(1):178–186.
- [Zenke et al., 2015] Zenke, F., Agnes, E. J., and Gerstner, W. (2015). Diverse synaptic plasticity mechanisms orchestrated to form and retrieve memories in spiking neural networks. *Nature Communications*, 6.
- [Zenke and Gerstner, 2017] Zenke, F. and Gerstner, W. (2017). Hebbian plasticity requires compensatory processes on multiple timescales. *Philosophical Transactions of the Royal Society B: Biological Sciences*, 372(1715).
- [Zhang et al., 2009] Zhang, J.-C., Lau, P.-M., and Bi, G.-Q. (2009). Gain in sensitivity and loss in temporal contrast of stdp by dopaminergic modulation at hippocampal synapses. *Proceedings of the National Academy of Sciences*, 106(31):13028–13033.
- [Ziegler et al., 2015] Ziegler, L., Zenke, F., Kastner, D. B., and Gerstner, W. (2015). Synaptic consolidation: from synapses to behavioral modeling. *Journal of Neuroscience*, 35(3):1319–1334.